A phase field model for cyclic fatigue

Zur Erlangung des akademischen Grades Doktor-Ingenieur (Dr.-Ing.)
Genehmigte Dissertation von Sikang Yan aus Hubei
Tag der Einreichung: August 5, 2024, Tag der Prüfung: September 26, 2024

1. Gutachten: Prof. Dr.-Ing. habil. Ralf Müller
2. Gutachten: Prof. Dr.-Ing. Wolfgang Dornisch
Darmstadt

TECHNISCHE UNIVERSITÄT DARMSTADT

Civil and Environmental Engineering Department
Institute for Mechanics
Continuum Mechanics

A phase field model for cyclic fatigue

Submitted doctoral thesis by Sikang Yan

Date of submission: August 5, 2024
Date of thesis defense: September 26, 2024

Darmstadt

Bitte zitieren Sie dieses Dokument als:
URN: urn:nbn:de:tuda-tuprints-288174
URL: http://tuprints.ulb.tu-darmstadt.de/28817
DOI: https://doi.org/10.26083/tuprints-00028817

Dieses Dokument wird bereitgestellt von tuprints,
E-Publishing-Service der TU Darmstadt
http://tuprints.ulb.tu-darmstadt.de
tuprints@ulb.tu-darmstadt.de

For the ultimate truth of the universe

Erklärungen laut Promotionsordnung

§ 8 Abs. 1 lit. c PromO

Ich versichere hiermit, dass die elektronische Version meiner Dissertation mit der schriftlichen Version übereinstimmt.

§ 8 Abs. 1 lit. d PromO

Ich versichere hiermit, dass zu einem vorherigen Zeitpunkt noch keine Promotion versucht wurde. In diesem Fall sind nähere Angaben über Zeitpunkt, Hochschule, Dissertationsthema und Ergebnis dieses Versuchs mitzuteilen.

§ 9 Abs. 1 PromO

Ich versichere hiermit, dass die vorliegende Dissertation selbstständig und nur unter Verwendung der angegebenen Quellen verfasst wurde.

§ 9 Abs. 2 PromO

Die Arbeit hat bisher noch nicht zu Prüfungszwecken gedient.

Darmstadt, August 5, 2024

S. Yan

Acknowledgements

In the beginning, I would like to acknowledge Prof. Dr.-Ing. Ralf Müller for his constant and valuable supervision. This work is not possible to be done without his expertise and insights.

I would like to deeply thank Distinguished Professor Bahram Ravani for his kind support during my stay at UC Davis. His encouragement and advice have been a constant source of inspiration.

I would like also to thank Prof. Dr.-Ing. Wolfgang Dornisch for agreeing to act as a second reviewer.

I want to thank all my colleagues, no matter whether they are from University of Kaiserslautern-Laudau (former: University of Kaiserslautern), Technical University of Darmstadt, University of California Davis, or somewhere else: The meaningful discussion and thoughtful feedback from all helped me shape the direction of my research. I appreciate sincerely my family and all my friends for their encouragement and support during my entire Ph.D. study. I especially want to thank Mr. Arsalan Jawaid for our delightful research cooperation. I am greatly thankful to the German Research Foundation (Deutsche Forschungsgemeinschaft *DFG*) within International Research Training Group (*IRTG* 2057) for funding this project.

Last but not least, I would like to express my deepest gratitude to Dr.-Ing. Alexander Schlüter for his unwavering support and guidance throughout my academic journey. He is not only a great colleague to me, but also a valued friend and a trustworthy mentor.

Zusammenfassung

Ermüdungsversagen ist eines der entscheidenden Probleme in Fertigungsprozesse und Ingenieuranwendungen. Spannungs- oder Verschiebungszyklen können dazu führen, dass Risse im Laufe der Zeit entstehen und wachsen, was schließlich zu einem strukturellen Versagen führt. Um solche Ausfälle zu vermeiden, ist es wichtig, das Verhalten der Ermüdungsrissentwicklung im Voraus vorherzusagen. In den letzten zehn Jahren hat die Phasenfeldmethode für die Ermüdungsanalyse viel Aufmerksamkeit erregt. Der größte Vorteil des Phasenfeldmodells besteht darin, dass alle Rissentwicklungsszenarien durch eine Evolutionsgleichung einheitlich beschrieben werden können. Es wurde gezeigt, dass das Phasenfeld-Ermüdungsmodell die wichtigsten Ermüdungseigenschaften reproduzieren und den Risswachstumspfad vorhersagen kann; dennoch hat es bei einigen komplexen Problemen in der Industrie noch Schwächen. Der erste Nachteil des Phasenfeld-Ermüdungsmodells ist sein hoher Rechenaufwand, da Ermüdungsbrüche normalerweise nach Tausenden von wiederholten Zyklen auftreten. Um die Simulationszeit in einem vernünftigen Rahmen zu halten, wird das Zyklenzahlinkrement in der Phasenfeldsimulation adaptiv gewählt. Im Anschluss zeigen wir, dass das Phasenfeld-Ermüdungsmodell komplexe Belastungssituationen simulieren kann, einschließlich unterschiedlicher Belastungstemperaturen und -frequenzen. Wir haben das Phasenfeldmodell auch auf thermomechanische Ermüdung erweitert, bei der eine zusätzliche Treibkraft berücksichtigt wird. Es ist bekannt, dass das Phasenfeldmodell auf einer energetischen Formulierung basiert, die nicht leicht verständlich ist. Daher greifen wir die Idee der Konfigurationskräfte auf und bieten eine einfache Möglichkeit, die energetischen Triebskräfte in der Phasenfeldsermüdungssimulation zu erklären.

Abstract

Fatigue failure is one of the most crucial issues in manufacturing processes and engineering applications. Stress or displacement cycles can cause cracks to form and grow over time, eventually leading to structural failure. To avoid these failures, predicting fatigue crack evolution behavior in advance is important. In the past decade, the phase field method for fatigue analysis has drawn much attention. The biggest advantage of the phase field model is its uniform description of all crack evolution scenarios by one evolution equation. It has been shown that the phase field fatigue model can reproduce the most important fatigue properties and predict the crack growth path; however, it still comes up short of some complex problems in the industry. The first drawback of the phase field fatigue model is its intense computational cost since fatigue fracture usually happens after thousands of repeated cycles. In order to keep the simulation time within a reasonable limit, the cycle number increment is therefore adaptively chosen in the phase field simulation. Following that, we show that the phase field fatigue model can simulate complex loading situations including different loading temperatures and frequencies. We also extended the phase field model for thermomechanical fatigue, in which an additional fatigue driving force is considered. It is known that the phase field model is based on an energetic formulation, which can not be easily understood straightforwardly. Thus, we take the idea of configurational forces and provide a simple way to explain the energetic driving forces in the phase field fatigue simulation.

Contents

1. Introduction

In manufacturing processes, dynamic loads typically do not result in immediate tool failure; instead, the failure of tools occurs as a result of fatigue fracture development over multiple loading cycles. Thus, it is important to know the fatigue behavior of tools in advance for the benefit of safety. Different from fatigue experiments, computational methods overcome the disadvantages of those classical methods since they require less cost and time. One of the most popular methods for fracture mechanics is the so-called phase field method.

This work aims to present a phase field model for cyclic fatigue under complex environments. The seed of the energetic study of fracture mechanics was first planted by Griffith [41] more than one hundred years ago. In general, fracture is understood as the material being separated into two or more pieces due to the action of stress. Thanks to Griffith's brilliant idea, the breaking of atomic bonds is associated with an energy density of the crack surface. The crack propagation is explained by a competition of elastic energy which is stored in the solid, and surface energy, which is required to generate cracks. This newly established energetic fracture criterion was later realized by Irwin [52] by the introduction of the stress intensity factor. However, this failure criterion is only capable of predicting the crack propagation along a priori known crack path. Thus, different studies, e.g., [33, 39, 79] were aiming to solve this issue, but they failed to solve the crack nucleation as well as the transition process from the nucleation to the crack extension. The next great leap was completed by Francfort and Marigo [36] with their variational formulation of brittle fracture, where the entire crack evolution is obtained by minimizing the total energy of the body. This model was later regularized by Bourdin et al. [22] for numerical accessibility. Especially, the regularized variational model with the introduction of the order parameter resembles a phase field model. The phase field method had been originally applied for solving interface problems like solidification. However, the word "phase field" for fracture mechanics was first brought by Kuhn and Müller [58], in which the phase field method demonstrates its high potential in fracture mechanics for its simplicity and generality in various scenarios.

Recently, the phase field model has been extended to simulate the fatigue fracture [53]. On the one hand, some models try to degrade the fracture toughness to model the

material under fatigue [26, 2, 94, 43, 46, 95, 96, 100, 4]; on the other hand, some models introduce an additional energy term accounting for the fatigue driving force [9, 25, 91, 65, 47]. The presented work was based on the phase field fatigue model from Schreiber et al. [91], which is later extended to incorporate the mean stress effects for various loading situations [92]. This model introduces an additional energy term representing the accumulated fatigue driving forces, in which a fatigue damage parameter is directly coupled to Wöhler curves. It has been shown that the phase field model can reproduce the most important fatigue properties; however, further investigation is required in order to let the phase field fatigue model be employed for more general and complex problems.

This thesis is devoted to giving a comprehensive study of the phase field model for cyclic fatigue. It is a cumulative work summarizing my research results during the project of International Research Training Group *IRTG* at the University of Kaiserslautern-Landau (former: University of Kaiserslautern), the University of California Davis, and the Technical University of Darmstadt. The essential part of this work consists of three publications: All the publications have already been pressed in the journal.

The thesis has six chapters and proceeds as follows: In Chapter 2, some theoretical preliminaries and information related to continuum mechanics (Sec. 2.1), fracture mechanics (Sec. 2.2), fatigue fracture (Sec. 2.3), J-integral (Sec. 2.4) and phase field model (Sec. 2.5) are provided. In Chapter I, a numerical implementation for the phase field fatigue model aiming at reducing the computational time is proposed. The key idea is to divide the entire fatigue fracture simulation into three stages and apply different cycle number increments in each damage stage. Three numerical examples highlight this solution strategy and validate the results against experimental results and previous works. The second contribution discusses the extension of the phase field model to thermomechanical fatigue. Besides the classical material fatigue due to repeated mechanical loading, fatigue failure can also result from fluctuating temperature changes. In Chapter II, we propose a phase field model for thermomechanical fatigue, where the thermal stress is considered as an additional fatigue driving force. Although it has been shown that the phase field fatigue model can reproduce the most important fatigue properties as well as predict crack evolution in complex scenarios, it is still hard to explain the phase field method based on Griffith's energy framework. In Chapter III, we borrow the idea of configurational forces onto the phase field model, which provides a straightforward way to understand the phase field simulations of fatigue fracture. In Chapter 3, the work of this thesis is summarized, and the outlook for future work is given. In Appendix, we provide an additional publication contribution in which the phase field model is applied to manufacturing and engineering problems.

2. Preliminary information

2.1. Continuum mechanics

Continuum mechanics provides a very useful and common abstraction of the real behavior of solids and fluids, by imagining the considered body – the continuum – to be continuously filled with material. The continuum is considered to consist of material points, i.e., the so-called particles. The subject of continuum mechanics focuses on material bodies that can undergo motions and deformations. In order to provide basic notation and relations for later chapters, a brief introduction to classical continuum mechanics is given here. Comprehensive information can be found, for example, in Gurtin [44], Lai et al. [60], and Becker et al. [16].

2.1.1. Kinematics

Over time, the body occupies different regions of physical space: it is convenient to choose one of those regions as the *reference configuration* $\mathcal{B}_0$, where it is usually to set the time to $t = 0$ for this state. Here, the particles of the body can be identified with their reference positions $\mathbf{X}$. Consider now a motion happens, which drives the material points to their position $\mathbf{x}$ at time t in the *actual configuration* $\mathcal{B}$. This motion defines the following mapping (see Fig. 2.1):

$$\mathbf{x} = \varphi(\mathbf{X}, t). \tag{2.1}$$

The change of positions in the physical space of the particle from the reference configuration to the actual configuration is given by the difference

$$\mathbf{u} = \mathbf{x} - \mathbf{X}, \tag{2.2}$$

where the vector $\mathbf{u}$ is called the *displacement vector*. Besides, the *velocity* is given by the total or material time derivative of the actual position

$$\mathbf{v} = \frac{\mathrm{d}\mathbf{x}}{\mathrm{d}t} = \dot{\mathbf{x}} \tag{2.3}$$

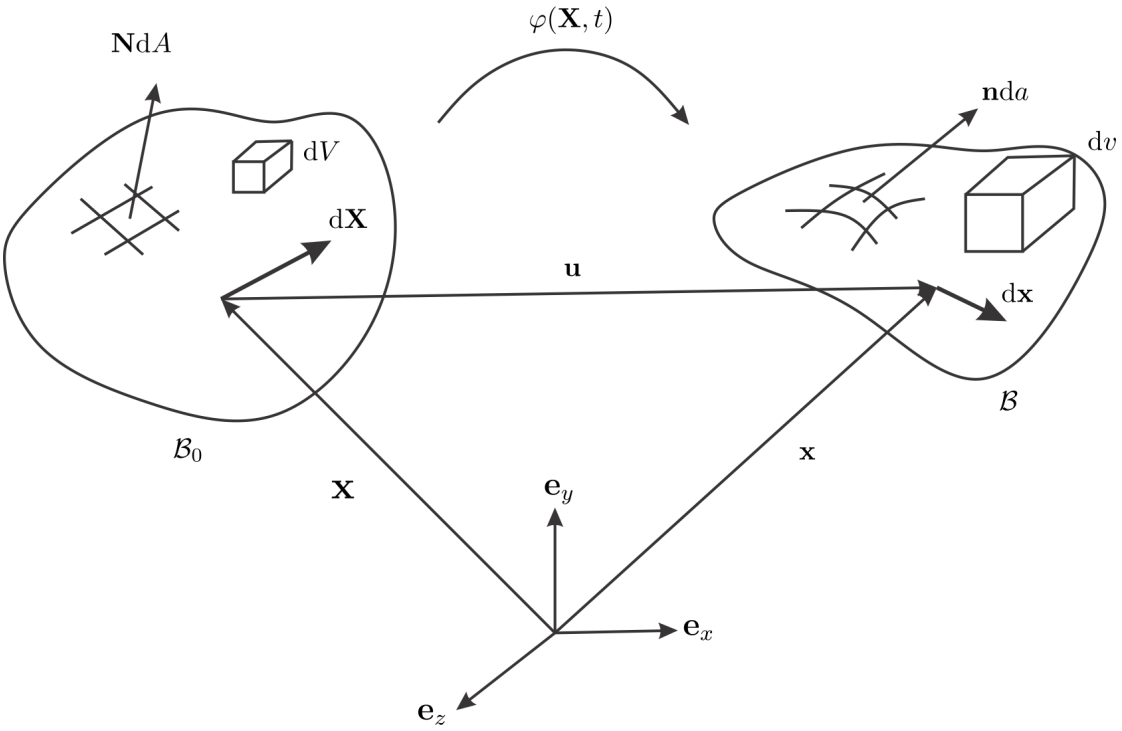

Figure 2.1.: A mapping φ gives a transformation of particle positions between the reference configuration $\mathcal{B}_0$ and actual configuration $\mathcal{B}$.

and the *acceleration* is again the total or material time derivative of the velocity

$$\mathbf{a} = \frac{\mathrm{d}\mathbf{v}}{\mathrm{d}t} = \dot{\mathbf{v}} = \ddot{\mathbf{x}}. \tag{2.4}$$

Furthermore, the gradient of the mapping

$$\mathbf{F} = \frac{\partial \varphi(\mathbf{X}, t)}{\partial \mathbf{X}} = \frac{\partial \mathbf{x}}{\partial \mathbf{X}} \tag{2.5}$$

is called the *deformation gradient*, describing how a line element in the reference configuration maps into the current configuration

$$\mathrm{d}\mathbf{x} = \mathbf{F}\mathrm{d}\mathbf{X}. \tag{2.6}$$

Since the mapping φ must be invertible and orientation persevering to represent the motion of a continuum, the determinant of the deformation gradient has to be positive

$$\det\mathbf{F} = J > 0, \tag{2.7}$$

where the determinant J is called the *Jacobian*. It is to show that the Jocabian connects the surface and volume change between the configurations. The mapping of surface elements of the reference configuration $\mathrm{d}A$ with normal vector $\mathbf{N}$ into the actual configuration $\mathrm{d}a$ with normal vector $\mathbf{n}$ can be done with the help of *Nanson formula*

$$\mathbf{n}\mathrm{d}a = J\mathbf{F}^{-T}\mathbf{N}\mathrm{d}A. \tag{2.8}$$

Respectively, the transformation between the volume elements between the reference configuration $\mathrm{d}V$ and actual configuration $\mathrm{d}v$ is given by

$$\mathrm{d}v = J\mathrm{d}V. \tag{2.9}$$

The gradient of the displacement vector $\mathbf{u}$ is called *displacement gradient*, which is closely related to the deformation gradient

$$\mathbf{H} = \frac{\partial\mathbf{u}}{\partial\mathbf{X}} = \mathbf{F} - \mathbf{I}, \tag{2.10}$$

where the tensor $\mathbf{I}$ denotes the second order identity tensor. The spatial *velocity gradient* indicates the velocity regarding the deformation gradient to the displacement

$$\mathbf{L} = \frac{\partial\dot{\mathbf{v}}}{\partial\mathbf{x}} = \dot{\mathbf{F}}\mathbf{F}^{-1}. \tag{2.11}$$

2.1.2. Stress tensor

Consider an infinitesimal surface $\mathrm{d}a$ exerting a force $\mathrm{d}\mathbf{f}$ with outward normal vector $\mathbf{n}$ in the current configuration (see 2.2), the *traction* is defined as

$$\boldsymbol{t} = \frac{\mathrm{d}\mathbf{f}}{\mathrm{d}a}. \tag{2.12}$$

The *Cauchy theorem* gives the state of the stress at a point inside a material in the actual configuration, allowing to compute the traction on any surface element with outward normal vector $\mathbf{n}$

$$\boldsymbol{t} = \boldsymbol{\sigma}\mathbf{n}, \tag{2.13}$$

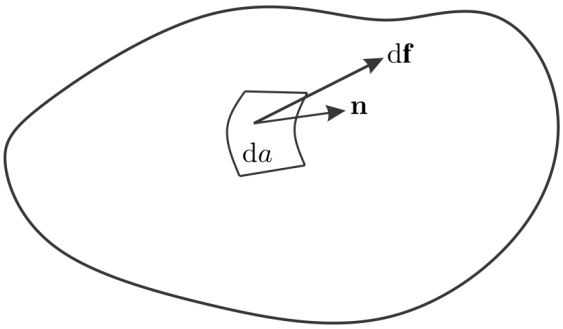

Figure 2.2.: The traction is defined as the ratio between the force and the infinitesimal surface.

where the tensor $\boldsymbol{\sigma}$ is called *Cauchy stress tensor*. Similarly, the traction $\boldsymbol{t}$ measured in the reference configuration with respect to the normal vector $\mathbf{N}$ from the reference configuration is given by

$$\boldsymbol{t} = \mathbf{P}\mathbf{N}, \tag{2.14}$$

where the tensor $\mathbf{P}$ is called the *first Piola-Kirchhoff stress tensor*, describing the current stress based on an infinitesimal surface $\mathrm{d}A$ in the reference configuration. With Nanson's formula, the Cauchy stress tensor and first Piola-Kirchhoff stress tensor have the following relation

$$\mathbf{P} = J\boldsymbol{\sigma}\mathbf{F}^{-T}. \tag{2.15}$$

In order to define a stress measure that is purely formulated in the reference configuration, the *second Piola-Kirchhoff stress tensor* is introduced

$$\mathbf{S} = \mathbf{F}^{-1}\mathbf{P} = J\mathbf{F}^{-1}\boldsymbol{\sigma}\mathbf{F}^{-T}. \tag{2.16}$$

It is noticed that the traction $\tilde{\boldsymbol{t}} = \mathbf{S}\mathrm{d}A$ is only a virtual explain stress related to the surface in the reference configuration. Fig. 2.3 summarizes the relations between all stress measures graphically.

2.1.3. Strain tensor

A deformation of a body can be decomposed into a pure rotation – it does not generate stress since it represents a rigid body motion, and a pure stretch – it does contribute to the

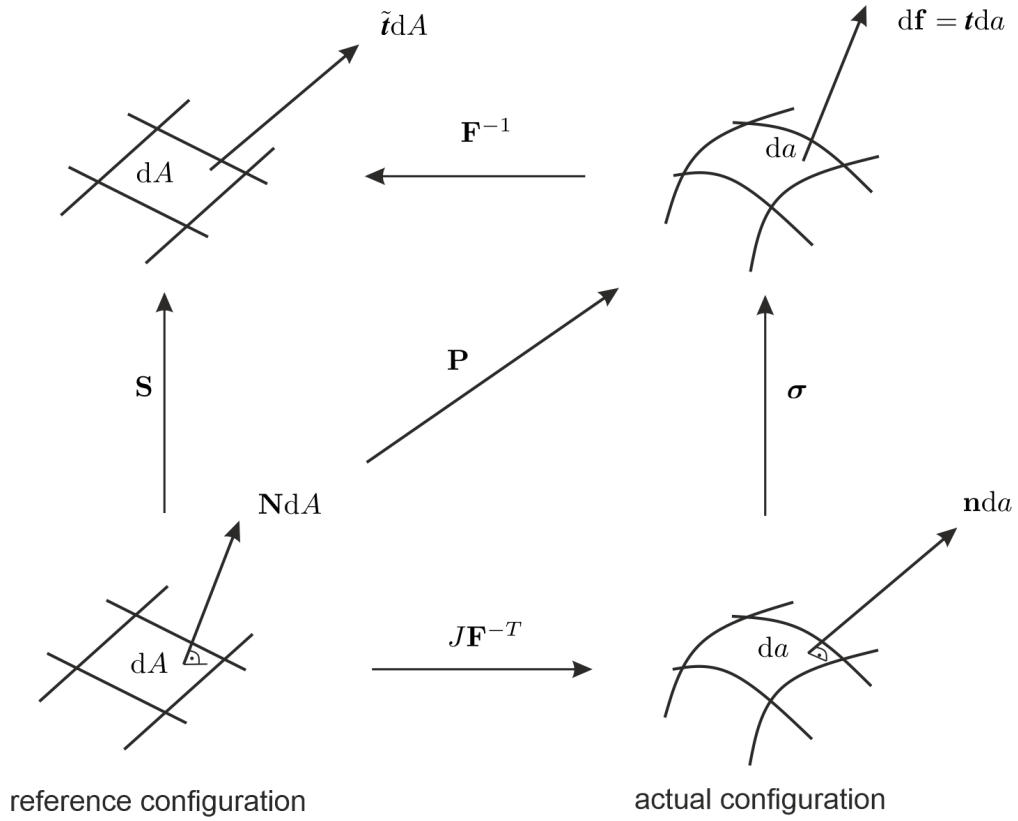

Figure 2.3.: A summary of all stress measures in reference and actual configuration.

stress and strain. In order to distinguish the quantity purely related to the stress property, a unique polar decomposition is introduced

$$\mathbf{F} = \mathbf{RU} = \mathbf{VR}. \tag{2.17}$$

The *rotation tensor* $\mathbf{R}$ is an orthogonal tensor, describing the pure rotation of a body; and the symmetric, positive definite *right stretch tensor* $\mathbf{U}$ or *left stretch tensor* $\mathbf{V}$ describes the stretching under deformation (see Fig. 2.4).

In order to eliminate the rotation part during the deformation and retain the pure stretching, the *right* and *left Cauchy-Green tensor* are introduced respectively

$$\mathbf{C} = \mathbf{F}^T\mathbf{F} = \mathbf{U}^T\mathbf{U} = \mathbf{U}^2 \tag{2.18}$$

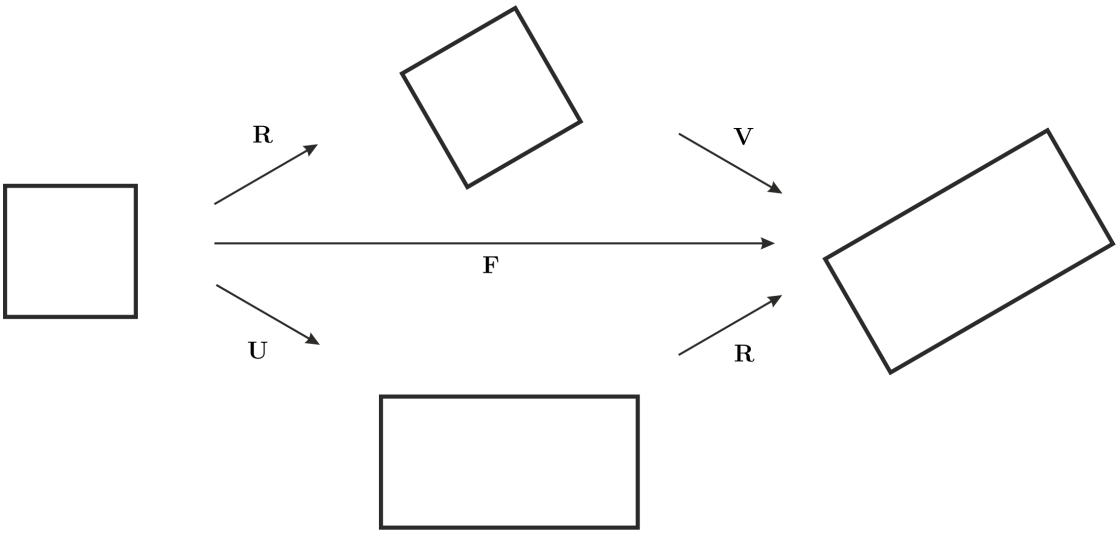

Figure 2.4.: With a deformed body, the deformation gradient $\mathbf{F}$ can be decomposed into a rotation part $\mathbf{R}$ and a stretching part $\mathbf{U}$ or $\mathbf{V}$.

and

$$\mathbf{b} = \mathbf{F}\mathbf{F}^T = \mathbf{V}\mathbf{V}^T = \mathbf{V}^2. \tag{2.19}$$

Furthermore, the *Green-Lagrange strain tensor*

$$\mathbf{E} = \frac{1}{2}(\mathbf{C} - \mathbf{I}) = \frac{1}{2}(\mathbf{H} + \mathbf{H}^T + \mathbf{H}^T\mathbf{H}) \tag{2.20}$$

and the *Euler-Almansi strain tensor*

$$\mathbf{e} = \frac{1}{2}(\mathbf{1} - \mathbf{b}^{-1}) \tag{2.21}$$

are introduced to describe the strain measure in more general cases.

In this work, the displacement $\mathbf{u}$ is assumed much smaller compared to the dimension of the body and in particular the components of the displacement gradient H_{ij} are assumed to be much smaller than 1

$$|H_{ij}| = \left|\frac{\partial u_i}{\partial X_j}\right| \ll 1, \tag{2.22}$$

where the indices i, j denote the entry from the i-th row and j-th column of the tensor. Thus, if the assumptions from above are applied, then only the linear part of the Green-Lagrange strain tensor remains, which is the *linearized strain tensor*, i.e.,

$$\boldsymbol{\varepsilon} = \frac{1}{2}(\mathbf{H} + \mathbf{H}^T). \tag{2.23}$$

2.1.4. Constitutive law

Although the stress tensors and stain tensors are introduced in the past section, the connection between them is still missing. The constitutive law gives the relation between the strain measures and stress measures. One of the most common constitutive laws is the generalized Hooke's law

$$\boldsymbol{\sigma} = \mathbb{C}\boldsymbol{\varepsilon}, \quad \sigma_{ij} = \mathbb{C}_{ijkl}\varepsilon_{kl}, \tag{2.24}$$

with the 4th order stiffness tensor $\mathbb{C}$ or in the index notation $\mathbb{C}_{ijkl}$. It is noted that the tensor component $\mathbb{C}_{ijkl}$ is symmetric

$$\mathbb{C}_{ijkl} = \mathbb{C}_{jikl} = \mathbb{C}_{ijlk} = \mathbb{C}_{klij}. \tag{2.25}$$

In particular, for isotropic materials, where elastic properties remain the same in different directions, the stiffness tensor $\mathbb{C}$ is related only to two independent *Lamé parameters* λ and μ

$$\mathbb{C}_{ijkl} = \lambda\delta_{ij}\delta_{kl} + \mu(\delta_{ik}\delta_{jl} + \delta_{il}\delta_{jk}), \tag{2.26}$$

where the symbol δ_{ij} denotes the Kronecker delta

$$\delta_{ij} = \begin{cases} 0 & \text{if} \quad i \neq j \\ 1 & \text{if} \quad i = j \end{cases}. \tag{2.27}$$

The Lamé parameters can be obtained from the other material parameters, e.g., the *Young's modulus* E, the *shear modulus* G, and the *Poisson's ratio* ν

$$\lambda = \frac{\nu E}{(1+\nu)(1-2\nu)} \quad \mu = G = \frac{E}{2(1+\nu)}. \tag{2.28}$$

2.1.5. Balance laws

The law of *conservation of mass* states that the mass of a closed system must remain constant over time

$$\frac{\mathrm{d}\rho}{\mathrm{d}t} + \mathrm{div}\big(\rho\mathbf{v}\big) = 0, \tag{2.29}$$

where the parameter ρ denotes the mass of density.

When forces are involved, assuming volume forces $\boldsymbol{f}$ applied in the system, the *balance of linear momentum* reads

$$\frac{\mathrm{d}\big(\rho\mathbf{v}\big)}{\mathrm{d}t} = \mathrm{div}\boldsymbol{\sigma} + \boldsymbol{f}. \tag{2.30}$$

Eq. (2.30) implies that the momentum can only be changed through the action of forces.

The last fundamental balance law in continuum mechanics states the *conservation of energy*, which is equivalent to the first law of thermodynamics

$$\rho\dot{\mathcal{E}}^* = \rho s_\theta^* + \boldsymbol{\sigma} : \mathbf{D} - \mathrm{div}\mathbf{q}_\theta. \tag{2.31}$$

The parameter $\dot{\mathcal{E}}^*$ denotes the specific internal energy per unit mass, the parameter $\mathbf{q}_\theta$ is the heat flux, and the parameter s_θ^* is the specific heat source. The tensor $\mathbf{D}$ is the symmetric part of the velocity gradient $\mathbf{L}$

$$\mathbf{D} = \frac{1}{2}(\mathbf{L} + \mathbf{L}^T). \tag{2.32}$$

Additionally, the *Clausius-Duhem inequality* expresses the second law of thermodynamics in continuum mechanics

$$\rho S^* + \mathrm{div}\left(\frac{\mathbf{q}_\theta}{\theta}\right) - \frac{\rho s_\theta^*}{\theta} \geq 0, \tag{2.33}$$

where $\mathcal{S}^*$ is the specific entropy density and θ is the absolute temperature.

2.1.6. Fourier law and thermal stress

As observed in nature, heat is transferred from the hotter end to the colder end of an object. This thermal conduction process can be described by *Fourier's law* of thermal conduction

$$\mathbf{q}_\theta = -\boldsymbol{\kappa}\nabla\theta, \tag{2.34}$$

where the positive semi-definite tensor $\boldsymbol{\kappa}$ is the heat conduction tensor and $\nabla\theta$ is the temperature gradient.

As the temperature of the material changes, thermal strain occurs if the final temperature θ is different from the initial temperature θ_0

$$\boldsymbol{\varepsilon}_T = \boldsymbol{\alpha}(\theta - \theta_0), \tag{2.35}$$

where $\boldsymbol{\alpha}$ is the thermal expansion coefficient. Furthermore, if the body is locally constrained such that the material cannot be extended or contracted freely, thermal stress is generated in those parts of the body, i.e,

$$\boldsymbol{\sigma}_T = E\boldsymbol{\alpha}(\theta - \theta_0), \tag{2.36}$$

where the parameter E is the Young's modulus. Isotropic materials do not have preferred directions of thermal expansion; thus, the thermal expansion coefficient is degenerated into a diagonal matrix

$$\boldsymbol{\alpha} = \alpha\mathbf{I}. \tag{2.37}$$

It is noted that a positive temperature difference $\theta - \theta_0 > 0$ generates compressive forces and the opposites exert tensile forces.

2.2. Fracture mechanics

Fracture mechanics studies the crack propagation in materials. In classical fracture mechanics, materials are treated as a continuum; and the macroscopic quantities like stresses, strain, and energy are analyzed in order to predict the fracture behavior. In this section, a brief outline of linear elastic fracture theory is provided, where the plastic material behaviors are neglected. This introduction follows relevant textbooks, e.g., [42, 11], that can be consulted for more details by interested readers.

2.2.1. Failure hypotheses

Historically, the failure of materials is determined by hypotheses. The simplest failure hypothesis is the *principal stress hypothesis*, where the failure is to take place when the maximum principal stress reaches a threshold. The principal stresses are eigenvalues of the stress tensor. The principal stresses ($\sigma_1 > \sigma_2 > \sigma_3$) can be computed with *singular value decomposition* (SVD) [14] or given by formula in 2D cases from stress tensor $\boldsymbol{\sigma} = \sigma_{ij}$

$$\sigma_{1,2} = \frac{\sigma_{11} + \sigma_{22}}{2} \pm \sqrt{\left(\frac{\sigma_{11} - \sigma_{11}}{2}\right)^2 + \sigma_{12}^2}. \tag{2.38}$$

In particular, the maximum stress σ_1 is called *first principal stress*, which denotes the maximum value of tensile stress on the plane. The principle stress hypothesis is dominated by the failure of brittle materials. Similar hypotheses can be made for principal strain, as known as the *principal strain hypothesis*. It is to assume that failure occurs when the maximum principal strain reaches a critical value.

The *von Mises yield criterion* has been applied widely for ductile materials, and it assumes that the failure of materials is due to material yielding and plasticity. It is postulated that the yielding of ductile materials happens when the *von Mises stress* σ_v is greater than a threshold – the yield strength σ_y

$$\sigma_v > \sigma_y, \tag{2.39}$$

where the von Mises stress is given as

$$\sigma_v = \sqrt{\frac{(\sigma_{11} - \sigma_{22})^2 + (\sigma_{22} - \sigma_{33})^2 + (\sigma_{33} - \sigma_{11})^2 + 6(\sigma_{12} + \sigma_{23} + \sigma_{31})^2}{2}}. \tag{2.40}$$

For the other failure hypotheses, the reader may refer to Gross et al. [42].

2.2.2. Fracture modes

In linear fracture mechanics, the fracture solid is considered a linear elastic material. As shown in Fig. 2.5, a crack is considered as a cut inside a body, where the *crack surface* consists of the opposite boundaries of this cut, and the end of the crack is called the *crack tip* or *crack front*. Depending on the deformation of the crack tip, the crack loading can be

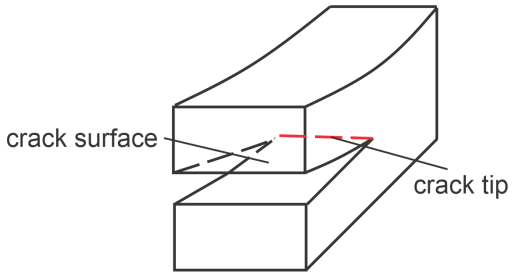

Figure 2.5.: The crack is assumed as a cut in the body.

classified into three modes (see Fig. 2.6): mode I, where the crack opens symmetrically and orthogonal to the crack surface; mode II, where the crack opening is parallel to the crack surface but orthogonal to the crack tip; mode III, where the deformation of the crack tip is both parallel to the crack surface and the crack tip.

2.2.3. Stress intensity factor and the *K*-concept

The *process zone* is defined as the region close to a crack tip, in which the process of material separation takes place (see Fig. 2.7). Generally, complicated processes of bonds breaking are involved in the process zone during the fracturing. In order for linear elastic fracture mechanics to be applicable, some assumptions must be made:

1. The process zone is considered very small compared to the macroscopic dimensions of the body.
2. The region in which the plastic material behavior near the crack tip occurs is assumed to be very small and can be neglected

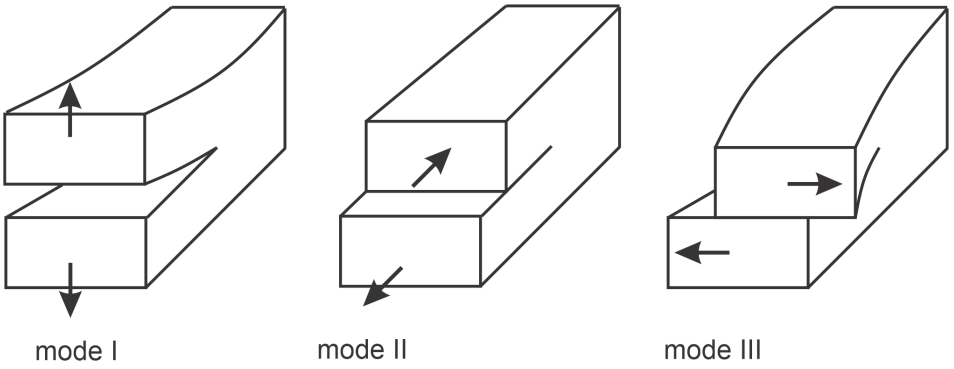

Figure 2.6.: depending on the deformation of the crack tip, the crack loading can be classified into three modes.

For a two-dimensional setting of linear elastic plane strain and plane stress problems, the dominating solution close to the crack tip can be solved analytically by means of complex functions. The stress fields around the crack tip are given in [42] and read

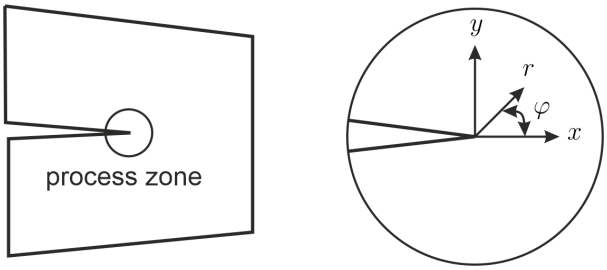

Figure 2.7.: The process zone is a small region in the vicinity of the crack tip in which the process of material separation takes place.

$$\text{mode I} \quad \begin{bmatrix}\sigma_x\\ \sigma_y\\ \tau_{xy}\end{bmatrix} = \frac{K_I}{\sqrt{2\pi r}}\cos(\frac{\varphi}{2}) \begin{bmatrix}1-\sin(\frac{\varphi}{2})\sin(\frac{3\varphi}{2})\\ 1+\sin(\frac{\varphi}{2})\sin(\frac{3\varphi}{2})\\ \sin(\frac{\varphi}{2})\cos(\frac{3\varphi}{2})\end{bmatrix} \tag{2.41}$$

$$\text{mode II} \quad \begin{bmatrix}\sigma_x\\ \sigma_y\\ \tau_{xy}\end{bmatrix} = \frac{K_I}{\sqrt{2\pi r}} \begin{bmatrix}-\sin(\frac{\varphi}{2})\Big(2+\cos(\frac{\varphi}{2})\cos(\frac{3\varphi}{2})\Big)\\ \sin(\frac{\varphi}{2})\cos(\frac{\varphi}{2})\cos(\frac{3\varphi}{2})\\ \cos(\frac{\varphi}{2})\Big(1-\sin(\frac{\varphi}{2})\sin(\frac{3\varphi}{2})\Big)\end{bmatrix} \tag{2.42}$$

$$\text{mode III} \quad \begin{bmatrix}\tau_{xz}\\ \tau_{yz}\end{bmatrix} = \frac{K_I}{\sqrt{2\pi r}} \begin{bmatrix}-\sin(\frac{\varphi}{2})\\ \cos(\frac{\varphi}{2})\end{bmatrix}, \tag{2.43}$$

where r and φ are the polar coordinates around the crack tip with the crack tip as the origin (see Fig. 2.7). The stress intensity factors K [52] are intensity parameters, that describe the stress singularity near the tip of a crack. They are determined by the specimen geometry, the size, and location of the crack, the magnitude, and the distribution of loads applied on the material. A crack is assumed to propagate if the stress intensity factor reaches the critical stress intensity factor or fracture toughness according to Irwin [52]

$$K_I = K_{Ic}, \quad K_{II} = K_{IIc} \quad \text{or} \quad K_{III} = K_{IIIc}. \tag{2.44}$$

For mixed mode loading, a generalized fracture criterion must be satisfied

$$f(K_I, K_{II}, K_{III}) = 0. \tag{2.45}$$

Eq. (2.44) and Eq. (2.45) are referred as the *K-concept*.

2.3. Fatigue fracture

A material failure due to extended cyclic loading is known as a fatigue fracture. The entire fatigue crack evolution process can be segmented into three phases of life: crack initialization, crack propagation and fracture [17]. Here, we briefly introduce the mechanism of crack initiation and crack propagation from a microstructural point of view based on the review of Sandig [85] and Ritchie [84]. Fatigue is well-known under consistently fluctuating loading, and this accumulated cyclic loading generates defects in the form of multiple dislocations within the material, which becomes denser as the fatigue progresses [82].

At the same time, mechanical strain in many materials is localized in the so-called *slip bands* in order to form a unique structure to maintain the minimum energy of the system. As cycles increase, the slip bands become wider; the material separates at points within those slip bands and finally develops into small cracks [34].

The mechanism of fatigue crack propagation is similar but slightly different depending on the types of materials (ductile or brittle). In general, the fatigue crack growing process is determined by a competition between *intrinsic* and *extrinsic* mechanisms [84]. The intrinsic mechanism is the crack extending ahead of the crack tip and the extrinsic mechanism is the crack closure behind the crack tip, which prevents the crack from growing. Furthermore, the concept of *crack intensity factor range* ΔK provides a powerful tool to analyze the fatigue crack propagation behavior [52]. The crack propagation stage includes also the microcrack propagation and macrocrack propagation [86].

The fatigue test is a mechanical experiment to determine the *fatigue life*, which is the number of loading cycles that a specimen sustains before its failure occurs [106]. The fatigue test proceeds as follows: one side of the specimen is fixed, and the other side is applied with cycle loading periodically [13]. In order to compare materials in an adequate way, the different cyclic loads are converted to respective stress acting on the cross-section of the specimen, which alternates sinusoidally around a mean stress $\boldsymbol{\sigma}_m$ with a stress amplitude $\boldsymbol{\sigma}_a$. The fatigue life of a specimen is usually graphically represented in an *SN-diagram*(see Fig. 2.8). In the vertical axis of the SN-diagram, the stress amplitude $\boldsymbol{\sigma}_a$ is plotted; and the number to the fatigue failure N_f is plotted right on the horizontal axis with a logarithmic scaling. Depending on the number of cycles to the mechanical fatigue failure, the fatigue life concept is classified into *low-cycle fatigue*(LCF), where the fatigue life is up to $10^4 \sim 10^5$ cycles; *high-cycle fatigue*(HCF), where the fatigue life is usually more than 10^5 [87]. The LCF is characterized by its plastic deformation, high stress, and low frequency; and the HCF results from repeated elastic deformation with a low stress and high loading frequency. The slope k of the log-log SN-Curve gives the relationship between the load amplitude and the number of cycles to failure. For many materials, if the stress levels are below a certain level A_D, an infinite number of cycles can be applied without causing a failure, and this threshold cycle number is called the knee point cycle number n_D.

It is worth mentioning that several researches [56] [54] have shown that some metals could still fail after 10^7 cycles, which is beyond the range of 10^6 cycles for a classical infinite life proposed by Wöhler [93, 15]. In this work, we will however only focus on the HCF region since the applied phase field fatigue model is an extension of Kuhn and Müller's model for brittle materials, i.e., it is not suitable to capture the dominated plasticity as it occurs in LCF.

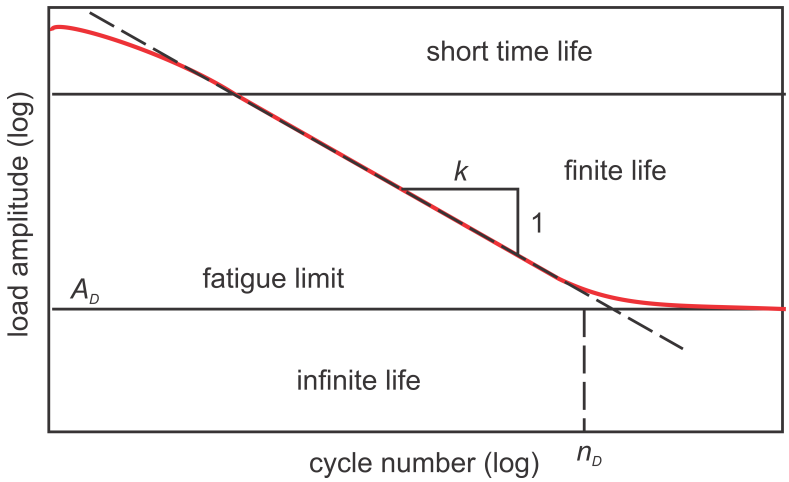

Figure 2.8.: The entire crack propagation phases is classified into: microcrack propagation, macrocrack propagation, and failure [108].

2.3.1. Crack propagation and Paris' law

Let $\frac{\mathrm{d}a}{\mathrm{d}N}$ be the crack growth rate and ΔK be the stress intensity factor range, Fig. 2.9 reports the entire crack propagation stages: microcrack propagation, macrocrack propagation, and failure.

As the microcracks are formed inside the slip bands, the barriers of grain boundary impede the growth of microcracks. After the crack penetrates the first grain boundary, the crack growth rate increases until it reaches the boundary of the next grain. Finally, the microcrack grows at a steadily increasing rate when it passes the last grain boundary.

The macrocrack growth is a bulk material phenomenon, and it is usually perpendicular to the main principal stress. During continuous loading, the crack will be opened by crack tip plastic deformation, and the slip deformation causes the crack extension. The Paris' law [80] is the most essential equation to describe the macro crack propagation behavior. According to Paris' law, the fatigue crack growth rate is in relation to the stress intensity factor range

$$\frac{\mathrm{d}a}{\mathrm{d}N} = C(\Delta K)^m \quad \text{with} \quad \Delta K = K_{\max} - K_{\min}, \tag{2.46}$$

where C and m are material dependent parameters.

As the macrocrack successively grows, the crack growth rate becomes steep and finally leads to the failure of structures.

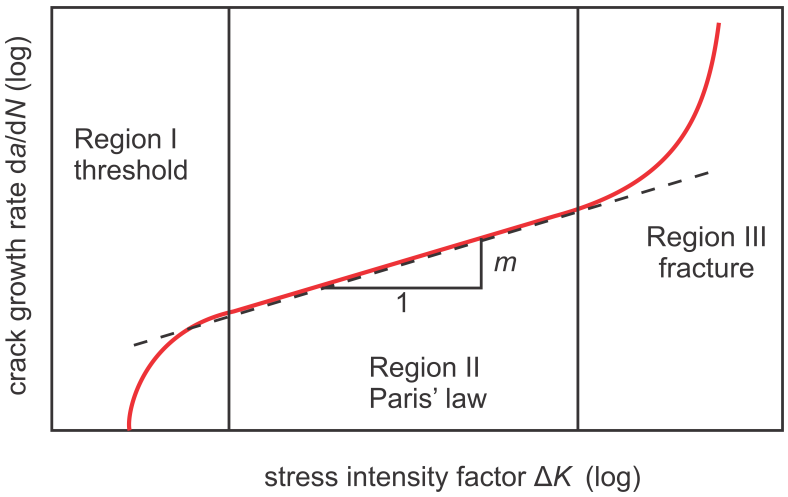

Figure 2.9.: The entire crack propagation phases are classified into: microcrack propagation, macrocrack propagation, and failure [108].

2.3.2. Mean stress effect

Studies show that the fatigue life is reduced when the material is subject to a high mean stress loading, which is called *mean stress effect*.

In the past decade, many mean stress correction models have been proposed, which aim to include the mean stress effect in the Wöhler's curve. In 1919, Goodman [40] firstly exploits a straight line to include the relationship between the mean stress σ_m and the stress amplitude σ_a as well as the ultimate tensile strength σ_u

$$\frac{\sigma_a}{\sigma_{ar}} + \frac{\sigma_m}{\sigma_u} = 1, \tag{2.47}$$

where σ_{ar} is the equivalent stress as the mean stress effect is considered. The *Goodman line* is generally conservative, especially when the mean stress becomes large [32]. As an alternative, Smith, Watson, and Topper (*SWT*) proposed a simple model, in which only the maximum stress $\sigma_{\max}$ and the stress amplitude σ_a are involved

$$\sigma_{ar} = \sqrt{\sigma_{\max}\sigma_a}. \tag{2.48}$$

The SWT model is frequently used due to its straightforward form and not independent of the material; however, it is found to be inaccurate for small mean stresses [57]. In

addition to the SWT models, Walker model [101] supposed the mean stress effect as

$$\sigma_{ar} = \sigma_{\max}\left(\frac{1-R}{2}\right)^{\gamma}, \tag{2.49}$$

where $R = \dfrac{\sigma_m}{\sigma_{\min}}$ is the stress ratio, which gives the ratio of the mean stress σ_m and the minimum stress $\sigma_{\min}$. The parameter γ is a material constant, where a higher γ alleviates the mean stress effect [32]. It is noted that the SWT model can be seen as a special case of Walker model with $\gamma = 0.5$.

2.3.3. Miner's rule

For a case of variable amplitude loading, the Miner rule [73] is widely used to approximate the accumulated fatigue damage on the material. It is postulated that the cumulative damages done by different stress magnitudes all contribute to the eventual fatigue failure. Let k be the number of the various stress magnitudes S_k, Miner rule is formulated as

$$\sum_{i=1}^{k} \mathrm{d}D_i = \sum_{i=1}^{k} \frac{n_i}{N_i} = D_c, \tag{2.50}$$

where n_i is the load cycles and N_i is the fatigue life cycles bearing the i-th stress magnitude, so the fatigue damage caused by higher stress is indeed higher since N_i is smaller for higher stress σ_i. The failure occurs when the sum of damage fractions $\mathrm{d}D_i$ reaches a constant D_c.

Originally, the damage constant is taken as 1 as the material goes to failure. However, in practical applications this is not always the case: The Miner's rule does not take into account the order of the loading sequence applied at the object. A high-low loading sequence typically increases the damage constant ($D_c \approx 2 \sim 3$) and a low-high loading sequence decreases the damage constant below 1. Fig. 2.10 quantitatively illustrates the damage accumulation mechanism. Assuming n_1 cycles are applied for the first block with stress S_1 and N_1 is the fatigue life of this stress level, the portion $\dfrac{n_1}{N_1}$ of the entire fatigue life will be expanded. This repeats for the stress level S_2 and so on. Once the summation of all the portion $\sum \dfrac{n_i}{N_i}$ reaches the constant D_c, the material is predicted to fail.

While Miner's rule gives a linear damage accumulative mechanism, some other nonlinear cumulative damage models, e.g. [27] can also be found in the literature. Moreover, a connection between Miner's rule and Paris' law has already been shown in the study of Ciavarella et a. [28].

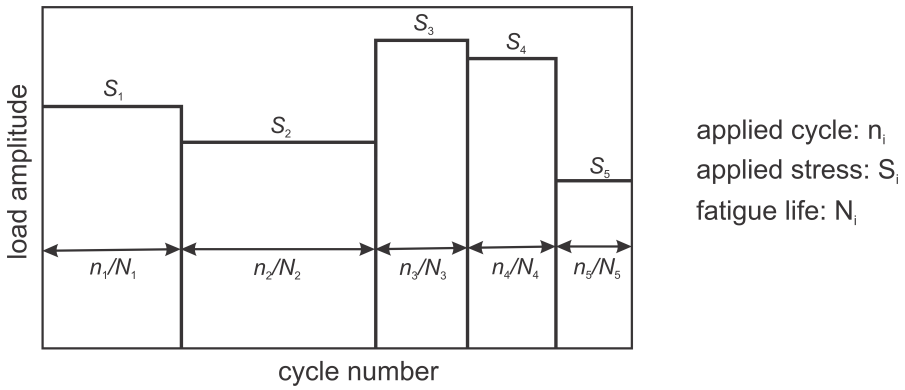

Figure 2.10.: An illustration of Miner rule. When the sum of damage fractions reaches a constant D_c, the material is fatigue fractured.

2.3.4. Thermo-mechanical fatigue

Besides the mechanical loading, a cyclic thermal loading can also lead to the fatigue of the material. Typically, thermal stresses are generated by repeated heating and cooling of material under geometric constraints [105]. Thermo-mechanical fatigue is the combination of cyclic mechanical loading, that leads to fatigue of a material, with a cyclic thermal loading.

In general, there are three damage mechanisms acting in thermo-mechanical fatigue process [77]:

1. creep: material undergoes slow deformation at high temperatures.
2. fatigue: the growth and propagation of cracks due to repeated loading.
3. oxidation: the reaction of material and oxygen changes its chemical composition.

Due to the complex interaction behavior, huge research effect has been given to find models predicting the thermo-mechanical fatigue life [98, 66, 29, 110].

2.4. J-intergral and configurational forces

Classical mechanics is well-known and typically defined within the usual Euclidean physical space. However, when defects are present in a material, rather than a perfect continuum, it becomes practical to define the "forces" directly acting on the "defects" within the material.

Consider a body C_R defined in a reference configuration, that deforms under mechanical loading and occupies the configuration C_r as shown in Fig. 2.11. The mapping of the line elements in the body is usually described by the deformation gradient $\mathbf{F}$. Let the body be unloaded, the occupying of the body back into the stress-free configuration C'_R can be defined by a reversed deformation gradient $\mathbf{f}$. If the material of the body is perfectly elastic, the reverse deformation $\mathbf{f}$ can be formulated as $\mathbf{f} = \mathbf{F}^{-1}$ and the body in the original reference configuration C_R and the stress-free configuration C'_R are identical. However, if irreversible microstructural changes like cracking are involved during the deformation, the gradients $\mathbf{f}$ and $\mathbf{F}^{-1}$ are close but not equal.

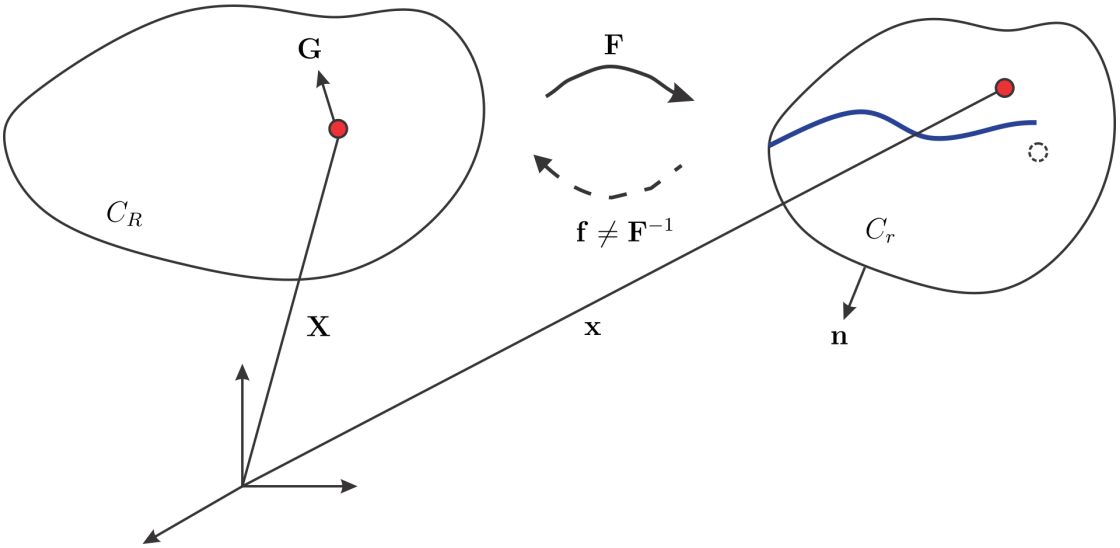

Figure 2.11.: If cracks occur, the deformation $\mathbf{f}$ and the inverse of the original deformation $\mathbf{F}^{-1}$ are not equal. Configurational force describes the phenomena associated with the material itself (red point).

To describe such irreversible changes of the material, a new perspective based on the material manifold but not the spatial coordinates is required, which must provide a unified and elegant framework for the analysis of various kinds of material imperfections. The concepts of the *J-Integral* and the *configurational force* are born from this reason. The J-Integral was first introduced by Rice [83], which is widely used especially in nonlinear fracture mechanics. The J-integral gives the strain energy release rate associated with crack growth, and it can be seen as a measure of the intensity of deformation around the crack tip.

Let ψ be the strain energy density of a homogeneous, elastic body. The material is assumed to be arbitrarily nonlinear and anisotropic. Without volume forces, the J-Integral vector is defined as

$$\boldsymbol{\mathcal{J}} = \int_{\partial V} \boldsymbol{\Sigma} \mathbf{n} \mathrm{d}A, \tag{2.51}$$

where ∂V is a closed surface that includes the crack tip, and $\mathbf{n}$ is the outward unit normal vector. The quantity

$$\boldsymbol{\Sigma} = \psi \mathbf{I} - \left(\nabla \mathbf{u}\right)^{\mathrm{T}} \boldsymbol{\sigma} \tag{2.52}$$

is called *Eshelby*'s stress tensor and the tensor $\mathbf{I}$ is the identity tensor. The Eshelby's stress tensor is an energy-momentum tensor, which captures the local structural rearrangement, for example, the cracking of the body. One of the favorable advantages of using Eshelby's stress tensor is that its divergence vanishes $\mathrm{div}\boldsymbol{\Sigma} = 0$ if no cracks or defects are contained in the domain V [42].

2.5. Introduction to phase field model

The phase field method is originally used to solve interfacial problems, like ferromagnetism [102, 109, 31], ferroelectrics [76, 1, 89], solidification dynamics [67, 103], phase transitions [104, 81] etc. In general, the phase field method employs a continuous field order parameter with a smooth transition to model a discrete interface between multiple physical phases. As speaking of fracture mechanics, this order parameter describes the smooth transition between fully broken and intact material. Phase field fracture models can be derived from the Landau-Ginzburg phase transition [38] or can be seen as an extension of Griffith's fracture theory [7]. In the first interpretation, the phase field model [12, 55, 48] does not diffuse the crack with the idea of a length scale parameter; additionally, the fracture energy is not included in the free energy. The second type of phase field fracture model, despite its similarity to the Landau-Ginzburg phase transition explicitly, introduces a length scale parameter to regularize a fracture surface energy. In this section, we follow the path of Griffith's theory to introduce a phase field model for cyclic fatigue.

2.5.1. Griffith's energy approach

The root of the phase field model for fracture can be found back in the Griffith theory [41]. In the year of 1921, A. A. Griffith (1893-1963) advanced the work of Inglis [51], who first

studied the fracture in glass and determined the stresses around a hole in a plate. Griffith proposed an energy-balance approach to predict the fracture process. The Griffith energy criterion states the following: Let $\mathrm{d}A$ be an infinitesimal surface increment during crack propagation, the infinitesimal *fracture surface energy* $\mathrm{d}\Gamma$ is assumed proportional to the size of the crack

$$\mathrm{d}\Gamma = \mathcal{G}_c \mathrm{d}A \tag{2.53}$$

with the parameter $\mathcal{G}_c$ as the *critical energy release rate*. The energy release rate is defined as the change of the internal energy

$$\mathcal{G} = -\frac{\mathrm{d}\Pi}{\mathrm{d}A}, \tag{2.54}$$

where Π denotes the total potential of the body. Furthermore, let $\mathcal{E}$ be the internal energy and $\mathcal{W}$ be the work of external forces, the complete energy balance reads

$$\dot{\Gamma} + \dot{\mathcal{E}} = \dot{\mathcal{W}}. \tag{2.55}$$

Eq. (2.55) correlates to the first principle of thermodynamics, and takes into account the fracture surface energy Γ representing the energy to separate the material and causing fractures. Assuming the external forces are conservative and related to a potential Π^e, Eq. (2.55) can be rewritten as in the perspective of energy

$$\frac{\mathrm{d}\Gamma}{\mathrm{d}t} + \underbrace{\frac{\mathrm{d}\Pi^i}{\mathrm{d}t} + \frac{\mathrm{d}\Pi^e}{\mathrm{d}t}}_{\frac{\mathrm{d}\Pi}{\mathrm{d}t}} = 0 \quad \text{with} \quad \mathcal{E} = \frac{\mathrm{d}\Pi^i}{\mathrm{d}t} \text{ and } \mathcal{W} = -\frac{\mathrm{d}\Pi^e}{\mathrm{d}t}, \tag{2.56}$$

where Π^i is the strain energy density. Considering an infinitesimal crack increment $\mathrm{d}A$, Eq. (2.56) leads to Griffith's theory

$$\frac{\mathrm{d}\Gamma}{\mathrm{d}t} + \frac{\mathrm{d}\Pi}{\mathrm{d}t} = \left(\frac{\mathrm{d}\Gamma}{\mathrm{d}A} + \frac{\mathrm{d}\Pi}{\mathrm{d}A}\right)\frac{\mathrm{d}A}{\mathrm{d}t} = 0 \tag{2.57}$$

$$\rightarrow \frac{\mathrm{d}\Gamma}{\mathrm{d}A} + \frac{\mathrm{d}\Pi}{\mathrm{d}A} = 0. \tag{2.58}$$

With Eq. (2.53) and Eq. (2.54), Griffith's theory states that there is a balance of the release of the internal energy and the increase of the surface energy during crack extension, i.e.,

$$\mathcal{G} = \mathcal{G}_c. \tag{2.59}$$

For straight growing cracks, the relation of the K-concept and the energy release rate is given as

$$\mathcal{G} = \frac{K_I^2 + K_{II}^2}{E'} + \frac{K_{III}^2}{2G} \tag{2.60}$$

with

$$E' = \begin{cases} E & \text{plane stress} \\ \dfrac{E}{1-\nu} & \text{plane strain or 3D cases.} \end{cases} \tag{2.61}$$

2.5.2. A variational model of quasistatic crack

In general, Griffith's energetic fracture criterion has three shortcomings:

- it is not able to predict the nucleation of a new crack
- it is not able to predict the crack propagation path
- it is not able to model complicated patterns like kinking and branching of cracks.

Along the path of the Griffith theory, Francfort and Marigo introduced a *variational formulation*[36] of brittle fracture to address the difficulties encountered in the original Griffith criterion. In order to free itself of the constraints of the Griffith criterion, the variational formulation creates a unified framework for the crack evolution behavior, where the crack nucleation, propagation, branching, and kinking are included. The basic idea of the fracture criterion for the variational formulation is to minimize the total energy of an elastic body.

Let $\mathcal{S}(t)$ be a crack set, which is the discontinuity set of the displacement $\mathbf{u}$ at time t. Assuming that there is no crack healing, thus, the crack set $\mathcal{S}$ must contain all its predecessors

$$\mathcal{S}(\tau) \subset \mathcal{S}(t) \quad \text{for all} \quad \tau < t. \tag{2.62}$$

In the variational formulation of brittle fracture, the crack set $\mathcal{S}$ is allowed to grow discontinuously; particularly, the cracks are allowed to nucleate from undamaged material. The possible crack sets are considered as all closed subdomains of the elastic body and its boundary $\hat{\Omega} = \Omega \cap \partial\Omega$ with the dimensions not greater than $n-1$[1], where n denotes the

[1] In this work, we only consider the dimension of the subdomains is $n-1$.

dimension of the elastic body. Following the idea of Griffith, the fracture surface energy Γ of a crack set $\mathcal{S}$ is proportional to the crack area

$$\Gamma(\mathcal{S}) = \mathcal{G}_c \mathcal{H}^{n-1}(\mathcal{S}), \tag{2.63}$$

where $\mathcal{H}$ is the $n-1$ dimensional Hausdorff measure, which is a general measure for hypersurfaces and here to be understood as a "surface" measure of the crack surface. The strain energy associated with the body is given as

$$\mathcal{E}^e(\mathcal{S}, \mathbf{u}) = \int_{\Omega/\mathcal{S}} \frac{1}{2} \boldsymbol{\varepsilon}(\mathbf{u}) : (\mathbb{C} : \boldsymbol{\varepsilon}(\mathbf{u})) \mathrm{d}V. \tag{2.64}$$

Furthermore, the not debonded parts of the boundary are considered to be subject only to Dirichlet boundary conditions

$$\mathbf{u}(\mathbf{x}, t) = \mathbf{u}^* \quad \text{on} \quad \partial\Omega_u / \mathcal{S}(t), \tag{2.65}$$

and Neumann boundary conditions as well as the volume forces are not covered in the original work. Figure (2.12) illustrates the crack set $\mathcal{S}$ in the variational formulation of brittle fracture, where Ω denotes the elastic body and $\partial\Omega$ is its boundary.

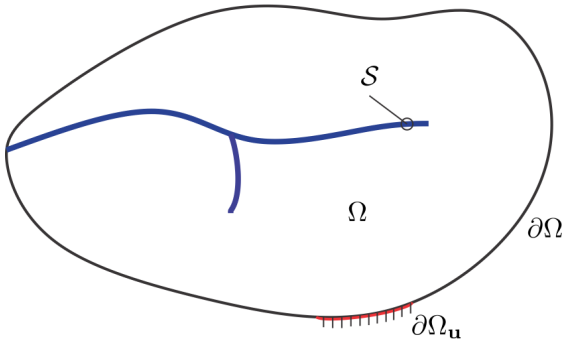

Figure 2.12.: The crack set $\mathcal{S}$ of the variational formulation of brittle fracture.

It is postulated that for at any time t, among all cracks sets $\mathcal{S}$ obeying Eq. (2.62) and all displacement fields $\mathbf{u}$ obeying Eq. (2.65), the pair $(\mathcal{S}, \mathbf{u})$ minimizes the total energy

$$\mathcal{E}(\mathcal{S}, \mathbf{u}) = \mathcal{E}^e(\mathcal{S}, \mathbf{u}) + \Gamma(\mathcal{S}). \tag{2.66}$$

This criterion enforces a global energy minimization, in which Griffith's formulation can be seen as a first-order necessary condition for a local minimum of the total energy [37].

2.5.3. A regularized approximation of the energy functional

The variational formulation is a powerful tool to describe the fracture phenomena in a unified framework, however, a suitable numerical implementation is nevertheless required to handle more general and complex situations. Solving the variational fracture problem allows an infinite number of arbitrary evolution of crack sets to be taken into consideration, which is numerically unfeasible without prior knowledge of the crack path. The introduction of regularization formulation shall be retrieved back to the model from Mumford and Shah [75] for the image segmentation process. Their algorithm to segment images can be seen as the minimization problem: find a pair (K, ϕ) to minimize

$$\mathcal{F} = \int_{\Omega/K} |\nabla\phi|^2 \mathrm{d}x + k\mathcal{H}^1(K) + \int_{\Omega} |\phi - g|^2 \mathrm{d}x, \tag{2.67}$$

where Ω is the domain of the entire image, the parameter K is compact of the domain Ω representing the contours of the image, the parameter ϕ is an element of Ω/K representing the pixel intensity of each point of the picture in real world, and the parameter g is the pixel intensity to be measured. Later, Ambrosio and Tortorelli [8] used an elliptic functional defined on Soblev spaces to approximate the Mumford-Shah image segmentation functional

$$\mathcal{F}_{\mathrm{AT}} = \int_{\Omega/K} \left[(|\nabla\phi|^2 + |\nabla z|^2)(1 - z^2)^{2h} + \frac{1}{4}(\alpha^2 h^2) z^2 \right] \mathrm{d}x + \beta \int_{\Omega} |\phi - g|^2 \mathrm{d}x, \tag{2.68}$$

where the variable z controls the gradient of ϕ and α, $\beta > 0$ are fixed parameters. This approximation of the Mumford-Shah functional takes place as the parameter $h \to \infty$, meaning the Ambrosio-Tortorelli approximation $\mathcal{F}_{\mathrm{AT}}$ is equivalent to the Mumford-Shah functional $\mathcal{F}$ when the parameter h nears infinite.

Inspired by this equivalence, Bourdin et al. [22, 21] introduce an additional scalar field $s(\mathbf{x}, t)$ to indicate the cracks, which is a regularized version of the variational formulation amenable to numerical implementation. This secondary scalar field s, called *crack field parameter*, interpolates continuously from a broken state ($s = 0$) to an undamaged state ($s = 1$) of the material shown in Fig. 2.13.

The regularized approximation of the total energy functional for linear elastic material reads

$$\mathcal{E}(s, \boldsymbol{\varepsilon}(\mathbf{u})) = \int_{\Omega} \left[(s^2 + \eta)\psi^e(\boldsymbol{\varepsilon}(\mathbf{u})) + \mathcal{G}_c \left(\frac{(1-s)^2}{4\epsilon} + \epsilon |\nabla s|^2 \right) \right]. \tag{2.69}$$

The parameter ϵ is the length parameter controlling the width of the transition zone of s, and the small parameter η is used to avoid numerical difficulties when the material is

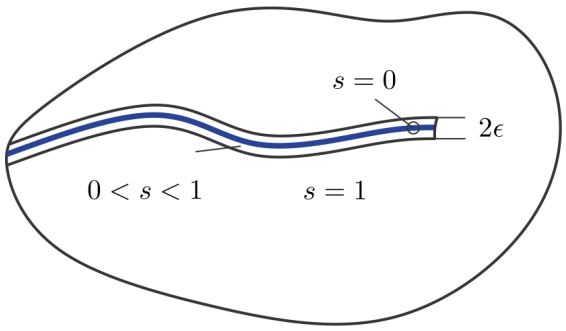

Figure 2.13.: The main attribute of this regularized variational formulation is to introduce an additional scalar field to present the cracks.

totally broken ($s = 0$). The functional ψ^e is the strain energy density. The main advantage of this regularization version is that the cracks are no longer mesh or geometry-dependent. It is noted that Eq. (2.69) approximates Eq. (2.66) in the sense of Γ-convergence. The Γ-convergence describes the convergence of functionals, ensuring that minimizers of approximating functionals converge to minimizers of a target functional in variational problems. Therefore, it creates a link between the regularized and free-discontinuous fracture energy. Furthermore, this regularized version gives birth to the so-called fracture phase field models, building a simple path to model fracture phenomenon.

2.5.4. A phase field model for brittle fracture

Although the Bourdin's regularization of the variational formulation of brittle fracture resembles the phase field model, the evolution law for the crack field parameter s is still missing. Kuhn and Müller [58] used the framework of Gurtin [45] on a thermodynamics consistent based model, in which the minimization problem Eq. (2.69) leads to a coupled Euler-Lagrange equation system

$$\mathrm{div}\boldsymbol{\sigma} = 0 \tag{2.70}$$

and

$$\dot{s} = -M\left[2s\psi^e - \mathcal{G}_s\left(2\epsilon\Delta s + \frac{1-s}{2\epsilon}\right)\right]. \tag{2.71}$$

Eq. (2.70) describes the equilibrium of the stress field

$$\boldsymbol{\sigma} = (s^2 + \eta)\frac{\partial\psi^e}{\partial\nabla\mathbf{u}}, \tag{2.72}$$

and Eq. (2.71) is a Ginzburg-Laudau type evolution equation of the crack field. The parameter $M > 0$ is a mobility parameter, which models the "viscosity"(rate dependency) of the phase field fracture model. The limit case $M \to \infty$ approximates the quasi-static case

$$0 = 2s\psi^e - \mathcal{G}_s\left(2\epsilon\Delta s + \frac{1-s}{2\epsilon}\right). \tag{2.73}$$

Along this path, the Kuhn and Müller's model has been extended to dynamic fracture [88], ductile fracture [59] and fatigue fracture [91, 92]. Additionally, some selected other phase field fracture models are summarized in Tab. 2.5.4. Due to the large amount of literature, this table is not meant to be complete.

2.5.5. Extension of the phase field model for cyclic fatigue

Kuhn and Müller's model establishes a powerful framework for fracture simulation; however, this formulation considered only elastic energy and surface energy, which is not suitable for a fatigue fracture simulation. The required cyclic load amplitude to induce fatigue fracture is typically much lower than in other fracture simulation cases; thus, it is not effective to minimize the total energy. Additionally, the continuous loading and unloading process consumes also much energy because of the irreversible fatigue processes as shown in [74] and this is not included in the Kuhn and Müller's model.

Based on that, Schreiber et al. [91, 92] introduced a phase field model for cyclic fatigue by incorporating an additional energy contribution

$$\mathcal{E} = \mathcal{E}^e + \Gamma + \mathcal{P}. \tag{2.74}$$

Besides the elastic energy $\mathcal{E}^e$ and fracture surface energy Γ from [58], the additional energy term $\mathcal{P}$ stands for an additional free energy term representing the sum of additional driving forces caused by fatigue damage

$$\mathcal{P} = \int_\Omega h(s)\psi^{\mathrm{ad}}(D)\mathrm{d}V = \int_\Omega h(s)q < D - D_c >^b \mathrm{d}V, \tag{2.75}$$

where $h(s)$ is a degradation function and the function ψ^{ad} is an additional fatigue energy density. The parameter D is introduced to represent the accumulated fatigue damage

$$D = D_0 + \mathrm{d}D, \tag{2.76}$$

Fracture types	Literature
Quasi-static fracture	Kuhn and Müller model [58] Aranson-Kalatsky-Vinokur model [12] Amor, Marigo, Maurini model [10] Miehe et al. model [72, 70] Borden et al. model [19]
Dynamic fracture	Karma-Kessler-Levine model [55] Henry and Levine model [48] Larsen-Ortner-Süli model [61] Borden et al. model [23, 20] Hofacker and Miehe model [49, 50]
Ductile fracture	Miehe et al. model [69, 71] Ambati and de Lorenzis model [6] Borden et al. model [18] Shanthraj et al. model [97] Alessi et al. model [3] Dittmann et al. model [30] Tsakmakis et al. model [99]
Hydraulic fracture	Lee et al. model [62] Zhou et al. model [111]
Anisotropic fracture	Nguyen et al. [78] Li et al. model [63] Bryant and Sun model [24]
Fatigue fracture	Carrara et al. model [26] Mesgarnejad et al. model [68] Seiler et al. model [94] Alessi et al. model [5] Lo et al. model [64]

Table 2.1.: Summary of different phase field fracture models.

where D_0 denotes the previous damage, and $\mathrm{d}D = \frac{\mathrm{d}N}{n_D}\left(\frac{\hat{\sigma}}{A_D}\right)^k$ denotes the damage increment. The fatigue parameters A_D, k and n_D can be obtained from the S-N curve. In the presented work, the fatigue driving force $\hat{\sigma}$ is considered as the first principle stress σ_1. The parameter D_c is a threshold, together with Macaulay brackets $<>$, models fatigue crack nucleation, and the parameters q and b control how fast the fatigue energy grows in the crack propagation.

It has been shown [91, 92, 90], that the introduced phase field model can capture the key fatigue properties such as Paris' law, the mean stress effect, and the loading sequence effect. However, it remains inapplicable to complex engineering problems, as further modifications are still necessary. This thesis aims to advance the phase field model proposed by Schreiber, which will be presented in Chapters I, II, and III in detail. In Chapter I, an adaptive cycle number adjustment algorithm is proposed, in which the cycle increment in each simulation step is adaptively chosen based on the damage increment

$$\mathrm{d}N = n_D\left(\frac{\hat{\sigma}}{A_D}\right)^{-k}\mathrm{d}D. \tag{2.77}$$

Results show that using the adaptive cycle simulation schema can dramatically reduce computing time compared to classical simulation methods. In Chapter II, the phase field fatigue model is extended to thermomechanical fatigue, where the thermal stress is considered as a second fatigue driving force in the crack evolution. Here, thermal strain $\boldsymbol{\epsilon}_T$ is introduced into the stain energy density

$$\psi^e = \frac{1}{2}(\boldsymbol{\epsilon} - \boldsymbol{\epsilon}_T) : \mathbb{C} : (\boldsymbol{\epsilon} - \boldsymbol{\epsilon}_T), \tag{2.78}$$

such that the driving force consists of both a mechanical stress part and a thermal stress part. The overall conclusion is that thermal stress is primarily responsible for fatigue crack nucleation, while mechanical stress drives crack extension. In Chapter III, the concept of configurational forces is used as a powerful tool to examine the energetic forces during crack propagation. A configurational force balance is derived

$$\nabla \cdot \boldsymbol{\Sigma} + \mathbf{g} = \mathbf{0}, \tag{2.79}$$

where the generalized Eshelby stress tensor $\boldsymbol{\Sigma}$ captures the local changes such as the fatigue fracturing, and the generalized configurational force $\mathbf{g}$ is the energetic force which leads the crack propagation.

I. First paper

Published in:
International Journal of Fracture, 237(1), p. 47–60 (2022).
DOI: https://doi.org/10.1007/s10704-022-00628-0

I.1. Objectives of the first paper

Despite the well-established phase field fatigue model in Sec. 2.5.5, it suffers from the huge computational effort since the fatigue cracks usually happen after a large number of cycles, especially in a high-cycle domain. Schreiber et al. [91] presents a time-cycle transfer to resolve the number of similar cycles per time into the block. However, the question of how to choose the size of the block is still open. If the block size is chosen too small, the simulation will take a very long time, and it is not realistic to apply the model to problems raised in the industry; in contrast, if the block size is chosen too large, the fatigue energy will grow impulsively, and the crack pattern will be thus irregular and unstable.

The paper aims to present an adaptive cycle number adjustment algorithm, which keeps the computation time in a reasonable number without losing accuracy. The key idea is to divide the entire fatigue fracture simulation into three stages and apply different cycle number increments which are associated with the damage increments for each damage stage. Three numerical examples highlight this solution strategy and validate the results against experimental results and previous works.

Int J Fract
https://doi.org/10.1007/s10704-022-00628-0

ORIGINAL PAPER

An efficient implementation of a phase field model for fatigue crack growth

Sikang Yan · **Christoph Schreiber** · **Ralf Müller**

Received: 19 August 2021 / Accepted: 16 March 2022

Abstract Recently, phase field modeling of fatigue fracture has gained a lot of attention from many researches and studies, since the fatigue damage of structures is a crucial issue in mechanical design. Differing from traditional phase field fracture models, our approach considers not only the elastic strain energy and crack surface energy, additionally, we introduce a fatigue energy contribution into the regularized energy density function caused by cyclic load. Comparing to other type of fracture phenomenon, fatigue damage occurs only after a large number of load cycles. It requires a large computing effort in a computer simulation. Furthermore, the choice of the cycle number increment is usually determined by a compromise between simulation time and accuracy. In this work, we propose an efficient phase field method for cyclic fatigue propagation that only requires moderate computational cost without sacrificing accuracy. We divide the entire fatigue fracture simulation into three stages and apply different cycle number increments in each damage stage. The basic concept of the algorithm is to associate the cycle number increment with the damage increment of each simulation iteration. Numerical examples show that our method can effectively predict the phenomenon of fatigue crack growth and reproduce fracture patterns.

S. Yan ( ) · C. Schreiber · R. Müller
Institute of Applied Mechanics, Technische Universität Kaiserslautern, Gottlieb-Daimler-Straße, 67653 Kaiserslautern, Germany
e-mail: yan@rhrk.uni-kl.de

Keywords Phase field modeling · Fatigue fracture · Computing efficient · FEniCS

1 Introduction

In the last decade, the phase field method was developed to simulate fracture processes (Francfort and Marigo 1998; Bourdin et al. 2000; Bourdin 2007). The core idea of the phase field model is to represent a discrete discontinuous phenomenon by a smooth function. The biggest advantage of phase field modeling is its unified framework, in which the entire fracture evolution (nucleation, propagation, branching, kinking) is covered. Griffith (1921) initially proposes the idea of using an energetic criterion to predict the onset of crack propagation. Later, Francfort and Marigo (1998) generalize the classical Griffith theory by a variational formulation of brittle fracture, but it is nevertheless numerically difficult. A regularized approximation of the model is presented by Bourdin (Bourdin 2007; Bourdin et al. 2008), which is more suitable for numerical implementation. This regularized version gives birth to the so-called fracture phase field models, building a simple path to model fracture phenomenon. The phase field method has been successfully established for quasi-static fracture (Kuhn and Müller 2010; Miehe et al. 2010; Borden et al. 2014), dynamic brittle fracture (Schlüter et al. 2014), ductile fracture (Ambati et al. 2015; Kuhn et al. 2016), hydraulic fracture (Wilson and Landis 2016; Yoshioka and Bourdin 2016) so far. However, the real

Published online: 06 April 2022

manufacturing processes usually involve oscillating loads, which usually do not lead to an immediate failure, but rather a failure caused by fatigue crack growth after numerous loading cycles. In this spirit, a phase field model that can handle complex cyclic fatigue process is required.

Some research contributions are given to find phase field models for the fatigue fracture process. On the one hand, Boldrini et al. (2016) proposed a phase field model to describe the fracture behavior coupling thermal and fatigue problems, where fatigue behavior is related to an additional scalar variable. On the other hand, fatigue fracture can be modeled by adopting the Ginzburg-Landau formalism (Gurtin 1996): In Caputo and Fabrizio (2015) and Amendola et al. (2016), the fatigue damage evolution is derived by incorporating a fatigue potential to degrade the material under cyclic loading. However, those methods fail to reproduce the important known feature of fatigue behavior like the Paris' law, the Wöhler curve with the transition between low- and high-cyclic fatigue, and the Palmgren-Miner law. Recently, (Alessi et al. 2018; Carrara et al. 2020; Seiler et al. 2020; Seleš et al. 2021; Hasan and Baxevanis 2021) advance the fatigue phase field model by taking both degradation of stiffness and reduction of fracture energy in the fatigue damage evolution, where the major feature of fatigue behavior can be recovered into account. Differing from the above approaches, Schreiber et al. (2020a, b) extend the model from Kuhn and Müller (2010), where an additional energy density contribution is proposed as an additional driving forces caused by the increasing number of load cycles. In Schreiber et al. (2020a, b), a realistic fatigue crack growth behavior, including the mean stress effects and different stress ratios, can be predicted.

In phase field simulation of fatigue fracture, huge computational effort is usually required before crack nucleation or propagation can be observed on a macroscopic level. As an efficient scheme, the computing time must be kept below a reasonable limit with respect to a large number of load cycles. In this work, we provide an efficient adaptive cycle number adjustment algorithm based on the work of Schreiber et al. (2020a, b). The platform FEniCS (Alnæs et al. 2015) is used for the implementation.

2 Phase field modeling for cyclic fatigue cracks

2.1 Phase field modeling

A phase field fracture model introduces an additional field variable to represent cracks. In the phase field model from Kuhn and Müller (2010), the crack field s is 1 if the material remains undamaged and is 0 where cracks occur. Furthermore, it is to postulate that the displacement field $\mathbf{u}$ and crack field s locally minimize the total energy of a loaded body Ω. The total energy E is given as

$$E = \int_{\Omega} \frac{1}{2}\Big((s^2+\eta)\boldsymbol{\varepsilon} : [\mathbb{C}\boldsymbol{\varepsilon}]\Big)\mathrm{d}V + \int_{\Omega} \mathcal{G}_c\left(\frac{(1-s)^2}{4\epsilon} + \epsilon|\nabla s|^2\right)\mathrm{d}V \tag{1}$$

with the infinitesimal strain tensor $\boldsymbol{\varepsilon} = \frac{1}{2}(\nabla\mathbf{u} + \nabla^T\mathbf{u})$ and stiffness tensor $\mathbb{C}$. The dimensionless parameter η is used to avoid numerical difficulties, and $\mathcal{G}_c$ is the cracking resistance. The parameter ϵ controls the width of the transition zone between the broken and undamaged material. Figure 1 shows the influence of ϵ to the crack width. The internal length parameter ϵ is taken

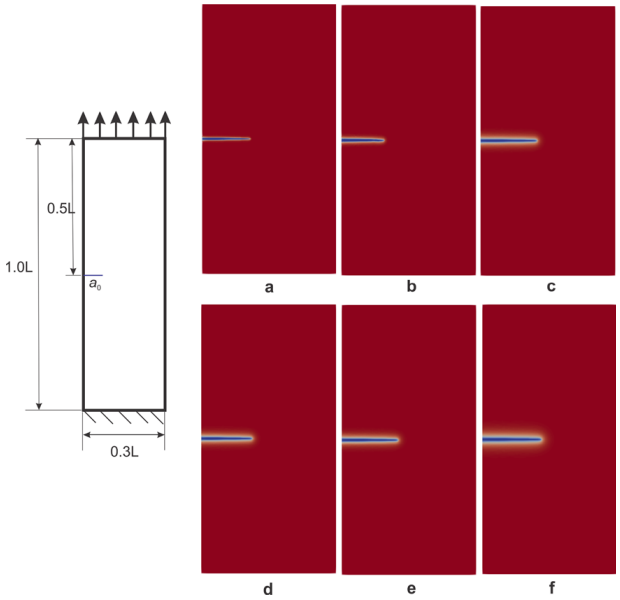

Fig. 1 A quadratic geometry is loaded at the top of the surface and the pre-defined crack a_0 is with length of $0.05L$. The model parameter ε controls the width of the transition zone (**a**: $\epsilon = 0.001$; **b**: $\epsilon = 0.002$; **c**: $\epsilon = 0.003$; **d**: $\epsilon = 0.004$; **e**: $\epsilon = 0.005$ **f**: $\epsilon = 0.006$)

as four times the mesh size in order to solve the phase field governing equation in the presented examples of this work.

In a classical phase field fracture mode, e.g. Kuhn and Müller (2010), only the elastic energy and the fracture surface energy is considered in the total free energy. The crack will propagate in such a way that the total energy is minimized. However, this is not suitable in a fatigue fracture simulation. The cyclic loading involved in the fatigue simulation is much lower than the other fracture simulation cases, thus, with this load it is not effective to minimize the total energy. Additionally, the continuous loading and unloading process consumes also much energy as shown in Mughrabi (2015) and this is not included in the Kuhn and Müller's model. Different from the work proposed in (Alessi et al. 2018; Carrara et al. 2020; Hasan and Baxevanis 2021), where a fatigue degradation function related to a history variable is applied directly on the fracture energy term and the fracture toughness of the material is reduced during the fatigue process, we keep the surface energy term untouched and extend the phase field model from Kuhn and Müller (2010) by an additional term for cyclic fatigue. The total energy now reads

$$\begin{aligned} E(\boldsymbol{\varepsilon}, s, \nabla s) &= \int_{\Omega} \psi(\boldsymbol{\varepsilon}, s, \nabla s) \mathrm{d}V \\ &= \int_{\Omega} \frac{1}{2}\Big((s^2+\eta)\boldsymbol{\varepsilon} : [\mathbb{C}\boldsymbol{\varepsilon}]\Big)\mathrm{d}V + \\ &\quad \int_{\Omega} \mathcal{G}_c\left(\frac{(1-s)^2}{4\epsilon} + \epsilon|\nabla s|^2\right)\mathrm{d}V + \\ &\quad \int_{\Omega} \psi^{ac}\mathrm{d}V, \end{aligned} \tag{2}$$

Among them, ψ is the total energy density, and ψ^{ac} is the energy density, standing for the sum of additional driving forces caused by fatigue damage. The energy density for fatigue crack ψ^{ac} is given as (Schreiber et al. 2020b)

$$\begin{aligned} \psi^{ac} &= h(s) q \Big\langle D - D_c \Big\rangle^b \\ &= h(s) q \left\langle D_0 + \frac{\mathrm{d}N}{n_D}\left(\frac{\hat{\sigma}(1-L)}{f(L)}\right)^k - D_c \right\rangle^b, \end{aligned} \tag{3}$$

which is related to a new introduced parameter D, representing the damage related to fatigue.

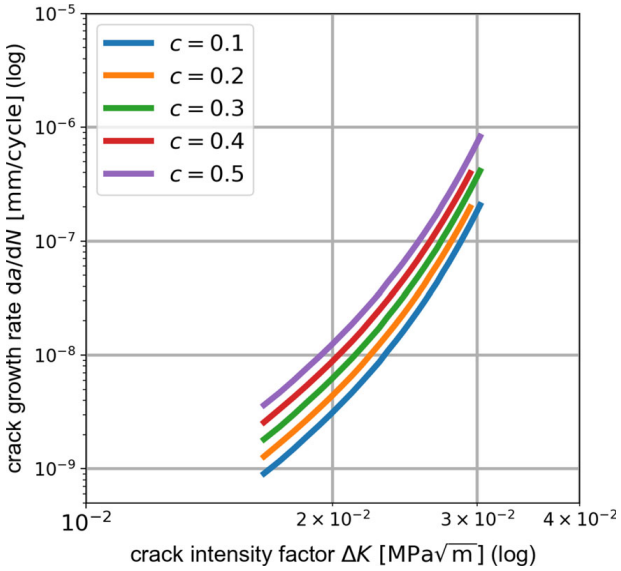

Fig. 2 A higher number of c increases the crack growth rate

The function $f(L) = A_D(1-L)^c$ is a threshold, where L is the ratio of the mean external load and the maximum external load; and the parameter c is a constant. In general, the function $f(L)$ can be chosen arbitrarily as long as it captures the mean stress effect of a specific material. Fig. 2 shows the influence of the parameter c on the crack growth rate by unidirectional cyclic load, where a higher value of c increases mean stress effect. The increments with load amplitude below this threshold is not taken into damage accumulation. The term $\hat{\sigma}(\boldsymbol{\varepsilon})$ is the driving force, corresponding to the first principal stress of the stress tensor $\boldsymbol{\sigma} = \mathbb{C}\boldsymbol{\varepsilon}$ in this case, of which we only consider positive entries and negative entries are neglected. However, it is not claimed that this choice of driving force is generally valid for all materials with complex properties or effects. Other effective stress quantities, as e.g. the von-Mises stress, might be more suitable in different cases. The parameters A_D, k and n_D can be obtained from the S-N curve (see Fig. 3). Here, the mathematical model of the phase field is coupled with the fatigue parameters from experiments, which allows for a general and elegant incorporation of influences, like the temperature effect or ambient environment into the fatigue propagation behavior. Furthermore, D_0 is the previous state of fatigue damage; D_c is a threshold to determine the critical fatigue damage stage. The idea, to use a damage parameter D, is inspired by Miner's rule from Miner (1945). Miner's rule describes the mechanism of damage accumulation until macro crack initiation. The con-

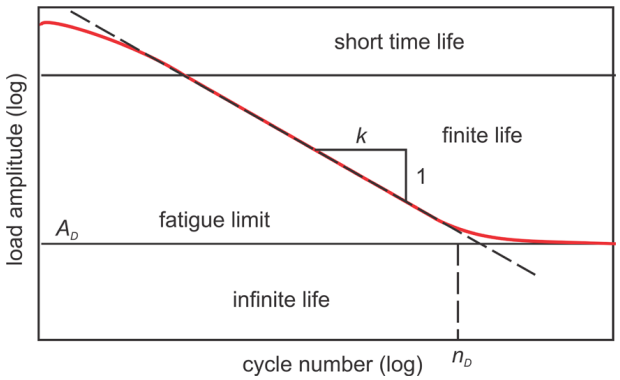

Fig. 3 A simplified explanation of S-N curve

nection between Paris' law and Miner's rule is shown in Ciavarella et al. (2018). Thus, we define the damage parameters in cooperation with fatigue parameters from the S-N curve. The regularization parameters q and b determine the speed of fatigue damage energy growth, which should be chosen appropriately to ensure a stable energy growth speed. Figure 4 shows the influence of different parameter settings on the crack length and crack growth rate. It is to notice that the parameters q and b are merely numerical parameters, which are only used to construct the fatigue energy term from the damage parameter D. The crack growth rate is mostly determined by the fatigue parameters from the S-N curve with the help of experiments, as shown in Fig. 5

The degradation function $h(s) = s^2$ models the loss of stiffness in broken material caused by cyclic fatigue. This choice of degradation function is for the sake of simplicity. For a comprehensive overview of the model parameters, we provide a summary in Table 1.

With the Macauley brackets, which is defined by

$$\langle x \rangle^n = \begin{cases} 0 & \text{if } x \leq 0 \\ x^n & \text{if } x > 0, \end{cases} \tag{4}$$

the fatigue crack will only occur after the damage D reaches the threshold D_c. After that, the fatigue energy grows rapidly controlled by parameters q and b; and it eventually decreases again due to the degradation function.

The fatigue damage D is updated for every simulation iteration

$$D_{n+1} = D_n + \mathrm{d}D_n \tag{5}$$

with

$$\mathrm{d}D_n = \frac{\mathrm{d}N}{n_D} \left(\frac{\hat{\sigma}_n (1 - L)}{f(L)} \right)^k. \tag{6}$$

With the help of variational principle, Eq. (2) yields the equilibrium of the displacement field $\mathbf{u}$ and the evolution of the crack field s.

2.2 Paris' law

The crack growth behavior is the main focus of the present investigation. The growth behavior of a macro crack can be described by Paris' law (Paris and Erdogan 1963). The Paris' law describes the fatigue crack growth rate in relation to the stress intensity factor range, it reads

$$\frac{\mathrm{d}a}{\mathrm{d}N} = C(\Delta K)^m, \tag{7}$$

where C and m are material dependent parameters. The stress intensity factor K (Irwin 1997) is an intensity parameter, which describes the stress singularity near the tip of a crack. It is determined by the specimen geometry, the size and location of the crack, the magnitude and the distribution of loads applied on the material. The crack growth rate is discretized as

$$\left(\frac{\mathrm{d}a}{\mathrm{d}N} \right)_p \approx \frac{a_p - a_{p-1}}{N_p - N_{p-1}}, \tag{8}$$

where a_p and N_p denote the crack length and cycle number from the p-th data point. According to Paris' law, the crack growth rate has a linear behavior with scope m in a diagram with logarithmic scales (see Fig 6).

3 FEniCS implementation of the phase field fatigue fracture model

3.1 Simulation settings

Let $\boldsymbol{t}^*$ be the external traction on the part $\partial\Omega_{\boldsymbol{t}}$ of the boundary of the domain Ω. The variational formulation of our problem reads

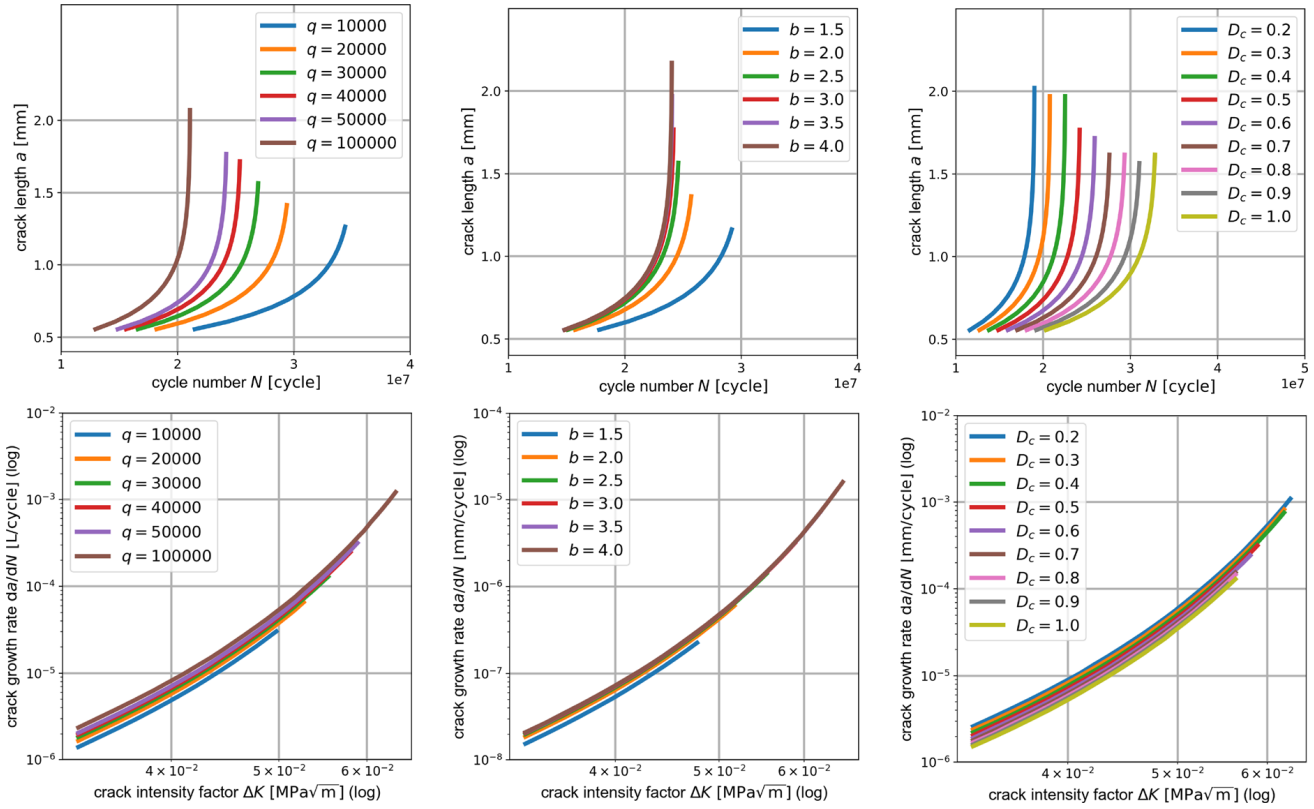

Fig. 4 The influence of the model parameters q, b and D_c on the crack length and crack growth rate

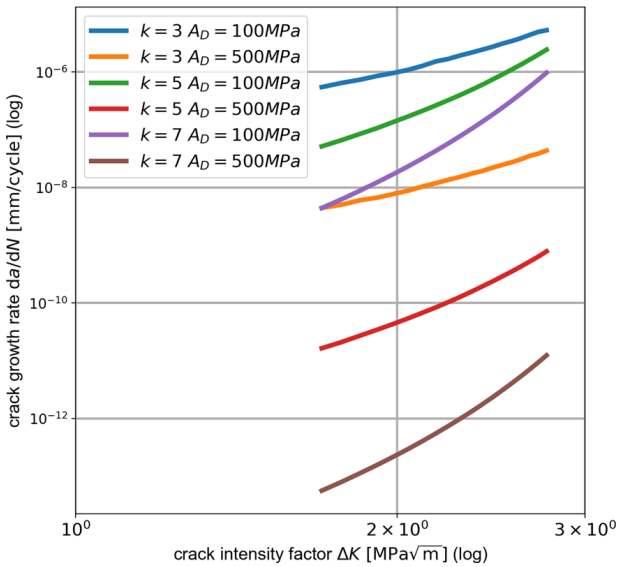

Fig. 5 The influence of the fatigue parameters on the crack growth rate

Table 1 Model parameters

Symbol	Meaning	Function
s	Crack field	Crack state
$\boldsymbol{\varepsilon}$	Infinitesimal strain tensor	
$\mathbb{C}$	Stiffness tensor	Material property
$\mathcal{G}_c$	Critical energy release rate	Fracture resistance
ϵ	Internal length	Control crack width
η	Residual stiffness parameter	Numerical stability
k	Lifetime exponent	Fatigue property
n_D	Knee point cycle number	Fatigue property
A_D	Threshold stress	Fatigue property
D_0	Current fatigue damage	History variable
D_c	Fatigue damage threshold	Critical damage state
q	Regularization parameter	Fatigue energy growth
b	Regularization parameter	Fatigue energy growth
c	Mean stress parameter	Mean stress effect

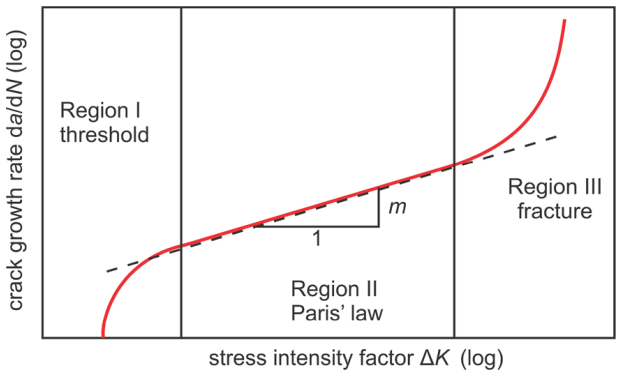

Fig. 6 The crack growth rate has a linear behavior in a diagram with logarithmic scales

$$\int_{\Omega} \delta E \, \mathrm{d}V + \int_{\partial\Omega_t} \boldsymbol{t}^* \cdot \delta\mathbf{u} \, \mathrm{d}A = 0. \tag{9}$$

Computing the variation of total energy E with regard to displacement field $\mathbf{u}$ and fracture field s yields

$$\delta E = \int_{\Omega} \left(\frac{\partial \psi}{\partial \boldsymbol{\varepsilon}} : \delta\boldsymbol{\varepsilon} + \frac{\partial \psi}{\partial s}\delta s + \frac{\partial \psi}{\partial \nabla s} \cdot \delta\nabla s \right) \mathrm{d}V. \tag{10}$$

Employing the product rule

$$\frac{\partial \psi}{\partial \boldsymbol{\varepsilon}} : \delta\boldsymbol{\varepsilon} = -\mathrm{div}\left(\frac{\partial \psi}{\partial \nabla \mathbf{u}} \right) \delta\mathbf{u} + \mathrm{div}\left(\left(\frac{\partial \psi}{\partial \nabla \mathbf{u}} \right)^T \delta\mathbf{u} \right) \tag{11}$$

and

$$\frac{\partial \psi}{\partial \nabla s} \cdot \delta\nabla s = -\mathrm{div}\left(\frac{\partial \psi}{\partial \nabla s} \right) \delta s + \mathrm{div}\left(\frac{\partial \psi}{\partial \nabla s} \delta s \right), \tag{12}$$

as well as the divergence theorem on Eq. (10) results in

$$\begin{aligned} \delta E = & \int_{\Omega} -\mathrm{div}\left(\frac{\partial \psi}{\partial \nabla \mathbf{u}} \right) \delta\mathbf{u} \, \mathrm{d}V \\ & + \int_{\Omega} \left(\frac{\partial \psi}{\partial s} - \mathrm{div}\frac{\partial \psi}{\partial \nabla s} \right) \delta s \, \mathrm{d}V \\ & + \int_{\partial\Omega} \frac{\partial \psi}{\partial \nabla s} \cdot \mathbf{n} \, \delta s \, \mathrm{d}A \\ & + \int_{\partial\Omega} \left(\frac{\partial \psi}{\partial \nabla \mathbf{u}} \right)^T \cdot \mathbf{n} \, \delta\mathbf{u} \, \mathrm{d}A \end{aligned} \tag{13}$$

Thus, Eq. (9) yields four coupled Euler-Lagrange equations of the variational principle

$$\mathrm{div}\frac{\partial \psi}{\partial \nabla \mathbf{u}} = 0 \tag{14}$$

$$\frac{\partial \psi}{\partial s} - \mathrm{div}\frac{\partial \psi}{\partial \nabla s} = 0 \tag{15}$$

$$\frac{\partial \psi}{\partial \nabla s} \cdot \mathbf{n} = 0 \quad \text{on } \partial\Omega_{\nabla s} \tag{16}$$

$$\left(\frac{\partial \psi}{\partial \nabla \mathbf{u}} \right)^T \cdot \mathbf{n} + \boldsymbol{t}^* = 0 \quad \text{on } \partial\Omega_t. \tag{17}$$

With the constitutive law $\frac{\partial \psi}{\partial \nabla \mathbf{u}} = \boldsymbol{\sigma}$, Eq. (14) represents the equilibrium condition

$$\mathrm{div}\boldsymbol{\sigma} = 0. \tag{18}$$

Eq. (15) provides the evolution equation of the crack field. As shown in Gurtin (1996), the most general form of the evolution of the crack field s, which is in consistent with a mechanical view of the second law of thermodynamics reads

$$\frac{\mathrm{d}s}{\mathrm{d}N} = -M\frac{\delta \psi}{\delta s} = -M\left(\frac{\partial \psi}{\partial s} - \mathrm{div}\frac{\partial \psi}{\partial \nabla s} \right), \tag{19}$$

where $M > 0$ is the mobility parameter, which models the "viscosity"(rate dependency) of the phase field fracture model. The $M \to \infty$ approximates the quasi static limit case with $\frac{\delta \psi}{\delta s} = 0$. Therefore, the evolution of crack field is modeled by

$$\begin{aligned} \frac{\mathrm{d}s}{\mathrm{d}N} = & -M\Big\{ g(s)' \frac{1}{2}\boldsymbol{\varepsilon} : [\mathbb{C}\boldsymbol{\varepsilon}] \\ & - \mathcal{G}_c\left(2\epsilon\nabla \cdot \nabla s - \frac{s-1}{2\epsilon} \right) \\ & + h(s)'\psi^{ac}(D) \Big\}. \end{aligned} \tag{20}$$

Eqs. (16) and (17) are the Neumann boundary conditions for the crack field

$$\nabla s \cdot \mathbf{n} = 0 \quad \text{on } \partial\Omega_{\nabla s} \tag{21}$$

and the stress field

$$\boldsymbol{\sigma}\mathbf{n} = \boldsymbol{t}^* \quad \text{on } \partial\Omega_t. \tag{22}$$

Solving Eqs. (18) and (20) by means of the Newton method yields the displacement field $\mathbf{u}$ and fracture field s.

3.2 Adaptive cycle number adjustment algorithm

To reduce the total number of load cycles, we transfer the simulation step to cycles: The simulation step is defined as the incremental change of "time" in one simulation iteration, and each simulation step represents a certain increment of load cycles. Furthermore, the real cyclic loading is approximated with its envelope loading. In general, this "time-cycle" transfer concept is also suitable for any arbitrary loading process. Noting Eq. (6), the cycle number increment can be rewritten as

$$\mathrm{d}N = n_D \left(\frac{\hat{\sigma}_n (1-L)}{f(L)} \right)^{-k} \mathrm{d}D. \tag{23}$$

The choice of the cycle number increment is a crucial point in the phase field model: not only because it determines the computational time; it also strongly influences the shape of the crack pattern. The crack trace is wide and irregular when the cycle number increment is too large. Besides, the fatigue energy grows dramatically by over-large cycle number increments, and it might result in a simulation with an unstable energy state. Several crack patterns from unsuitable cycle number increment are demonstrated in Fig. 7.

Additionally, the displacement field $\mathbf{u}_n$, the crack field s_n and the cycle number N_n from the previous simulation step are stored as reference values. These values will be reused if the simulation needs to be restarted. In Alg. 2, we provide the details of the restart-algorithm.

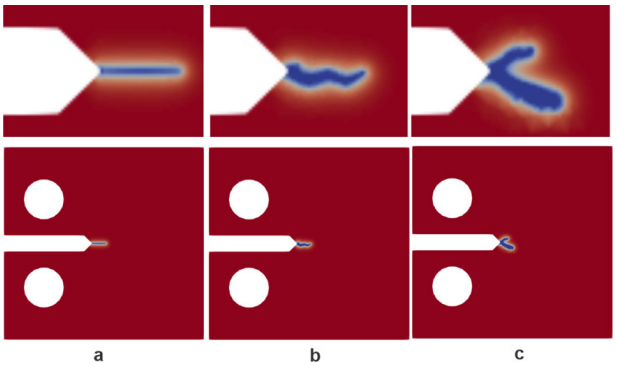

Fig. 7 The crack pattern is strongly influenced by the cycle number increment $\mathrm{d}N$; **a**: $\mathrm{d}N$ chosen by our algorithm; **b**: crack pattern is wide and irregular ($\mathrm{d}N = 50$); **c**: unstable state ($\mathrm{d}N = 500$)

Algorithm 1: adaptive cycle increment adjustment algorithm

Input: input parameter: D_c, D_α, D_β
/* damage threshold: D_c */
/* regulation parameter at stage ②: D_α */
/* regulation parameter at stage ③: D_β */
/* regulation parameter at stage ③: D_γ */
static is *TRUE*;
crack is *FALSE*;
while simulation **do**
  if $\max[\mathrm{d}D_{n+1}] + \max[\mathrm{d}D_n] < D_c$ and static is *TRUE* **then**
    /* stage ① */
    $\mathrm{d}N = 2\mathrm{d}N$;
  end
  else if $\max[\mathrm{d}D_{n+1}] + \max[\mathrm{d}D_n] > D_c$ and crack is *FALSE* **then**
    /* stage ② */
    static is *FALSE*;
    if $\max[\mathrm{d}D_n] > D_\alpha$ **then**
      $\mathrm{d}N = 0.1\mathrm{d}N$;
      restart;
    end
    else if $\max[\mathrm{d}D_n] < D_\alpha$ **then**
      /* fatigue damage begins now */
      crack is *TRUE*;
    end
  end
  if crack is *TRUE* **then**
    /* stage ③ */
    if $\max[\mathrm{d}D_n] < D_\beta$ **then**
      $\mathrm{d}N = \mathrm{d}N \frac{D_\gamma}{D_\beta}$;
      restart;
    end
    else if $\max[\mathrm{d}D_n] > D_\gamma$ **then**
      $\mathrm{d}N = \mathrm{d}N \frac{D_\beta}{D_\gamma}$;
      restart;
    end
  end
end

The simulation of fatigue fracture is divided into three stages: ① the damage D is below the threshold D_c. In this stage, it behaves in a pure static mechanical state. Thus, the cycle number increment should be chosen as large as possible. ② the damage D is at the limit

Algorithm 2: restart-algorithm

```
while simulation do
    if restart is TRUE then
        /* overwrite using previous cycle */
        N = N* + dN ;
        u = u* ;
        s = s* ;
    else
        /* store field from previous cycle */
        N* = N_n ;
        u* = u_n ;
        s* = s_n ;
        /* update field                    */
        D_{n+1} = D_n + dD_n ;
        N_{n+1} = N_n + dN_n ;
        u_{n+1} = u_n ;
        s_{n+1} = s_n ;
```

threshold D_c. The fatigue crack is about to begin and the cycle number increment $\mathrm{d}N$ should be chosen suitable to ensure $\mathrm{d}D$ small enough to simulate the transient process. ③ the damage D is bigger than D_c. We control the maximum damage increment $\max[\mathrm{d}D]$ between a control parameter D_β and D_γ to obtain a moderate growth rate of the fatigue energy. Since the damage increment $\mathrm{d}D$ is controlled by this algorithm, the fatigue damage at the previous step and current step will not change much. As a result, it is suitable to take the stress from the previous step as the driving force even if the cycle number increment $\mathrm{d}N$ is large. This adaptive algorithm will stop once the cycle number increment $\mathrm{d}N$ reach a minimal cycle number increment. Figure 8 reports the maximum damage increment $\max[\mathrm{d}D]$ and cycle number increment $\mathrm{d}N$ by applying the adaptive cycle increment adjustment algorithm. The cyclic loading is applied within four phases in this example, where both the influence of the maximum external load and mean stress are taken into consideration. According to our algorithm, small cyclic loading increases the increment of cycle number of one simulation step. It is to noticed that in this algorithm only two global values (the maximum damage increment $\max[\mathrm{d}D]$ and cycle number increment $\mathrm{d}N$) are involved. The algorithm is suitable for a fatigue fracture scenario with only one crack or multiple cracks are simultaneously at the same stage.

For a better comprehension of our algorithm, we summarize this in Alg. 1.

4 Numerical examples

For validation of the introduced implementation of the proposed model, several simulations are used. The compact tension (CT) specimen is widely used as testing sample in the field of fracture mechanics. The definition of the geometry is given in the ASTM E 399 standard (ASTM 2009).

For the CT specimen, the stress intensity factor can be approximated by

$$\begin{aligned}\Delta K = \frac{\Delta F}{\mathrm{B}\sqrt{\mathrm{L}}} \frac{2+\frac{a}{\mathrm{L}}}{\left(1-\frac{a}{\mathrm{L}}\right)^{3/2}} \cdot \\ \left[0.886 + 4.64\left(\frac{a}{\mathrm{L}}^2\right) - 13.32\left(\frac{a}{\mathrm{L}}\right)^3 \right. \\ \left. + 14.72\left(\frac{a}{\mathrm{L}}\right)^4 - 5.69\left(\frac{a}{\mathrm{L}}\right)^5\right].\end{aligned} \tag{24}$$

This equation was proposed in Srawley (1976). Here F is the applied force, and B is the thickness of the specimen. The simulation result is depicted in Fig. 9, where the upper semi-circle of the bolt hole is loaded with a distributed vertical pulsating load. The evolution of the crack field is demonstrated in Fig. 9b and c. Figure 9d shows the evolution of the field values (driving force $\hat{\sigma}$, damage D and crack field s) along the crack ligament at cycle N_1, N_2 and N_3. It is recognized, the driving force $\hat{\sigma}$ increases at the crack tip as the crack propagates; as a consequence, the specimen is easier to break than the early stage. In other words, the fatigue crack will propagate faster, and the crack growth rate will be higher. The fatigue damage parameter D is accumulated continuously during the crack propagation, whereas the crack field s decreases from 1 to 0. Figure 10 shows the comparison using cycle adjustment against the "classical" simulation scheme. As depicted in Fig. 10a, our algorithm can accelerate the simulation process significantly. The computing time has dropped to nearly 3% using our method, compared to constant cycle number increment $\mathrm{d}N = 5$. Figure 10b and c show, although the cycle number is adjusted, the proposed method yields almost the same crack growth rate and crack pattern. Using the applied forces as a variable, Fig. 11 shows the crack growth rate related to the stress intensity factor for different simulations. In Fig. 11a, we present the crack growth rate for different levels of maximum external

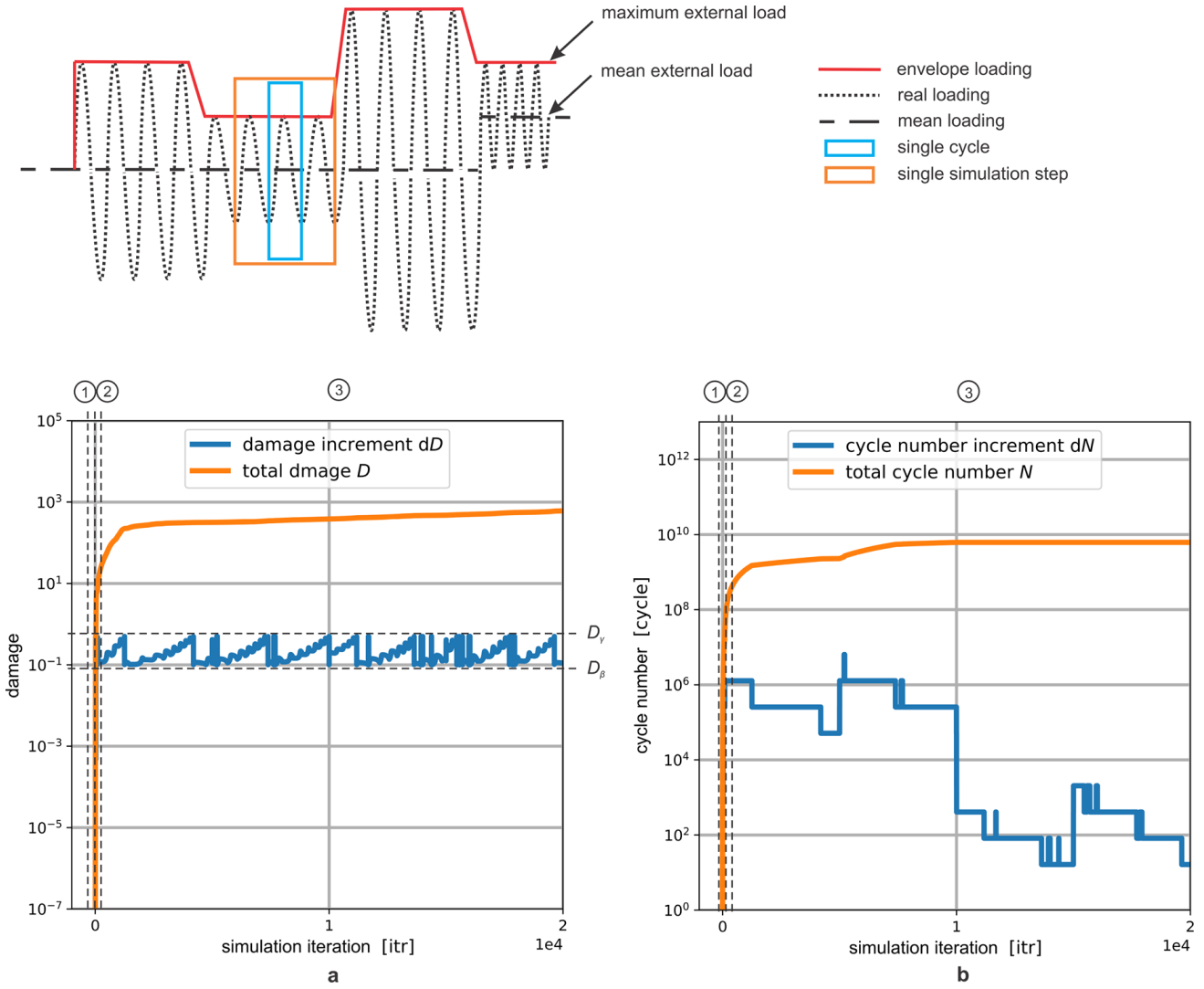

Fig. 8 Illustration of the proposed adaptive cycle adjustment. The upper figure is a schematic illustration of the approximation for cyclic loading in four phases; **a**: damage within the simulation; **b**: cycle number within the simulation

load. The result matches Paris' law with parameters $C = 3.724 \times 10^5 \frac{\text{mm/cycle}}{(\text{MPa}\sqrt{\text{m}})^m}$ and $m = 5.548$ very well. It is to observe that even though different force amplitudes for the simulation are applied, the rate of crack growth can be described with the same Paris' law. Figure 11b displays the effect of mean stress on the crack growth rate, where the stress ratio R is defined as the ratio between the minimum stress and the maximum stress. The depicted diagram reflects the fact that higher mean stress increases the rate of crack growth.

In the next example, we consider a block geometry with initial boundary values as proposed in Müller and Kuhn (2020). This example is straightforward and disregards special problems of distinction between tension and compression, since the cracks should only occur in tension region (Kuhn 2013). A half of its top surface is loaded with a displacement load, whereas the bottom of the block is fixed. Furthermore, we assume this upper half of the block will never break, given as a Dirichlet boundary condition $s = 1$ in the indicated area (in red) of width $0.5L$ (see Fig. 12). As seen in Fig. 12, the crack begins at the top of the surface, which is different from the pure elastic case shown in Müller and Kuhn (2020). The reason is that the fatigue crack is triggered at areas where the maximum first principal stress is found, which is the driving force for the fatigue crack propagation in our model.

Different loads, deformations and crack interactions can lead to complex crack propagation behav-

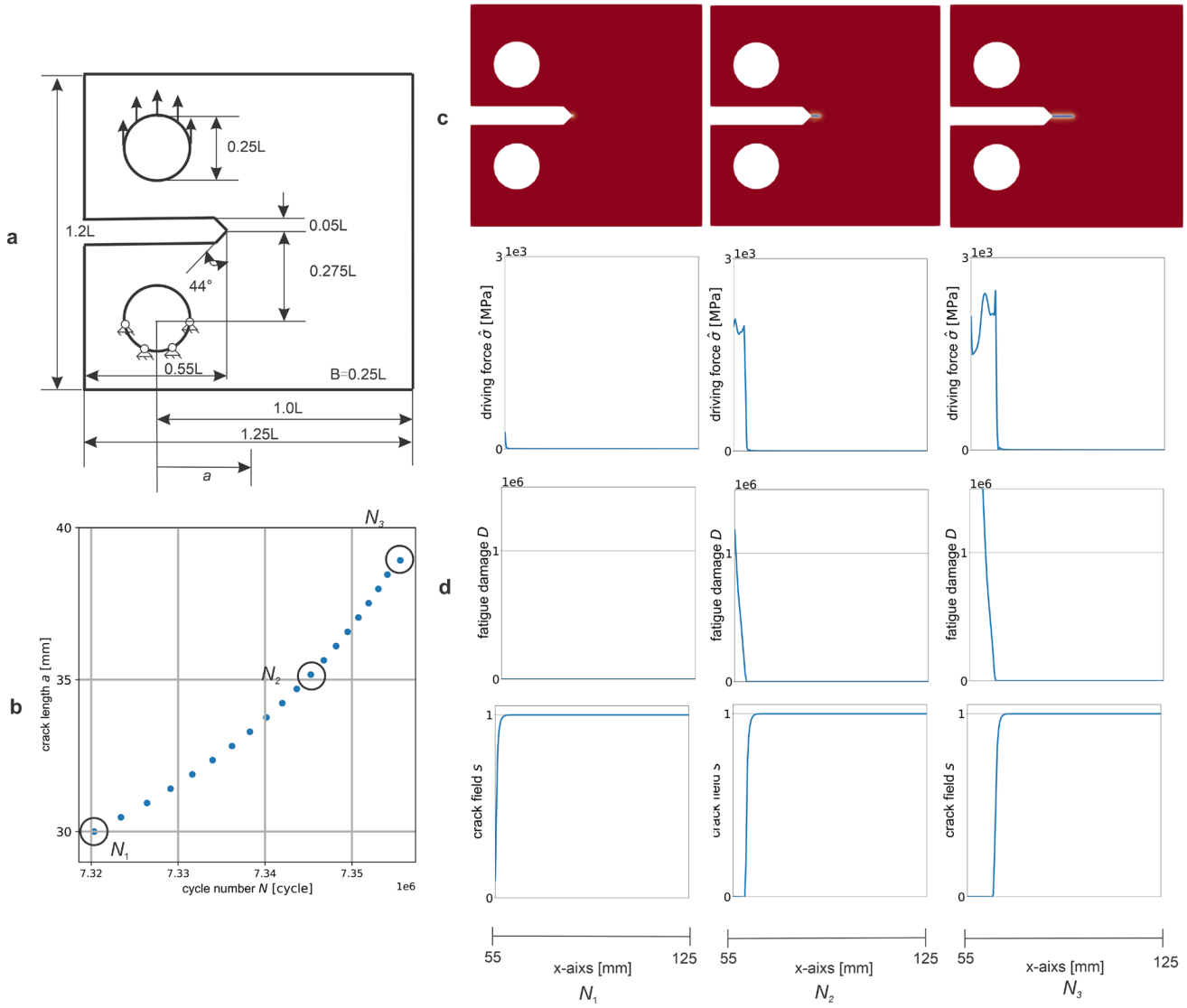

Fig. 9 **a**: The geometry definition of CT specimen; **b**: the crack length in relation to cycle number obtained from a simulation with vertical loads on the upper bolt hole; **c**: the evolution of crack field at cycle N_1, N_2 and N_3; **d**: the field value ($\hat{\sigma}$, D and s) at cycle N_1, N_2 and N_3

ior, depending on the applied load conditions on the geometry. A specimen of a rectangular geometry is set up to validate our model under mixed mode loading in traction conditions. The rectangular geometry is loaded with a purely alternating ($R = -1$) displacement load in the vertical direction on the upper edge, and the lower edge is fixed. Sharp notches on both vertical edges are defined for different situations. Figure 13 shows that the presented method is robust under mixed load situation. The first row at cycle number N_1 is the initial state of the crack pattern, where the predefined cracks are located at different positions. The simulation results at cycle number N_2 can be verified with the crack patterns illustrated in Yates et al. (2008). In the last row at cycle number N_3, we demonstrate the results at the last feasible simulation stages. At the early stage, the crack extends purely horizontal in all simulation settings. After this stage, the cracks begin to deviate from each other (see Fig. 13b and c), caused by the fatigue driving force. After this period, the cracks intend to change their directions to the horizontal level and grow towards each other again. The deviation of

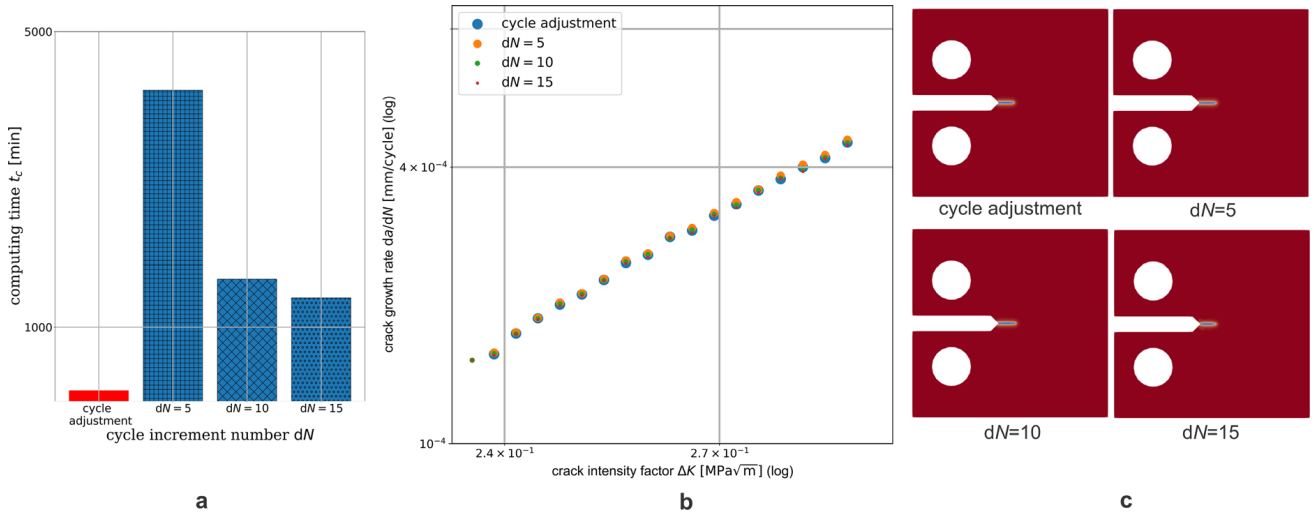

Fig. 10 Our method compared to the classical simulation scheme in **a**: the computational time; **b**: the crack growth rate; **c**: the crack pattern

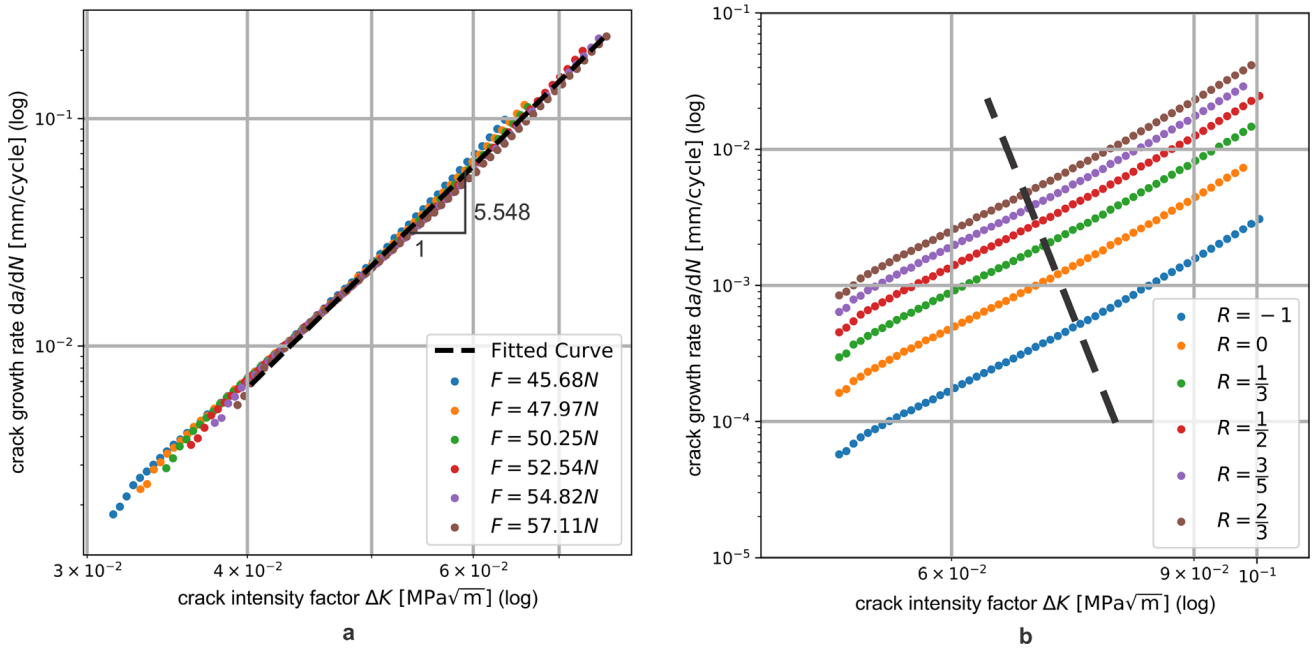

Fig. 11 The crack growth rate related to the stress intensity factor from simulations with the CT specimen. **a**: constant stress ratio with different force amplitudes; **b**: different stress ratio with the same force amplitude

the crack paths is influenced by the crack interaction, as shown in Fig. 13d. The crack propagation remains almost straight during the whole crack evolution due to the higher distance of the cracks. These crack paths simulated by the finite element method using our model is very similar comparing to experiments.

5 Conclusion

We present a phase field fracture model to predict the fracture behavior caused by fatigue damage. In the phase field modeling framework, the entire fatigue fracture behavior is simply derived by a single regu-

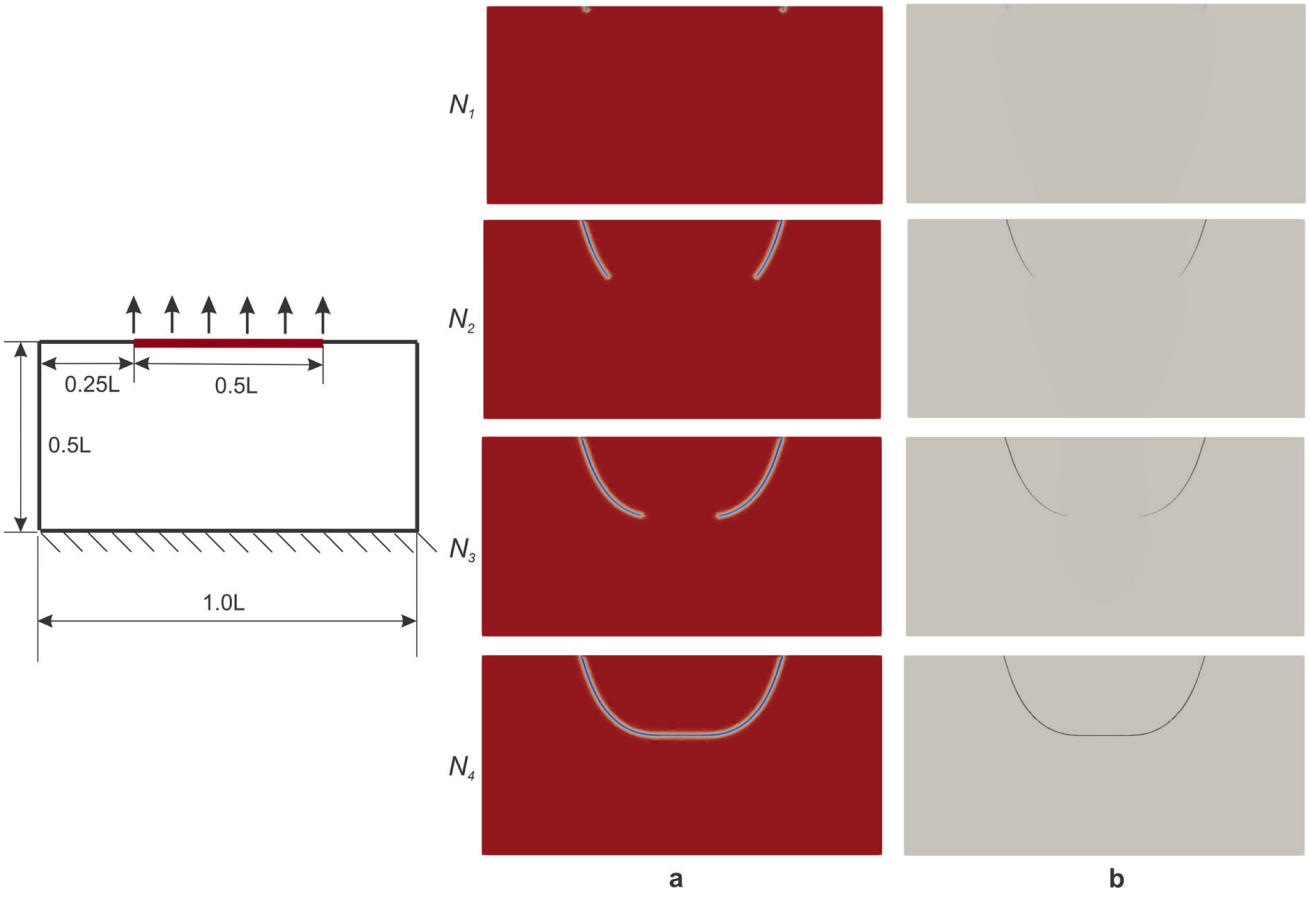

Fig. 12 The left figure is the definition of the block geometry; in the right figure, **a**: the evolution of crack field; **b**: the magnitude of the first principal stress $\hat{\sigma}$ (driving force) with color-map

larized energy density function. Differing from alternative fatigue phase field models (Alessi et al. 2018; Carrara et al. 2020; Seiler et al. 2020; Seleš et al. 2021), we introduce an additional energy term related to the fatigue damage into the total energy density function. The new method incorporates the experiment data directly into the phase field energy term, which is best to the author's knowledge, the first work to combine the experimental findings with the phase field fatigue model. Thus the proposed simulation setup has the potential to compactly simulate the fatigue propagation under complex circumstances. This fatigue energy part represents the accumulated driving force caused by fatigue damage. Furthermore, the fatigue energy is related to a damage parameter, which represents the damage caused by cyclic fatigue. The results show that our model is able to reproduce the significant properties of fatigue crack growth, as e.g. the mean stress effect. The main contribution of our study is to develop an adaptive cycle increment adjustment algorithm. The entire simulation is split into three stages: elastic stage; transient stage and fatigue stage. During the simulation, the damage increment is controlled to obtain a moderate fatigue energy growth, where the cycle number increment is chosen adaptively according to the damage increment. This algorithm can reduce the computational cost of simulation without sacrificing accuracy. The implementation of the phase field model is done on the open-source platform FEniCS. Thanks to its flexibility and simplicity, it enables elaborate and efficient simulations of complex problems. As a future work, the phase field fatigue damage model will be extended to three dimensions.

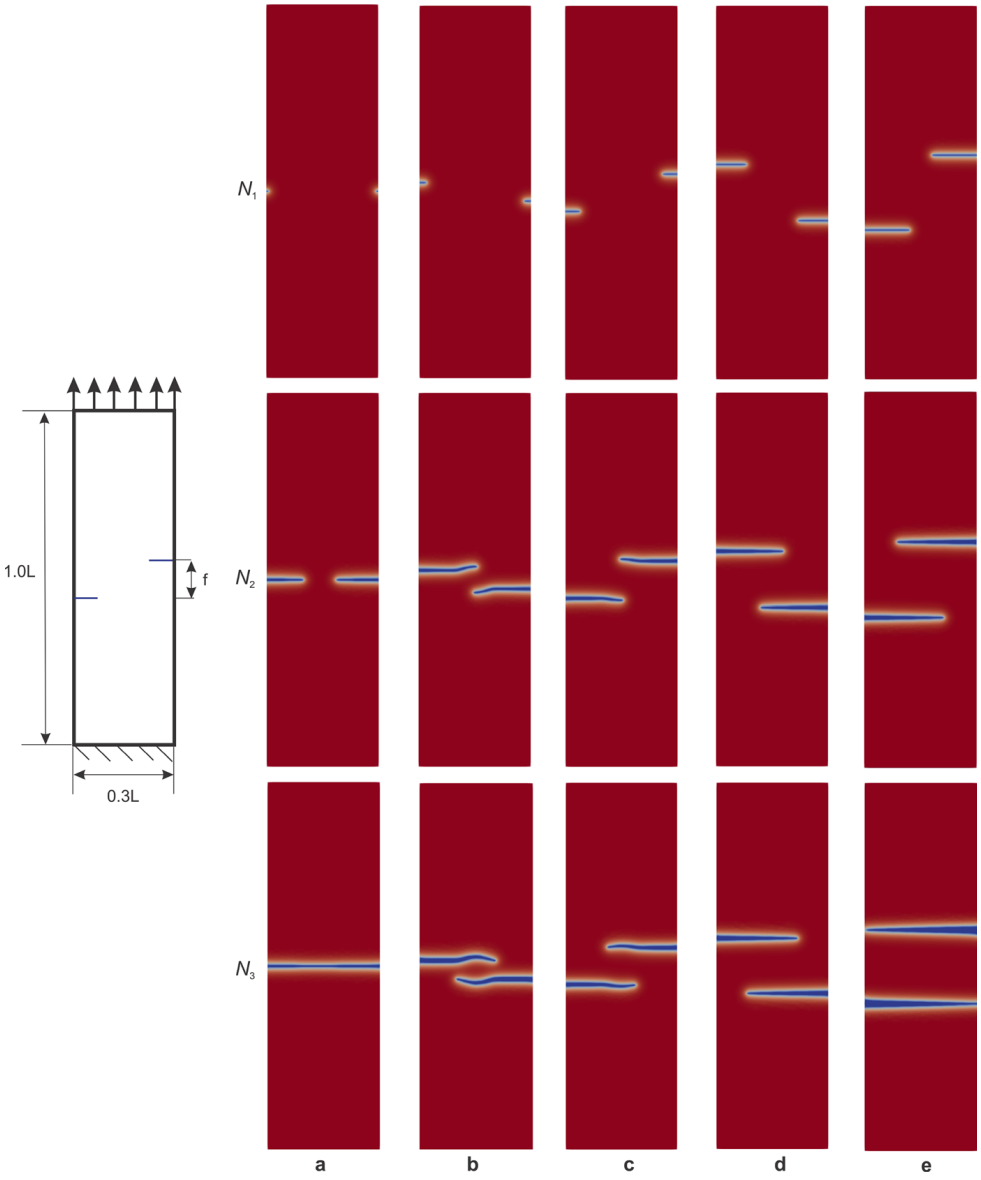

Fig. 13 The left figure is the definition of the rectangular specimen; the right figure (**a**-**e**) shows the evolution of the crack field loaded with different conditions (**a**: f=0; **b**: f=0.05L; **c**: f=0.1L; **d**: f=0.15L; **e**: f=0.2L)

Acknowledgements Funded by the Deutsche Forschungsgemeinschaft (DFG, German Research Foundation) -252408385 -IRTG 2057

Funding Open Access funding enabled and organized by Projekt DEAL.

References

Alessi R, Vidoli S, De Lorenzis L (2018) A phenomenological approach to fatigue with a variational phase-field model: the one-dimensional case. Eng Fract Mech 190:53–73

Alnæs MS, Blechta J, Hake J, Johansson A, Kehlet B, Logg A, Richardson C, Ring J, Rognes ME, Wells GN (2015) The fenics project version 1.5. Arch Numer Softw. https://doi.org/10.11588/ans.2015.100.20553

Ambati M, Gerasimov T, De Lorenzis L (2015) Phase-field modeling of ductile fracture. Comput Mech 55(5):1017–1040

Amendola G, Fabrizio M, Golden J (2016) Thermomechanics of damage and fatigue by a phase field model. J Therm Stresses 39(5):487–499

ASTM (2009) ASTM E399-09, Standard test method for linear-elastic plane-strain fracture toughness k ic of metallic materials. http://www.astm.org

Boldrini J, de Moraes EB, Chiarelli L, Fumes F, Bittencourt M (2016) A non-isothermal thermodynamically consistent phase field framework for structural damage and fatigue. Comput Methods Appl Mech Eng 312:395–427

Borden MJ, Hughes TJ, Landis CM, Verhoosel CV (2014) A higher-order phase-field model for brittle fracture: Formulation and analysis within the isogeometric analysis framework. Comput Methods Appl Mech Eng 273:100–118

Bourdin B (2007) Numerical implementation of the variational formulation for quasi-static brittle fracture. Interfaces Free Boundaries 9(3):411–430

Bourdin B, Francfort GA, Marigo JJ (2000) Numerical experiments in revisited brittle fracture. J Mech Phys Solids 48(4):797–826

Bourdin B, Francfort GA, Marigo JJ (2008) The variational approach to fracture. J Elast 91(1–3):5–148

Caputo M, Fabrizio M (2015) Damage and fatigue described by a fractional derivative model. J Comput Phys 293:400–408

Carrara P, Ambati M, Alessi R, De Lorenzis L (2020) A framework to model the fatigue behavior of brittle materials based on a variational phase-field approach. Comput Methods Appl Mech Eng 361:112731

Ciavarella M, D'antuono P, Papangelo A (2018) On the connection between palmgren-miner rule and crack propagation laws. Fatigue Fracture Eng Mater Struct 41(7):1469–1475

Francfort GA, Marigo JJ (1998) Revisiting brittle fracture as an energy minimization problem. J Mech Phys Solids 46(8):1319–1342

Griffith AA (1921) Vi, the phenomena of rupture and flow in solids. Philosophical transactions of the royal society of london Series A, containing papers of a mathematical or physical character 221(582–593):163–198

Gurtin ME (1996) Generalized ginzburg-landau and cahn-hilliard equations based on a microforce balance. Physica D 92(3–4):178–192

Hasan MM, Baxevanis T (2021) A phase-field model for low-cycle fatigue of brittle materials. Int J Fatigue 150:106297

Irwin GR (1997) Analysis of stresses and strains near the end of a crack traversing a plate

Kuhn C (2013) Numerical and analytical investigation of a phase field model for fracture. doctoralthesis, Technische Universität Kaiserslautern, http://nbn-resolving.de/urn:nbn:de:hbz:386-kluedo-35257

Kuhn C, Müller R (2010) A continuum phase field model for fracture. Eng Fract Mech 77(18):3625–3634

Kuhn C, Noll T, Müller R (2016) On phase field modeling of ductile fracture. GAMM-Mitteilungen 39(1):35–54

Miehe C, Welschinger F, Hofacker M (2010) Thermodynamically consistent phase-field models of fracture: variational principles and multi-field fe implementations. Int J Numer Meth Eng 83(10):1273–1311

Miner MA (1945) Cumulative damage in fatigue. J Appl Mech pp 159–164

Mughrabi H (2015) Microstructural mechanisms of cyclic deformation, fatigue crack initiation and early crack growth. Philosophical Transactions of the Royal Society A: Mathematical, Physical and Engineering Sciences 373(2038):20140132

Müller R, Kuhn C (2020) Spp-1748 benchmark collection phase field

Paris P, Erdogan F (1963) A critical analysis of crack propagation laws

Schlüter A, Willenbücher A, Kuhn C, Müller R (2014) Phase field approximation of dynamic brittle fracture. Comput Mech 54(5):1141–1161

Schreiber C, Kuhn C, Müller R, Zohdi T (2020) A phase field modeling approach of cyclic fatigue crack growth. Int J Fract 225(1):89–100

Schreiber C, Müller R, Kuhn C (2020b) Phase field simulation of fatigue crack propagation under complex load situations. Arch Appl Mech pp 1–15

Seiler M, Linse T, Hantschke P, Kästner M (2020) An efficient phase-field model for fatigue fracture in ductile materials. Eng Fract Mech 224:106807

Seleš K, Aldakheel F, Tonković Z, Sorić J, Wriggers P (2021) A general phase-field model for fatigue failure in brittle and ductile solids. Comput Mech 67(5):1431–1452

Srawley JE (1976) Wide range stress intensity factor expressions for astm e 399 standard fracture toughness specimens. Int J Fract 12(3):475–476

Wilson ZA, Landis CM (2016) Phase-field modeling of hydraulic fracture. J Mech Phys Solids 96:264–290

Yates J, Zanganeh M, Tomlinson R, Brown M, Garrido FD (2008) Crack paths under mixed mode loading. Eng Fract Mech 75(3–4):319–330

Yoshioka K, Bourdin B (2016) A variational hydraulic fracturing model coupled to a reservoir simulator. Int J Rock Mech Min Sci 88:137–150

II. Second paper

Published in:
Computational Materials Science, p. 112829 (2024)
DOI: https://doi.org/10.1016/j.commatsci.2024.112829

II.1. Objectives of the second paper

Subjecting mechanical components to repeated cycles of loading can lead to the development and extension of fatigue cracks. When such components operate in complex environments involving both thermal and mechanical loads fatigues cracks can be initiated and grow faster than when there is purely mechanical loading. Although various phase field models have been developed to simulate fatigue fractures over the years, they have mostly been limited to scenarios involving pure mechanical loading. This paper extends the phase field model to include thermomechanical fatigue. The phase field model utilizes the variational formulation, where the crack evolution is derived by minimizing the total energy by the crack field and displacement field. The propagation of the fatigue crack is conducted by a fatigue driving force, in this case, is taken as the first principal stress. However, for a thermomechanical fatigue scenario, some modifications must be adapted.

In this work, the thermal stress is added as an additional fatigue driving force within the phase field model. Through case studies, we demonstrate that the extended phase field fatigue model can predict thermomechanical fatigue behavior in a simple fashion.

Computational Materials Science 235 (2024) 112829

Contents lists available at ScienceDirect

Computational Materials Science

journal homepage: www.elsevier.com/locate/commatsci

Full length article

Thermomechanical fatigue life simulation using the phase field method

Sikang Yan [a,*], Ralf Müller [b], Bahram Ravani [c]

[a] Institute of Applied Mechanics, RPTU Kaiserslautern-Landau, Kaiserslautern, 67663, Germany
[b] Institute for Mechanics, Technical University of Darmstadt, Darmstadt, 64289, Germany
[c] Department of Mechanical and Aerospace Engineering, University of California Davis, CA, 95616, USA

ARTICLE INFO

Keywords:
Phase field
Thermomechanical fatigue

ABSTRACT

Putting a mechanical structure under repeated cyclic loading can lead to fatigue crack initiation and propagation. In engineering processes, a fatigue crack evolution behavior can be very complicated when the structure is in a complex environment and under complex loading conditions. Over the years, different phase field models have been developed to simulate fatigue fractures; however, they are mostly restricted to fatigue under pure mechanical loading. In this work, we show that the phase field model can simulate fatigue behavior in a complex environment. As a highlight of the presented paper, we extended the phase field fatigue model to handle thermomechanical fatigue. We consider thermal stress to be an additional fatigue driving force in the phase field model. It is shown, using case studies, that the extended phase field fatigue model is able to predict thermomechanical fatigue behavior.

1. Introduction

Finding ways to deal with fatigue failure is a crucial issue in mechanical design and manufacturing processes. Fatigue failure in structures is difficult to predict since unexpected cracks can occur at stress levels lower than the yield stress of the material. Moreover, unlike other fracture scenarios, fatigue failure does not happen immediately, but rather after a huge number of repeated load cycles. Depending on the types of loading, geometry, and environment of the technical component, the crack evolution behavior can be very complicated. Traditionally, fatigue life and crack patterns are determined by experiments, which are time-consuming and unfavorable in terms of economic and ecological aspects. Due to those intrinsic properties of the fatigue fracture, an innovative numerical tool is desired that can cover the mentioned fatigue features in a simple way.

In the past decade, the phase field method has been developed to simulate complicated fracture processes because of its energetic approach and its applicability to various application [1–3]. The phase field model can reproduce crack evolution, including initiation, propagation, branching, and kinking, by one single equation. Moreover, it can be simulated on a fixed mesh. Historically speaking, the phase field model is based on an extension of the Griffith fracture theory [4], where an energetic criterion is used to predict the onset of crack propagation. Following this idea, Francfort and Marigo [1] proposed a variational formulation to predict the crack evolution of brittle fracture. In order to numerically resolve the fracture behavior, a regularized formulation was devised by Bourdin et al. [2,3,5], where a crack field variable was introduced to indicate the crack status. This diffusive representation of cracks by a scalar field resembles the phase field method. Kuhn and Müller [6] proposed a phase field model for quasi-static fracture, where the variational problem yields an equation of stress equilibrium and an equation of crack evolution. Amor et al. [7] distinguished the fracture cases in tension and compression by decomposing the elastic energy density to avoid unrealistic crack propagation in compression. Later, an additional history field variable was introduced by Miehe et al. [8] in order to handle the irreversibility of the crack field. As solution methods, monolithic and staggered schemes are used in the literature [8–11].

The phase field method has been applied in different fracture scenarios. For the fatigue phase field model, there are two main strategies: to reduce the fracture toughness or to accumulate the fatigue damage. For the first variation: Alessi et al. [12] introduced a fatigue degradation function related to an accumulated strain history variable, which is applied to the fracture energy accounting for the fatigue effect. The fracture energy, which is associated with the fatigue degradation function, will decrease when the strain history variable increases. In other works like [13,14], the fatigue degradation function and history variable are chosen differently, but they are still used to reduce the fracture energy term. Different from those phase field formulations for fatigue fracture, Schreiber et al. [15,16], Yan et al. [17] follow the path from Kuhn and Müller [6] by extending the model by an additional fatigue driving term. This additional fatigue contribution represents

* Corresponding author.
E-mail addresses: yan@rhrk.uni-kl.de (S. Yan), ralf.mueller@mechanik.tu-darmstadt.de (R. Müller), bravani@ucdavis.edu (B. Ravani).

https://doi.org/10.1016/j.commatsci.2024.112829
Received 23 August 2023; Received in revised form 21 January 2024; Accepted 21 January 2024
Available online 24 January 2024

the sum of additional driving forces caused by fatigue damage. One major advantage of this formulation is that it directly couples the phase field model with the fatigue parameters of experiments, allowing us to handle complex environmental influences on crack growth. In addition, the efficiency of the phase field fatigue model must be discussed due to the high computation demand of fatigue simulation. On the one hand, Seleš et al. [18] enables a cycle skipping option for high cycle fatigue analysis with a two-part cycle skipping technique. Furthermore, Wu et al. [19,20] proposed a Broyden–Fletcher–Goldfarb–Shanno (BFGS) algorithm to solve the coupled governing equations monolithically. In this work, we show that the phase field fatigue model can take the effects of loading frequency and loading temperature into consideration. Additionally, the adaptive cycle number adjustment algorithm (ACNAA) [17] is employed in favor of efficient computations. It is shown that results from phase field simulations agree with existing experimental data.

Besides mechanical loading, the fatigue of materials can also be caused by rapid heating and cooling, known as thermal fatigue. Thermal fatigue is a special type of fatigue failure where the macroscopic cracks result from cyclic thermal stresses due to the repetitive fluctuations of temperature. Despite the phase field fatigue model being well-established for pure mechanical loading cases, studies of thermomechanical fatigue have not been widely reported. Amendola et al. [21] presented an isothermal phase field model for a nonisothermal system, where the thermal effects are defined in a fatigue functional. Recently, a thermal fatigue phase field model has been proposed by Du et al. [22], in which the thermal expansion and the effect of changing temperature are directly acting on material parameters. The key novelty of our work is that we consider thermal fatigue effects in the additional fatigue term of the phase field fracture model. The thermal stresses related to temperature gradients are considered to be the second fatigue driving force in the phase field model. It is shown that the extended phase field model can predict thermomechanical fatigue behavior. The outline of the paper is as follows: In Section 2, the phase field model for fatigue fracture is stated. In Section 3, phase field simulation results are compared with experimental data from the literature. In Section 4, a thermomechanical fatigue phase field model is presented, and in Section 5, conclusions are drawn and directions for future work are given. It is noted that since the original phase field fatigue model has been well presented in [15,17,23], we do not repeat the details of the model here in order to minimize any overlaps.

2. A phase field model for cyclic fatigue

The phase field fracture model introduces an additional field variable to represent cracks. The crack field s is 1 if the material is intact and is 0 where cracks occur [6]. The crack field s varies continuously from 0 to 1, modeling the transition zone similar to the Landau–Ginzburg phase transition [24]. Following a variational principle, it is postulated that the displacement field $\mathbf{u}$ and crack field s locally minimize the total energy of a loaded body Ω. This assumption yields two coupled equations – the equilibrium of the stress field and the evolution of the crack field – to describe fatigue fracturing. The total energy $\mathcal{E}$ for a case of fatigue fracture is given as

$$\mathcal{E} = \int_{\Omega} \psi(\boldsymbol{\varepsilon}, s, \nabla s, D)\mathrm{d}V = \int_{\Omega} \Big[(g(s)+\eta)\psi^{e}(\boldsymbol{\varepsilon}) + \psi^{s}(s,\nabla s) + h(s)\psi^{\mathrm{ad}}(D) \Big] \mathrm{d}V, \tag{1}$$

where ψ denotes the total energy density of the body, which consists of the elastic energy density ψ^{e}, the fracture surface energy density ψ^{s}, and an additional energy density ψ^{ad} [15]. The functions $g(s)$ and $h(s)$ are the degradation functions, which model the loss of stiffness in the broken material. In the rest of this work, the degradation function $h(s)$ is identical to $g(s) = s^2$ because of its simple form and better numerical robustness based on our studies. The parameter η describes a residual stiffness to avoid numerical difficulties. The stain energy density

$$\psi^{e}(\boldsymbol{\varepsilon}) = \frac{1}{2}\boldsymbol{\varepsilon} : (\mathbb{C}\boldsymbol{\varepsilon}) \tag{2}$$

models the energy stored inside a body, where $\mathbb{C}$ is the 4th order stiffness tensor and $\boldsymbol{\varepsilon} = \frac{1}{2}(\nabla\mathbf{u} + \nabla^{\mathrm{T}}\mathbf{u})$ is the infinitesimal strain tensor. The fracture surface energy density ψ^{s} denotes the energy required to separate the material and to generate cracks, which is assumed to be proportional to the crack surface. The formulation of the crack surface area is adapted from the work of Mumford and Shah in image processing [25]. Mumford and Shah proposed minimizing a functional to segment the image into nearly homogeneous regions separated by smooth boundaries. This functional captures the length of the boundary, the gradient of the image, and the image itself. As an analogy to this proposal, the surface density functional is given in relation to the gradient of the crack field ∇s and the crack field s itself. Therefore, the fracture surface energy density is given as

$$\psi^{s}(s,\nabla s) = \mathcal{G}_{c}\left(\frac{(1-s)^2}{4\epsilon} + \epsilon|\nabla s|^2 \right), \tag{3}$$

where the length parameter ϵ controls the width of the smooth transition zone between the broken ($s = 0$) and undamaged material ($s = 1$). When the length parameter ϵ goes to zero, the crack surface density functional approximates the crack surface area. The parameter $\mathcal{G}_{c}$ is the crack energy density, related to the fracture toughness. It describes the ability of a material to resist fracturing. The additional energy density term

$$\psi^{\mathrm{ad}}(D) = q < D - D_{c} >^{b} \tag{4}$$

is introduced to account for the accumulated fatigue driving force, which is associated with a fatigue damage parameter D. According to Borden et al. [16,26], the crack field s does not have any physical interpretation as a damage variable; actually, it is only an order parameter purely to denote the state of the interfacial problem. Thus, this parameter D is introduced to model the damage related to fatigue. Inspired by Miner's rule [27], the damage parameter will be accumulated during the entire simulation

$$D = D_{0} + \mathrm{d}D. \tag{5}$$

Although the original Miner's rule does not include the loading sequence effect, the phase field model is sensitive to cycle history and can reproduce the loading sequence effect as shown in [23]. We also want to mention that other choices e.g., the nonlinear damage accumulation model [28] might also be suitable. The parameter D_{0} is the previous damage and

$$\mathrm{d}D = \frac{\mathrm{d}N}{n_{D}}\left(\frac{\hat{\sigma}}{A_{D}} \right)^{k} \tag{6}$$

is the damage increment. The damage increment is associated with the cycle increment $\mathrm{d}N$, which provides a possibility to reduce the computational cost and simulation time by applying the adaptive cycle number adjustment algorithm [17]. The parameters n_{D}, A_{D}, and k are taken from Wöhler curves (SN curves) of experiments (see Fig. 1). Those parameters allow the phase model to incorporate the fatigue experiments directly, such that the information for complicated fatigue crack evolution can be integrated in a straightforward manner. It is noted that the microplasticity is implicitly modeled in the damage parameter D; with different loading scenarios (loading temperature or loading frequency), it would have different SN-curve from the experiments, where different fatigue parameters will be put into the damage parameter. In the phase field model, the fatigue driving force is the first principal stress of the undegraded stress field since the presented model aims at the high cycle fatigue and is based on the brittle phase field model from Kuhn and Müller [6]. It is noted that it is not claimed that

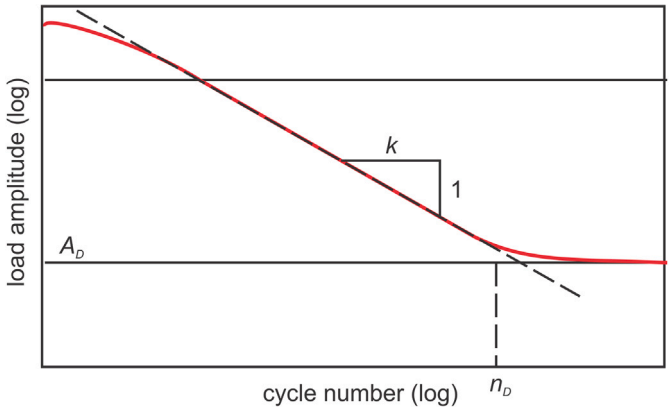

Fig. 1. An example of a typical SN curve.

this choice of driving force is suitable for all materials. Other effective stress quantities, e.g. the von-Mises stress, might be more suitable for ductile material and low cycle fatigue [30,31]. Fig. 2 reports the effects of the different choices of driving force (σ_1: first principal stress; σ_v: von-Mises stress) on the fatigue life and crack propagation rate in the example of CT-specimen [32]. It is noted that using the von-Mises stress as the fatigue driving force yields a shorter fatigue life and a lower crack propagation rate as compared to using the first principal stress. Moreover, the mean stress corrector can be applied to include the mean stress effect in the fatigue crack propagation [16]. The parameter D_c is a damage threshold, which models the crack nucleation process. The Macaulay brackets

$$\langle x \rangle^n = \begin{cases} 0 & \text{if} \quad x \leq 0 \\ x^n & \text{if} \quad x > 0, \end{cases} \tag{7}$$

enforces the fatigue contribution to vanish if the damage parameter is smaller than this threshold D_c. After the damage parameter overcomes this threshold D_c, the numerical parameters q and b control how fast the fatigue energy grows.

3. Phase field fatigue simulation of engineering problems

Fatigue tests are mechanical experiments to determine fatigue life. In the standard fatigue test, one side of the specimen is fixed, and on the other side, a periodic loading is applied. A detailed description of the fatigue test procedure can be found in [33]. Fig. 3 reports the fatigue life of different materials (**a**: AISI316L; **b**: Ti6Al4V; **c**: Al6061T6) using the phase field model. The material properties of those materials are listed in Table 1 [34–36], Table 2 [34,37,38] and Table 3 [34,39]. It should be noted that the tested materials possess different fatigue strengths and fatigue parameters, which yield different fatigue behaviors until the material is broken.

The specimen with Ti6Al4V appears to have a maximal fatigue strength among all samples, where it fails first after around 100,000 cycles under a stress amplitude of 505 MPa. It is shown that the number of cycles to failure using the presented methods is slightly lower than compared with the experimental data.

For further investigations, Fig. 4 reports the fatigue life of AISI316L under different maximum stresses. The experiment and simulation are

Table 1
AISI316L material property.

Material property	Value
Modulus of Elasticity E	193 GPa
Poissons ratio ν	0.25
Critical energy release rate $\mathcal{G}_c$	114000 N/m^2
Fatigue limit A_D	146.45 MPa
Knee point cycle number n_D	7 893 764
Slope Factor k	8.9

Table 2
Ti6Al4V material property.

Material property	Value
Modulus of Elasticity E	113 GPa
Poissons ratio ν	0.342
Critical energy release rate $\mathcal{G}_c$	27953 N/m^2
Fatigue limit A_D	460 MPa
Knee point cycle number n_D	550 000
Slope Factor k	7.4

Table 3
Al6061T6 material property.

Material property	Value
Modulus of Elasticity E	68.9 GPa
Poissons ratio ν	0.33
Critical energy release rate $\mathcal{G}_c$	13697 N/m^2
Fatigue limit A_D	82.73 MPa
Knee point cycle number n_D	10 000 000
Slope Factor k	9.36

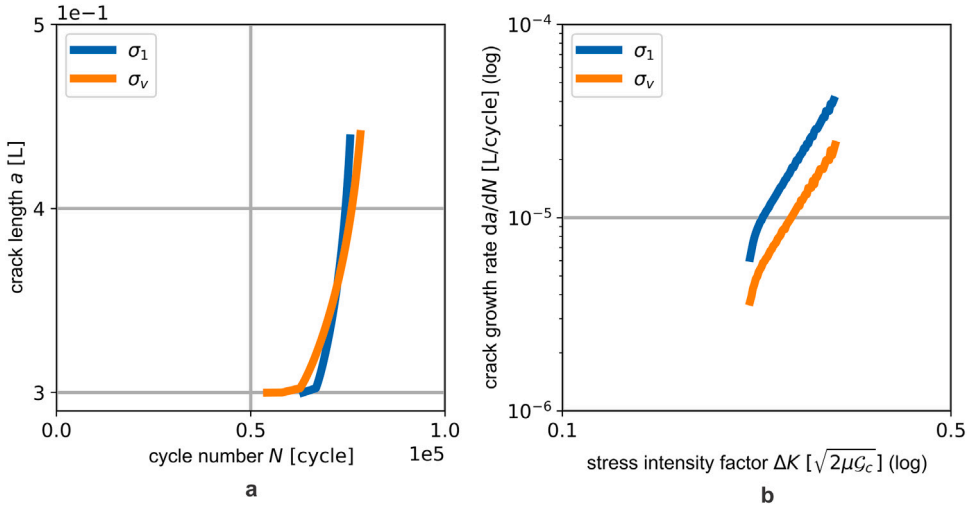

Fig. 2. Different choices (σ_1: first principal stress; σ_v: von-Mises stress) of the fatigue driving force and its effect on the crack evolution. The stress intensity factor is calculated from [29]. In the presented work, the fatigue driving force is taken as the first principal stress since the presented model is suitable for the high cycle fatigue regime.

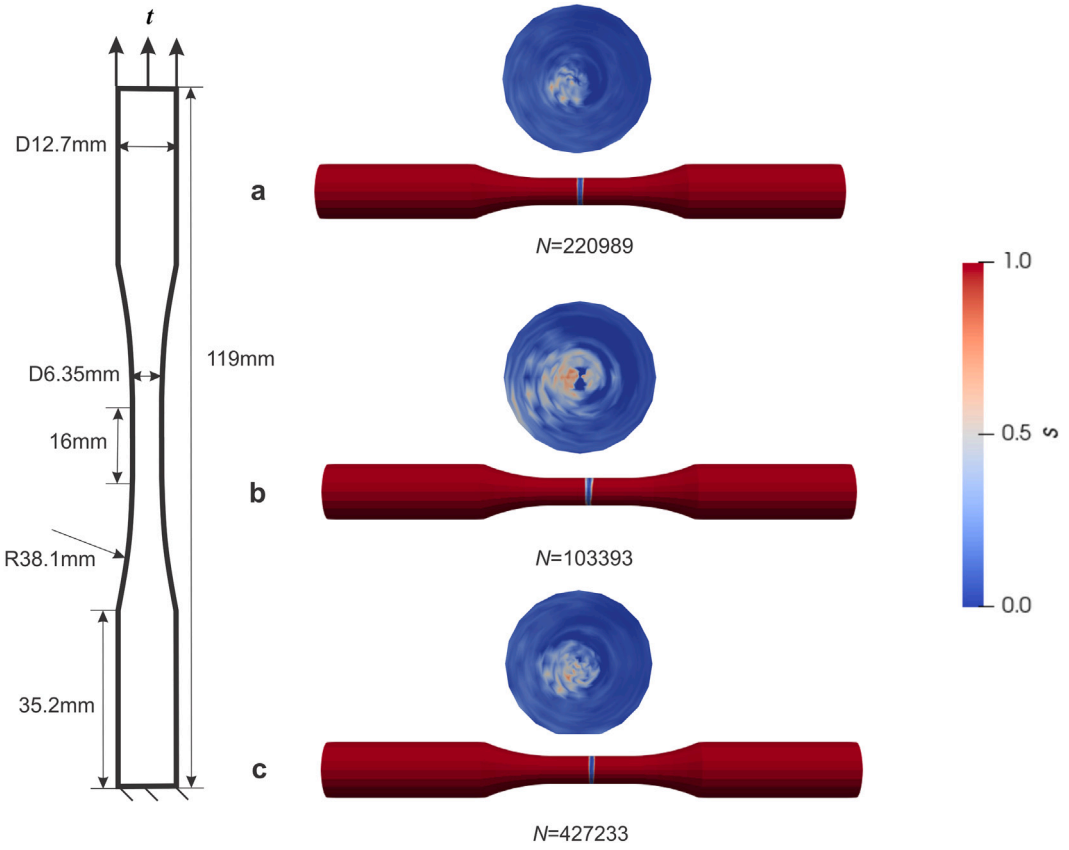

Fig. 3. Fatigue test using phase field model (**a**: AISI316L (236 MPa); **b**: Ti6Al4V (505 MPa); **c**: Al6061T6 (107 MPa)). The different fatigue life of materials are obtained from the phase field simulation.

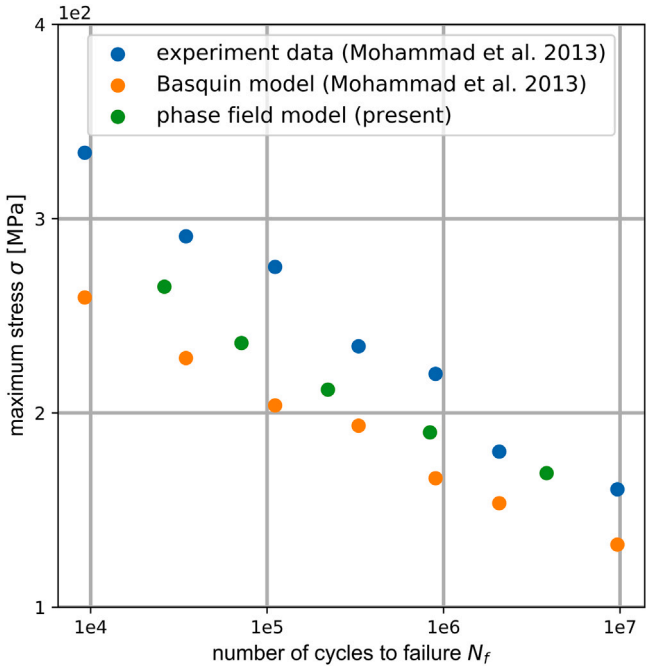

Fig. 4. Fatigue life of AlSl316L from simulation compared to experiment data and Basquin model. It is to notice that the results from the phase field simulation lie between the experiment data and the Basquin model.

set up with a stress ratio of $R = 0.1$ and a loading frequency of 5 Hz. It is noted that the results from the phase field model have a similar degradation tendency of fatigue life compared to the experiment. Moreover, it is shown that the results from the phase field simulation lie between the experiment data and the Basquin model [35,40]. Generally speaking, the results obtained from the phase field model yield a smaller number of cycles to failure compared to experiment data; however, this provides a safe estimate of the lifetime of engineering and manufacturing processes.

Unlike the degradation function-based phase field fatigue model, e.g., Carrara et al. [13], in our approach various fatigue parameters are put together into the damage parameter D, which would change based on how the fatigue damage is accumulated. Consequentially, it leads to different fatigue crack evolution behaviors. For example, as a result, the effect of the loading frequency is naturally considered by the choice of the different fatigue property parameters in the damage variable D. In the following phase field simulation, the material considered is low carbon steel S15C. The material fatigue properties are taken from the Wöhler curve, see [41,42].[1]

Material property	Value				
Modulus of Elasticity E	207 GPa				
Poissons ratio ν	0.285				
Critical energy release rate $\mathcal{G}_c$	29576 N/m^2				
Test frequency	0.2 Hz	2 Hz	20 Hz	140 Hz	20 kHz
Fatigue limit A_D	(185 MPa)	185 MPa	185 MPa	200 MPa	248 MPa
Knee point cycle number n_D	$(5 \cdot 10^5)$	$9 \cdot 10^5$	$1.1 \cdot 10^6$	$2 \cdot 10^6$	$6 \cdot 10^7$
Slope Factor k	4.09	9.55	11.01	18.57	37.91

[1] The fatigue limit A_D and the knee point cycle number n_D of 0.2 Hz frequency loading are not provided by [42].

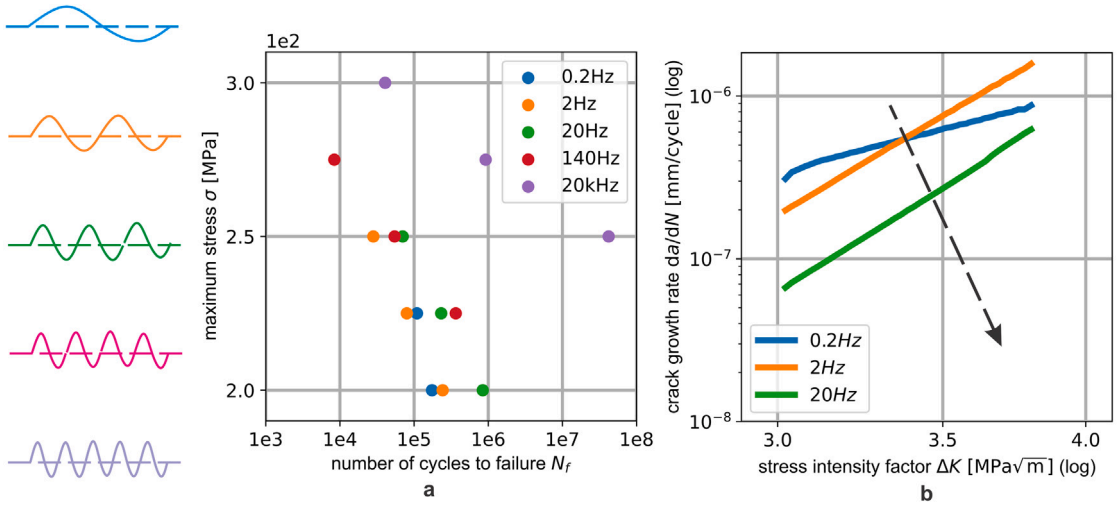

Fig. 5. Loading frequency influence on the **a** : fatigue life and **b** : crack growth rate. It is shown that the fatigue life increases with higher loading frequency.

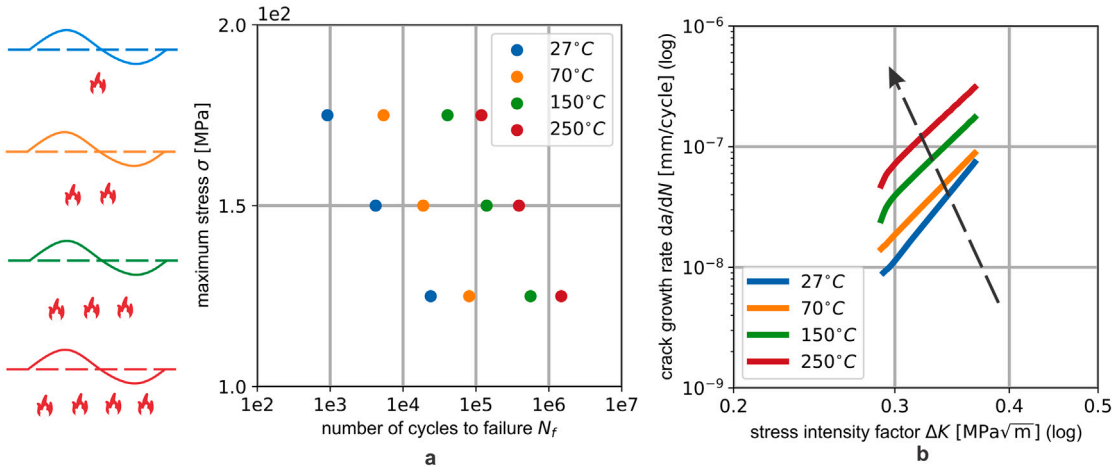

Fig. 6. Loading temperature influence on the **a** : fatigue life and **b** : crack growth rate. It is to notice that higher temperature leads to a longer fatigue life.

Fig. 5 depicts the fatigue life (using fatigue test [33]) and the stable crack propagation rate from the Paris' law (using CT-specimen [32]) for low carbon steel under different loading frequencies. It is shown that by increasing the loading frequency, the material has a longer fatigue life. In contrast, simulations on CT-specimen show that the fatigue crack growth rate of low carbon steel decreases with higher loading frequency. Those results can be verified by the experiment findings in [41,42]. Similarly, the phase field model assumes fatigue parameters (k, n_D, and A_D) cover all the loading temperature effects of the fatigue evolution. In the presented example, an Al6061T6 specimen is considered. The material fatigue properties are taken from [39].

Material property	Value			
Test temperature	27 °C	70 °C	150 °C	250 °C
Fatigue limit A_D	100 MPa	100 MPa	100 MPa	100 MPa
Knee point cycle number n_D	$9 \cdot 10^5$	$1.1 \cdot 10^6$	$2 \cdot 10^6$	$2.5 \cdot 10^6$
Slope Factor k	9.57	7.99	7.64	7.44

As shown in Fig. 6, the loading temperature has similar effects on both the fatigue life and the stable crack growth rate. Higher temperature allows for a higher fatigue life of the aluminum alloy, whereas for a given loading of 125 MPa, the aluminum specimen breaks first after 23,935 number of cycles at 27 °C but after 1,477,226 number of cycles at 270 °C. It is also interesting to notice that loading temperature has a positive correlation with the crack growth rate in simulations of CT-specimen: a high temperature can accelerate the speed of the crack propagation. Similar fatigue behavior of aluminum alloy can be found in the literature [39,43].

4. A phase field model for thermal fatigue fracture

When a material is under rapidly alternating heating and cooling, the temperature of the material's surface and interior will be different, leading to the expansion or contraction of the material. This non-uniform deformation of the material generates thermal stresses. In general, compressive stresses are produced when the loading process is at high temperatures; alternatively, tensile stresses occur when the material is cooled [44]. This cyclic expansion and contraction of material causes material fatigue. In order to include the thermal aspect in the phase field model, let us again look at the total energy density of the body ψ (Eq. (1)). Instead of using Eq. (2), the strain energy density is modified to consider an additional strain contribution generated by fluctuating temperature

$$\psi^e = \frac{1}{2}(\boldsymbol{\varepsilon} - \boldsymbol{\varepsilon}_T) : \mathbb{C}(\boldsymbol{\varepsilon} - \boldsymbol{\varepsilon}_T), \tag{8}$$

where $\boldsymbol{\varepsilon}_\mathrm{T}$ is the thermal strain, which can be calculated by [45]

$$\boldsymbol{\varepsilon}_\mathrm{T} = \kappa \mathbf{1} \Delta T. \tag{9}$$

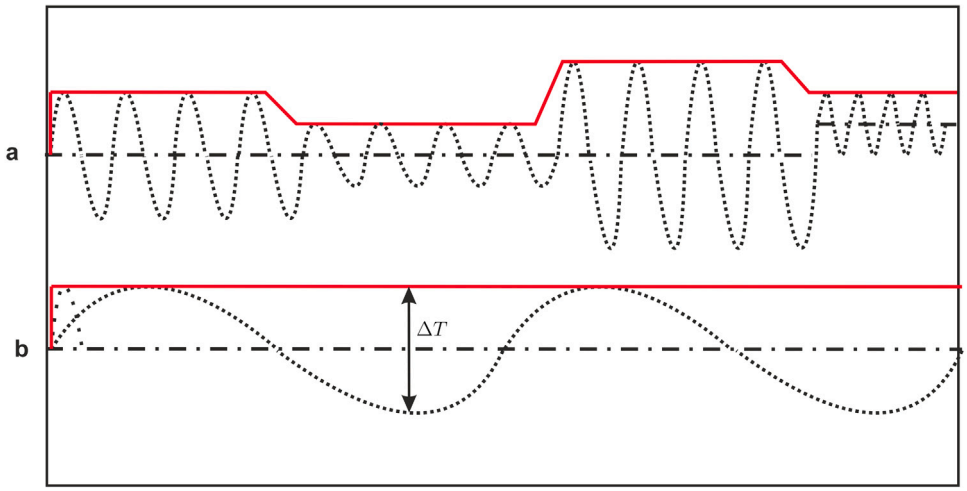

Fig. 7. An illustration of the "cycle"-"time" transfer: the simulation is using the continuous "time" (in red) for the purpose of efficiency. For the mechanical loading (**a**), the enveloping loading is taken for the simulation, and for the temperature loading (**b**) is the difference between the low- and high temperatures ΔT is taken.

The constant κ is the thermal expansion coefficient, which describes the amount of material expansion in relation to a temperature change. The tensor $\mathbf{1}$ denotes the second order unit tensor and ΔT is the temperature difference to a reference temperature. It is to be noted that a positive temperature difference $(T_{\text{high}} - T_{\text{low}})$ for a single heating process generates compressive stresses in the body, which will not lead to a fracture for many material [8]. However, in a cyclic thermal loading scenario, the material is subjected to repeated heating and cooling. As the temperature increases, the material becomes more ductile [46]; when it cools down, the thermal tensile stresses are developed and lead to thermal fatigue. Thus, the thermal effects are introduced in Eqs. (8) and (9) of the extended phase field fatigue model. Especially, a spatially varying temperature ΔT can be introduced via Eq. (9). However, heat conduction is not considered, thus the temperature gradient is considered in more detail.

Speaking of high cycle fatigue, the number of cycles to failure is usually in the order of tens of millions. As a result, simulating the accumulated cycles one after the other is not suitable for effective computing. The first step of an efficient computing concept is proposed by Chaboche [28] to bundle several cycles with similar loading into blocks. Recently, a "cycle"-"time" transfer of the phase field fatigue model is introduced, which assumes a constant block size of cycle number per time $\frac{\mathrm{d}N}{\mathrm{d}t}$ representing a certain evolution of fatigue damage [15,17]. The "cycle"-"time" transfer for the cyclic temperature loading is based on the same concept. For the phase field simulation, each single fluctuating temperature loading is not explicitly modeled; instead, the temperature change is taken as the difference between the high- and low temperatures $\Delta T = T_{\text{low}} - T_{\text{high}}$, and several cyclic temperature loads are bundled into the simulation "time" (see Fig. 7). However, it is not claimed that this model holds for any thermal boundary conditions. Our model is suitable for the thermal fatigue problem with an inhomogeneous temperature distribution in the body. If the spatial temperature rises in statically determined bodies, some further modifications of the model might be needed.

Let $\boldsymbol{t}$ be the external traction on the boundary of the body $\partial\Omega_t$, the variational formulation of our problem reads

$$\int_\Omega \delta\mathcal{E}\mathrm{d}V - \int_{\partial\Omega_t} \boldsymbol{t}\cdot\delta\mathbf{u}\mathrm{d}A = 0. \tag{10}$$

In order to minimize the total energy by the displacement field $\mathbf{u}$ and the crack field s, the variation of total energy $\mathcal{E}$ reads

$$\delta\mathcal{E} = \int_\Omega \left(\frac{\partial\psi}{\partial\boldsymbol{\epsilon}} : \delta\boldsymbol{\epsilon} + \frac{\partial\psi}{\partial s}\delta s + \frac{\partial\psi}{\partial\nabla s}\cdot\delta\nabla s\right)\mathrm{d}V. \tag{11}$$

Employing the product rule for the strain tensor $\boldsymbol{\epsilon}$

$$\frac{\partial\psi}{\partial\boldsymbol{\epsilon}} : \delta\boldsymbol{\epsilon} = -\mathrm{div}\left(\frac{\partial\psi}{\partial\nabla\mathbf{u}}\right)\delta\mathbf{u} + \mathrm{div}\left(\left(\frac{\partial\psi}{\partial\nabla\mathbf{u}}\right)^T\delta\mathbf{u}\right) \tag{12}$$

as well as on the crack field s

$$\frac{\partial\psi}{\partial\nabla s}\cdot\delta\nabla s = -\mathrm{div}\left(\frac{\partial\psi}{\partial\nabla s}\right)\delta s + \mathrm{div}\left(\frac{\partial\psi}{\partial\nabla s}\delta s\right), \tag{13}$$

and the divergence theorem on Eq. (11) yields

$$\begin{aligned}\delta\mathcal{E} = &\int_\Omega -\mathrm{div}\left(\frac{\partial\psi}{\partial\nabla\mathbf{u}}\right)\delta\mathbf{u}\mathrm{d}V + \int_\Omega\left(\frac{\partial\psi}{\partial s} - \mathrm{div}\frac{\partial\psi}{\partial\nabla s}\right)\delta s\mathrm{d}V\\ &+ \int_{\partial\Omega}\frac{\partial\psi}{\partial\nabla s}\cdot\mathbf{n}\delta s\mathrm{d}A + \int_{\partial\Omega}\left(\frac{\partial\psi}{\partial\nabla\mathbf{u}}\right)^T\mathbf{n}\delta\mathbf{u}\mathrm{d}A\end{aligned} \tag{14}$$

Eq. (14) state four coupled Euler–Lagrange equations to describe the entire crack evolution of the thermomechanical problem.

$$\mathrm{div}\frac{\partial\psi}{\partial\nabla\mathbf{u}} = 0 \tag{15}$$

$$\frac{\partial\psi}{\partial s} - \mathrm{div}\frac{\partial\psi}{\partial\nabla s} = 0 \tag{16}$$

$$\frac{\partial\psi}{\partial\nabla s}\cdot\mathbf{n} = 0 \quad \text{on } \partial\Omega_{\nabla s} \tag{17}$$

$$\left(\frac{\partial\psi}{\partial\nabla\mathbf{u}}\right)^T\mathbf{n} = \boldsymbol{t} \quad \text{on } \partial\Omega_t, \tag{18}$$

where the vector $\mathbf{n}$ denotes the normal vector outward to the domain; and the boundary $\partial\Omega_{\nabla s}$ and $\partial\Omega_t$ are the boundaries associated with the gradient of the crack field ∇s and traction $\boldsymbol{t}$. Eq. (15) describes the equilibrium of the stress field. It is noted that the stress field with the thermal effect taken into account is given now by

$$\boldsymbol{\sigma} = \frac{\delta\psi}{\delta\nabla\mathbf{u}} = (g(s)+\eta)\mathbb{C}(\boldsymbol{\epsilon}-\boldsymbol{\epsilon}_T) = (g(s)+\eta)\underbrace{\mathbb{C}\boldsymbol{\epsilon}}_{\boldsymbol{\sigma}_e} - (g(s)+\eta)\underbrace{\mathbb{C}\boldsymbol{\epsilon}_T}_{\boldsymbol{\sigma}_T}, \tag{19}$$

where the first term $\boldsymbol{\sigma}_e$ is the stress from the mechanical loading, and the later contribution $\boldsymbol{\sigma}_T$ is the stress resulting from the local temperature difference of the body. Similarly to [15], the fatigue driving force is taken as the first principal stress without degradation

$$\hat{\sigma} = \sigma_1 = [\mathbb{C}(\boldsymbol{\epsilon}-\boldsymbol{\epsilon}_\mathrm{T})]_1 = [\boldsymbol{\sigma}-\boldsymbol{\sigma}_T]_1, \tag{20}$$

which has a mechanical stress contribution and thermal stress contribution. Eq. (16) can be extended to a regularized form consistent with a mechanical view of the second law of thermodynamics [47], providing the evolution equation of the crack field

$$\frac{\mathrm{d}s}{\mathrm{d}N} = -M\frac{\delta\psi}{\delta s} = -M\left(\frac{\partial\psi}{\partial s} - \mathrm{div}\frac{\partial\psi}{\partial\nabla s}\right), \tag{21}$$

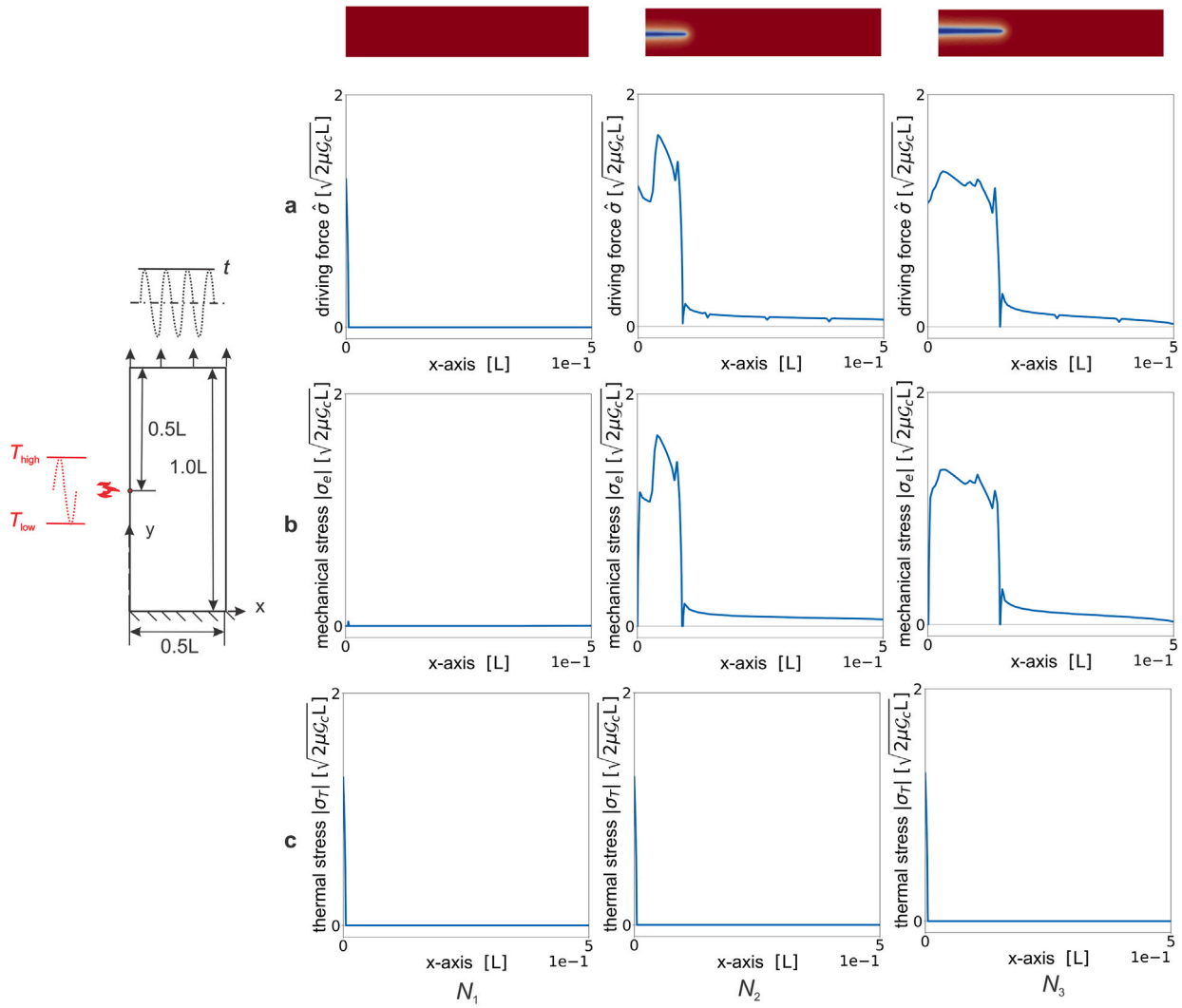

Fig. 8. An example of thermal fatigue with the stress development (**a**: driving force; **b**: mechanical stress; **c**: thermal stress) during the crack propagation. It is to conclude that the thermal stress is mainly responsible for the fatigue crack nucleation and mechanical load is the driving force for the crack extension.

where $M > 0$ is a mobility parameter, which models the "viscosity"(rate dependency) of the phase field fracture model for quasi static case. For M is a constant, Eq. (21) resembles the standard Ginzburg–Landau evolution equation [24,48]. Additionally, for a limit case of $M \to \infty$, Eq. (21) approximates the quasi-static limit case of the phase field fatigue model with $\frac{\delta\psi}{\delta s} = 0$. For fatigue fracture, the mobility parameter M controls the dependency for the crack propagation on cycle increment in the cyclic domain. The last two equations (Eqs. (17) and (18)) are the Neumann boundary conditions for the crack field and the stress field. Those equations (Eqs. (15)–(18)) are the governing equations of the presented thermomechanical problem.

Fig. 8 displays the crack propagation for a thermal point source. In this numerical example, a regular quadrilateral geometry is given, where the upper surface is loaded with uniform stresses of frequency 200 Hz and the bottom is fixed. In addition, a point of fluctuating thermal source with a frequency of 0.2 Hz is applied in the middle of the left side of the square geometry, providing inhomogeneous heating and cooling in the specimen. The results show that the first crack initializes after 4,610 cycles of thermal loading, and then the crack propagates in a straight line horizontally to the right. For further investigation of the crack evolution behavior, the magnitude of the fatigue driving force $\hat{\sigma}$, the mechanical stress $|\boldsymbol{\sigma}_e|$ and the thermal stress $|\boldsymbol{\sigma}_T|$ on the line of the crack propagation direction are provided. At cycle N_1, where the cracks are still in nucleation and not microscopically visible, the mechanical stress is at almost zero along the evaluated line. However, the thermal stress peaks on the left side of the line ($x = 0$), which provides the fatigue driving force for the crack nucleation. At later cycles N_2 and N_3, the mechanical stresses can be found to increase with the material breaking; at the same time, a small mechanical stress impulse is observed at the crack fronts, which is the driving force for the crack extending. On the other hand, the thermal stress remains unaltered during the simulation because heat transfer is not considered in the presented framework. Thermal point sources in different temperature gradients are used with the same numerical setup for further investigation of the effect of thermal stress. Fig. 9**a** shows that the thermal source with lower temperature gradient results in longer fatigue life, whereas a temperature difference of $\Delta T = 500$ K requires nearly 35% more number of cycles than $\Delta T = 800$ K to break the specimen. Although the temperature gradients are different, it is shown in Fig. 9**b** that the crack growth rate in those thermal conditions remains almost the same, which is inconsistent with the findings in the literature for many materials [49,50]. Thus, heat transfer as an additional field evolution for the temperature field should be considered in the future work. In Fig. 9**c**, the mechanical loading on

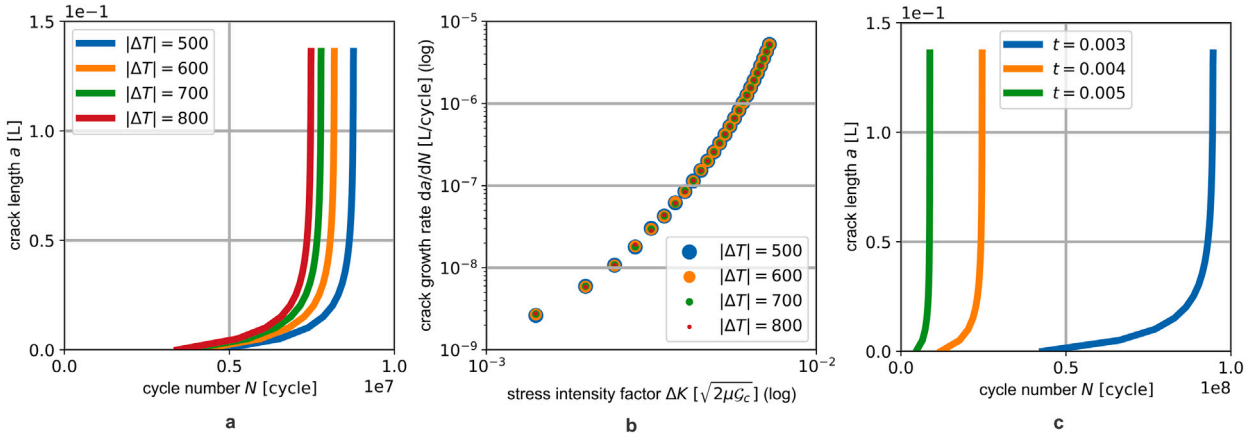

Fig. 9. Different temperature gradient differences result in different fatigue life (in **a**), but the crack growth rate remains almost the same (in **b**). In **c**, the mechanical loading t $[\sqrt{\frac{2\mu G_c}{L}}]$ is changed while the heat source is fixed.

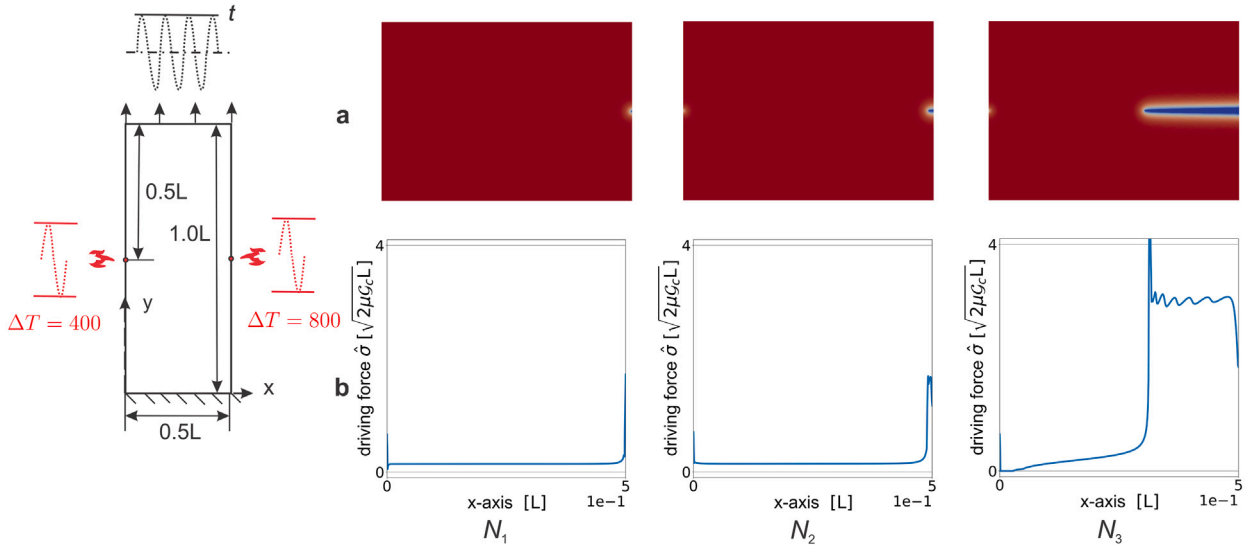

Fig. 10. The first crack nucleates at the higher temperature source (left) at $N_1 = 26{,}340$. The second crack subsequently nucleates at $N_2 = 821{,}292$, and the already nucleated crack from the right side propagates further. In **a**: the crack pattern; in **b**: the fatigue driving force.

the top of the square is changed, whereas the temperature difference of the heat source is fixed. As expected, a higher mechanical loading can accelerate the fatigue process overall.

Thermal expansion coefficient κ	1e-6 K^{-1}
Temperature difference $\lvert\Delta T\rvert$	500 K

Furthermore, we present two additional case studies involving various thermal loading scenarios. In the following example, two thermal sources are positioned on both sides of the geometry, each with different values of the temperature differences (left: $\Delta T = 400$ K and right: $\Delta T = 800$ K), as depicted in Fig. 10. It is noteworthy that the first crack initiates on the right side of the geometry, which has a higher temperature gradient. This behavior is attributed to the driving force mechanism of the presented phase field model: fatigue cracks initiate at locations where the maximum fatigue driving force is found. The higher temperature gradient on the right side contributes to a higher total stress compared to the left side, leading to crack nucleation there. As the cycle number continuously rises, a new crack also nucleates on the left side of the geometry (see cycle N_2) due to the increasing fatigue damage. At the same time, the crack from the right side propagates toward the middle, as illustrated in Fig. 10 at N_3.

In the last example, a single thermal source is specified at the center of the geometry (refer to Fig. 11). Here, crack nucleation occurs at the midpoint of the geometry, where higher thermal stress is present. Subsequently, cracks propagate in both directions, driven by the mechanical contribution of the fatigue driving force. It can be concluded here that the localized thermal stress is mainly responsible for the fatigue crack nucleation due to the high local stress, and the mechanical load is the driving force for the crack extension due to the global action of this load.

5. Conclusion

In this work, the thermomechanical fatigue problem is simulated by the proposed phase field model. The phase field model introduces a scalar variable to represent the crack state, and two coupled equations for the displacement field and the crack field are derived based on the variational principle to describe the crack evolution. The phase field fatigue model introduces an additional energy term to represent the accumulated fatigue driving force related to the fatigue damage. It is shown that the fatigue parameter, which is coupled with Wöhler curve (SN curve) from experiments, can take the complex effects of the environment into account. Besides the cyclic mechanical loading,

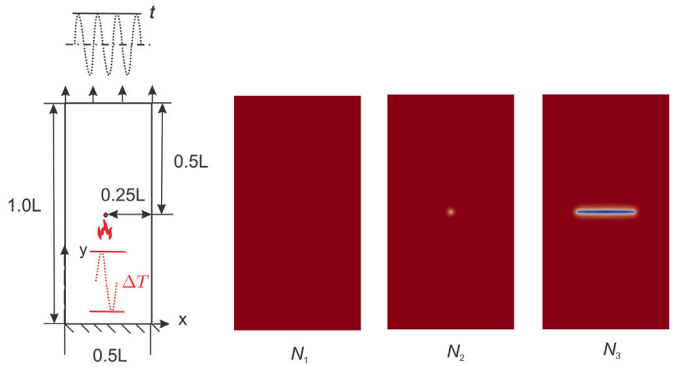

Fig. 11. A single thermal source is located at the center of the square. After a crack nucleates, it extends to both sides.

fatigue cracks can also be a result of the fluctuating temperature known as the thermal fatigue phenomenon. A contribution of this work is that we consider thermal stress as the second fatigue driving force in the phase field fatigue model, which allows the fatigue crack resulting from the repeated temperatures to be simulated. Results show that a higher temperature difference leads to a shorter fatigue life of the material. Overall, the localized thermal stress contributes more to crack nucleation and the mechanical stress has a global influence on crack evolution. In future work, heat transfer will be considered in the presented thermomechanical fatigue phase field model.

CRediT authorship contribution statement

Sikang Yan: Writing – original draft. **Ralf Müller:** Funding acquisition, Supervision, Writing – review & editing. **Bahram Ravani:** Supervision, Writing – review & editing.

Declaration of competing interest

The authors declare that they have no known competing financial interests or personal relationships that could have appeared to influence the work reported in this paper.

Data availability

Data will be made available on request.

Acknowledgments

Funded by the Deutsche Forschungsgemeinschaft (DFG, German Research Foundation) - 252408385 -IRTG 2057.

References

[1] G.A. Francfort, J.-J. Marigo, Revisiting Brittle fracture as an energy minimization problem, J. Mech. Phys. Solids 46 (8) (1998) 1319–1342.
[2] B. Bourdin, G.A. Francfort, J.-J. Marigo, Numerical experiments in revisited Brittle fracture, J. Mech. Phys. Solids 48 (4) (2000) 797–826.
[3] B. Bourdin, Numerical implementation of the variational formulation for quasi-static Brittle fracture, Interfaces Free Bound. 9 (3) (2007) 411–430.
[4] A.A. Griffith, VI. The phenomena of rupture and flow in solids, Philos. Trans. R. Soc. Lond. Ser. A Contain. Pap. Math. Phys. Charact. 221 (582–593) (1921) 163–198.
[5] B. Bourdin, G.A. Francfort, J.-J. Marigo, The variational approach to fracture, J. Elasticity 91 (1–3) (2008) 5–148.
[6] C. Kuhn, R. Müller, A continuum phase field model for fracture, Eng. Fract. Mech. 77 (18) (2010) 3625–3634.
[7] H. Amor, J.-J. Marigo, C. Maurini, Regularized formulation of the variational Brittle fracture with unilateral contact: Numerical experiments, J. Mech. Phys. Solids 57 (8) (2009) 1209–1229.
[8] C. Miehe, F. Welschinger, M. Hofacker, Thermodynamically consistent phase-field models of fracture: Variational principles and multi-field FE implementations, Internat. J. Numer. Methods Engrg. 83 (10) (2010) 1273–1311.
[9] A. Schlüter, A. Willenbücher, C. Kuhn, R. Müller, Phase field approximation of dynamic Brittle fracture, Comput. Mech. 54 (5) (2014) 1141–1161.
[10] T. Noll, C. Kuhn, R. Müller, A monolithic solution scheme for a phase field model of ductile fracture, PAMM 17 (1) (2017) 75–78.
[11] T. Gerasimov, L. De Lorenzis, A line search assisted monolithic approach for phase-field computing of Brittle fracture, Comput. Methods Appl. Mech. Engrg. 312 (2016) 276–303.
[12] R. Alessi, S. Vidoli, L. De Lorenzis, A phenomenological approach to fatigue with a variational phase-field model: The one-dimensional case, Eng. Fract. Mech. 190 (2018) 53–73.
[13] P. Carrara, M. Ambati, R. Alessi, L. De Lorenzis, A framework to model the fatigue behavior of brittle materials based on a variational phase-field approach, Comput. Methods Appl. Mech. Engrg. 361 (2020) 112731.
[14] M.M. Hasan, T. Baxevanis, A phase-field model for low-cycle fatigue of Brittle materials, Int. J. Fatigue 150 (2021) 106297.
[15] C. Schreiber, C. Kuhn, R. Müller, T. Zohdi, A phase field modeling approach of cyclic fatigue crack growth, Int. J. Fract. 225 (1) (2020) 89–100.
[16] C. Schreiber, R. Müller, C. Kuhn, Phase field simulation of fatigue crack propagation under complex load situations, Arch. Appl. Mech. (2020) 1–15.
[17] S. Yan, C. Schreiber, R. Müller, An efficient implementation of a phase field model for fatigue crack growth, Int. J. Fract. (2022) 1–14.
[18] K. Seleš, F. Aldakheel, Z. Tonković, J. Sorić, P. Wriggers, A general phase-field model for fatigue failure in Brittle and ductile solids, Comput. Mech. 67 (5) (2021) 1431–1452.
[19] J.-Y. Wu, Y. Huang, V.P. Nguyen, On the BFGS monolithic algorithm for the unified phase field damage theory, Comput. Methods Appl. Mech. Engrg. 360 (2020) 112704.
[20] J.-Y. Wu, Y. Huang, Comprehensive implementations of phase-field damage models in Abaqus, Theor. Appl. Fract. Mech. 106 (2020) 102440.
[21] G. Amendola, M. Fabrizio, J. Golden, Thermomechanics of damage and fatigue by a phase field model, J. Therm. Stress. 39 (5) (2016) 487–499.
[22] C. Du, H. Cui, H. Zhang, Z. Cai, W. Zhai, Phase field modeling of thermal fatigue crack growth in elastoplastic solids and experimental verification, Mech. Mater. 188 (2024) 104839.
[23] C. Schreiber, Phase Field Modeling of Fracture: Fatigue and Anisotropic Fracture Resistance, Technische Universität Kaiserslautern, 2021.
[24] V.L. Ginzburg, L.D. Landau, On the theory of superconductivity, in: On Superconductivity and Superfluidity, Springer, 2009, pp. 113–137.
[25] D. Mumford, J. Shah, Boundary detection by minimizing functionals, in: IEEE Conference on Computer Vision and Pattern Recognition. Vol. 17, San Francisco, 1985, pp. 137–154.
[26] M.J. Borden, T.J. Hughes, C.M. Landis, C.V. Verhoosel, A higher-order phase-field model for Brittle fracture: Formulation and analysis within the isogeometric analysis framework, Comput. Methods Appl. Mech. Engrg. 273 (2014) 100–118.
[27] M.A. Miner, Cumulative damage in fatigue, J. Appl. Mech. (1945).
[28] J. Chaboche, P. Lesne, A non-linear continuous fatigue damage model, Fatigue Fract. Eng. Mater. Struct. 11 (1) (1988) 1–17.
[29] J.E. Srawley, Wide range stress intensity factor expressions for ASTM E 399 standard fracture toughness specimens, Int. J. Fract. 12 (3) (1976) 475–476.
[30] R.V. Mises, Mechanik der festen Körper im plastisch-deformablen Zustand, Nachrichten von der Gesellschaft der Wissenschaften zu Göttingen, Mathematisch-Physikalische Klasse 1913 (1913) 582–592.
[31] A. Pineau, C. Bathias, Fatigue of Materials and Structures, Fundamentals, John Wiley & Sons, Inc, Hoboken, NJ, USA, 2010.
[32] ASTM, ASTM E399-09, Standard Test Method for Linear-Elastic Plane-Strain Fracture Toughness K Ic of Metallic Materials, Tech. rep., 2009, http://www.astm.org.
[33] ASTM, ASTM E606, Standard Test Method for Strain-Controlled Fatigue Testing, Tech. rep., 2021, http://www.astm.org.
[34] H.E. Boyer, T.L. Gall, Metals handbook; desk edition, 1985.
[35] K.A. Mohammad, E.S. Zainudin, S. Sapuan, N.I. Zahari, A. Aidy, Fatigue life for type 316l stainless steel under cyclic loading, in: Key Engineering Materials III, in: Advanced Materials Research, vol.701, Trans Tech Publications Ltd, 2013, pp. 77–81, http://dx.doi.org/10.4028/www.scientific.net/AMR.701.77.
[36] D. Roylance, Introduction to Fracture Mechanics, Department of Materials Science and Engineering, Massachusetts Institute of Technology, 2001.
[37] J. Lin, W. Li, S. Yang, J. Zhang, Vibration fatigue damage accumulation of Ti–6Al–4V under constant and sequenced variable loading conditions, Metals 8 (5) (2018) 296.
[38] S.A. Ojo, Use of Compact Specimens to Determine Fracture Toughness and Fatigue Crack Growth Anisotropy of DED Additive Manufactured Ti-6Al-4V (Ph.D. thesis), University of Akron, 2020.
[39] K. Zakaria, S. Abdullah, M. Ghazali, Elevated temperature fatigue life investigation of aluminium alloy based on the predicted SN curve, Jurnal Teknol. 63 (1) (2013).
[40] O. Basquin, The exponential law of endurance tests, in: Proc Am Soc Test Mater. Vol. 10, 1910, pp. 625–630.

[41] B. Guennec, A. Ueno, T. Sakai, M. Takanashi, Y. Itabashi, Effect of the loading frequency on fatigue properties of JIS S15C low carbon steel and some discussions based on micro-plasticity behavior, Int. J. Fatigue 66 (2014) 29–38, http://dx.doi.org/10.1016/j.ijfatigue.2014.03.005, URL https://www.sciencedirect.com/science/article/pii/S0142112314000875.
[42] N. Tsutsumi, Y. Murakami, V. Doquet, Effect of test frequency on fatigue strength of low carbon steel, Fatigue Fract. Eng. Mater. Struct. 32 (6) (2009) 473–483.
[43] X. Zhu, J. Jones, J. Allison, Effect of frequency, environment, and temperature on fatigue behavior of E319 cast aluminum alloy: Stress-controlled fatigue life response, Metall. Mater. Trans. A 39 (11) (2008) 2681–2688.
[44] Q. Xin, Diesel Engine System Design, Elsevier, 2011.
[45] W.D. Callister, D.G. Rethwisch, Materials Science and Engineering: An Introduction. Vol. 9, Wiley New York, 2018.
[46] W.F. Hosford, Mechanical Behavior of Materials, Cambridge University Press, 2010.
[47] M.E. Gurtin, Generalized Ginzburg-Landau and cahn-hilliard equations based on a microforce balance, Physica D 92 (3–4) (1996) 178–192.
[48] C. Kuhn, Numerical and Analytical Investigation of a Phase Field Model for Fracture (Ph.D. thesis), Technische Universität Kaiserslautern, 2013, p. X, 143, URL http://nbn-resolving.de/urn:nbn:de:hbz:386-kluedo-35257.
[49] J. Palmer, J. Jones, M. Whittaker, S. Williams, Thermo-mechanical fatigue crack growth and phase angle effects in Ti6246, Materials 15 (18) (2022) 6264.
[50] F. Palmert, J. Moverare, D. Gustafsson, Thermomechanical fatigue crack growth in a single crystal nickel base superalloy, Int. J. Fatigue 122 (2019) 184–198.

III. Third paper

Published in:
Forces in Mechanics, p. 100239 (2023)
DOI: https://doi.org/10.1016/j.finmec.2023.100239

III.1. Objectives of the third paper

In the last decades, the phase field method has drawn much attention for its application in fracture mechanics because it offers a simple unified framework for crack propagation. The core idea of phase field models for fracture is to introduce a continuous scalar field representing the discontinuous crack. Recently, a phase field model for fatigue has been proposed along this path. The fatigue failure differs from the other fracture scenarios, since cracks only occur after a considerable number of load cycles. As fracturing happens, changes in the material microstructure are involved, which causes the evolution of the structural configuration. Thus, a new mathematical description not based on traditional spatial coordinates, but on the material manifold is desired, which will serve as an elegant analysis tool to understand the energetic forces for crack propagation. Configurational forces are a suitable choice for this purpose, as they describe the energetic driving forces associated with phenomena changing the material itself.

In this work, we present a configurational forces-based tool, in which the energy terms of the phase field fatigue model are transformed to different “force” parts. Those different configurational forces play different roles during the crack propagation. Next, the phase field fatigue model is analyzed within the concept of configurational forces, which provides a straightforward way to understand the phase field simulations of fatigue fracture.

Forces in Mechanics 13 (2023) 100239

Contents lists available at ScienceDirect

Forces in Mechanics

journal homepage: www.sciencedirect.com/journal/forces-in-mechanics

Configurational forces in a phase field model for the cyclic fatigue of heterogeneous materials

Sikang Yan [*,a], Alexander Schlüter [a], Erik Faust [a], Ralf Müller [b]

[a] Institute of Applied Mechanics, RPTU Kaiserslautern-Landau, Erwin-Schrödinger-Straße 52, Kaiserslautern, 67655, Germany
[b] Institute for Mechanics, Technical University of Darmstadt, Karolinenplatz 5, Darmstadt, 64289, Germany

ARTICLE INFO

Keywords:
Phase field method
Fatigue fracture
Configurational forces

ABSTRACT

The phase field model - a powerful tool - has been well established to simulate the fatigue crack evolution behavior. However, it is still hard to understand how each energy component in the phase field model contributes to crack evolution since the phase field method is based on an energetic criterion. In this work, we borrow the concept of configurational forces and show a straightforward way to examine the energetic driving forces in the phase field fatigue model. Results show that different parts of the configurational forces provide different energetic contributions during crack propagation.

1. Introduction

Over the last decade, the phase field method has been successfully applied to various fracture mechanics scenarios. The phase field fracture model grew out of the classical Griffith theory's energetic point of view [13], unifying all the crack evolution behaviors in one single equation [5,6,12]. Along this path, the phase field model has been extended to quasi-static fracture [2,19,22], dynamic fracture [4,7] as well as fatigue fracture [1,9,16,29,31,32]. In general, regardless of the specific application of the phase field fracture models, the evolution of cracks is determined by a competition between the release of elastic energy and the growth of crack surface energy. In other words, the crack will propagate in such a way, which is favorable for the total energy. As a specialty of fatigue fracture compared to other cases, the elastic energy here is not the main factor driving crack growth since the applied loads are generally too low to drive macroscopic crack propagation alone. Thus, an additional energy term representing the accumulated fatigue driving forces is included in the total energy of the considered specimen [29].

Despite the phase field fatigue model being well established for fatigue fracture, it is still hard to explain how crack evolution is determined by the phase field model based on the framework of classical mechanics. As Newtonian forces remain invariant under configurational changes, it is convenient to consider motions between different configurations and derive the balance equations. However, fatigue fracture involves microstructural material rearrangement, it is not suitable to describe by the spatial coordinates since the evolution of material structure generally affects the working of standard forces. Thus, it is desired to have a tool which can analyze the fatigue crack evolution based on the material manifold itself. In this work, we provide a way to understand the phase field simulation of fatigue fracture based on the concept of configurational forces. The idea of configurational forces was first developed by Eshelby [11] to study inhomogeneities in elastic materials based on an energetic driving force. Later, a path from configurational forces to its application in fracture mechanics was discussed in [15,21] and examples of its finite element simulation can be found in [8,24]. In addition, a comparative study between the idea of configurational forces and phase field method is shown in Steinke et al. [33]. Recently, a first case to connect the generalized configuration forces and the phase field models of crack evolution is reported by Kuhn and Müller [18] for quasi-static crack propagation and later extended to heterogeneous materials [20]. Schlüter et al. [27] also discussed the configurational forces on dynamic phase field fracture model. In this work, we extend the concept of generalized configuration forces to the phase field fatigue model. Especially, the influences of different kinds of material inhomogeneities on fatigue fracturing are evaluated using the proposed configurational forces tool. The presented work is considered in the framework of linear continuum mechanics with small deformation theory.

* Corresponding author.
E-mail address: yan@rhrk.uni-kl.de (S. Yan).

https://doi.org/10.1016/j.finmec.2023.100239
Received 4 June 2023; Received in revised form 23 July 2023; Accepted 5 October 2023
Available online 6 October 2023

2. A phase field model for cyclic fatigue

Phase field models for fracture introduce an additional field variable to represent cracks [19]. The crack field s assumes a value of 1 if the material remains undamaged, and it is 0 where cracks occur. The crack evolution behavior is derived by applying the variational principle to the total energy of the body Ω [29,37]

$$\mathscr{E} = \int_\Omega \psi(\boldsymbol{\varepsilon}, s, \nabla s, D)\mathrm{d}V = \int_\Omega \left[(g(s)+\eta)\psi^e(\boldsymbol{\varepsilon}) + \psi^s(s,\nabla s) + h(s)\psi^{\mathrm{ad}}(D)\right]\mathrm{d}V, \tag{1}$$

where ψ denotes the total energy density, which is related to the strain tensor $\boldsymbol{\varepsilon}$, the crack field s and its gradient ∇s, as well as a scalar fatigue damage variable D. The strain $\boldsymbol{\varepsilon}$ is the symmetric part of the displacement gradient, i.e., $\boldsymbol{\varepsilon} = \frac{1}{2}(\nabla\mathbf{u} + (\nabla\mathbf{u})^{\mathrm{T}})$. The degradation functions $g(s)$ and $h(s)$ model the loss of stiffness of the broken material. While the function $g(s)$ is applied to the elastic contribution [17], the newly introduced degradation function $h(s)$ works on the fatigue energy part, which allows the fatigue damage directly to be coupled in the crack evolution and models the loss of stiffness of the material due to the cyclic fatigue. In this work, they are taken as $g(s) = h(s) = s^2$ for the benefit of simplicity.

The stain energy density

$$\psi^e(\boldsymbol{\varepsilon}) = \frac{1}{2}\lambda \mathrm{tr}^2(\boldsymbol{\varepsilon}) + \mu\boldsymbol{\varepsilon} : \boldsymbol{\varepsilon} \tag{2}$$

is the energy stored inside the body on account of elastic deformation and $\mathbf{u}$ denotes the displacement field. The parameters λ and μ are the Lamé constants. The fracture surface energy density

$$\psi^s(s,\nabla s) = \mathscr{G}_c\left(\frac{(1-s)^2}{4\epsilon} + \epsilon|\nabla s|^2\right) \tag{3}$$

is the energy required to separate the material in order to generate a crack, which is assumed to be proportional to the surface measure of the crack. The parameter $\mathscr{G}_c$ denotes the fracture resistance and can be related to the fracture toughness, which is the ability of a material to resist fracturing. The numerical parameter ϵ models the width of the smooth transition zone between the broken and unbroken material. The fatigue energy density

$$\psi^{\mathrm{ad}}(D) = q\langle D - D_c\rangle^b \tag{4}$$

is introduced to account for the fatigue driving forces. As shown in Bourdin et al. [3], the crack field does not have any physical interpretation as a damage variable but only indicates the field state. Thus, a new damage parameter D is introduced to model the fatigue damage. The damage parameter D is an internal variable, which does not directly enter into the variational procedure, and the evolution of this parameter is determined by $D = D_0 + \mathrm{d}D$, inspired by Miner's rule [23]. Here, we do not claim this linear damage accumulation model is the only choice for the phase field model, the other choices e.g., nonlinear damage accumulation model [10] might also be suitable. The value D_0 is the previous fatigue damage and $\mathrm{d}D = \frac{\mathrm{d}N}{n_D}\left(\frac{\widehat{\sigma}}{A_D}\right)^k$ is the fatigue damage increment, which is associated with the cycle increment $\mathrm{d}N$. The field $\widehat{\sigma}$ is the fatigue driving force, which is considered to be the first principal stress of the undegraded stress field. The fatigue parameters k, n_D and, A_D can be extracted from the Wöhler curve (SN curve) of fatigue experiments. The parameter D_c is a damage threshold, which is used alongside the Macaulay brackets ($\langle\cdot\rangle$) to model fatigue nucleation. The parameters q and b are used to calibrate the fatigue energy growth speed. Although the classical Miner's rule does not consider the load sequence effect, the presented phase field model is sensitive to cycle history and is able to reproduce the loading sequence effect in crack propagation simulations as shown in [28].

Considering traction forces $\boldsymbol{t}$ acting on the boundary of the domain $\partial\Omega$ and volume forces $\boldsymbol{f}$ acting inside of the domain Ω, our variational problem reads

$$\int_\Omega \delta\psi \mathrm{d}V - \int_{\partial\Omega} \boldsymbol{t}\cdot\delta\mathbf{u}\mathrm{d}A - \int_\Omega \boldsymbol{f}\cdot\delta\mathbf{u}\mathrm{d}V = 0. \tag{5}$$

It is noted that the cyclic repeated loading is approximated with its enveloping loading (maximum tension loading) to reduce the computing effort, which has been discussed in [29,37]. Additionally, the influence from mean stress is modeled by incorporating a mean stress corrector [30]. Since the individual cycle is not explicitly simulated and only tension load is taken within this approximation, a classic tension-compression split ci.e., in [2,22] is no longer necessary here. Applying the variational principle to Eq. (5) yields four coupled equations [37]

$$\mathrm{div}\frac{\partial\psi}{\partial\nabla\mathbf{u}} + \boldsymbol{f} = 0 \tag{6}$$

$$\frac{\partial\psi}{\partial s} - \mathrm{div}\frac{\partial\psi}{\partial\nabla s} = 0 \tag{7}$$

$$\frac{\partial\psi}{\partial\nabla s}\cdot\mathbf{n} = 0 \quad \text{on } \partial\Omega_{\nabla s} \tag{8}$$

$$\left(\frac{\partial\psi}{\partial\nabla\mathbf{u}}\right)\mathbf{n} = \boldsymbol{t} \quad \text{on } \partial\Omega_t. \tag{9}$$

With the constitutive law, Eq. (6) models the equilibrium of the stress field

$$\mathrm{div}\boldsymbol{\sigma} + \boldsymbol{f} = 0 \quad \text{with} \quad \frac{\partial\psi}{\partial\nabla\mathbf{u}} = \boldsymbol{\sigma}. \tag{10}$$

Eq. (7) can be extended to a regularized form consistent with a mechanical view of the second law of thermodynamics [14], which models the evolution of the crack field in a cyclic domain

$$\frac{\mathrm{d}s}{\mathrm{d}N} = -M\frac{\delta\psi}{\delta s} = -M\left(\frac{\partial\psi}{\partial s} - \mathrm{div}\frac{\partial\psi}{\partial\nabla s}\right), \tag{11}$$

where $M > 0$ is a mobility parameter accounting for the "viscosity" of the model [19]. In the presented phase field model, the plastic damage is modeled in the damage parameter D, and the irreversibility of the phase field model is accomplished by modeling Eq. (11) with fixing s if the crack field s is close to 0 [19]. It is noted that different formulations for irreversibility [25,34] can also be used here, and these formulations permit that the crack field may recover as long as $s > 0$. Furthermore, Eqs. (8) and (9) are the Neumann boundary conditions for the crack field and the stress field. It has been shown that the presented phase field model can reproduce the most important fatigue properties as well as predict crack evolution in complex scenarios [29,30,35,37]; however, this work focus to explain the results of phase field simulation using the framework of configurational forces. It is to show that the concept of the configurational forces provides a powerful tool to understand the crack propagation on the defect material.

3. Configurational forces in the phase field model for cyclic fatigue

The starting point to derive the phase field model in the framework of configurational forces is the total energy density of the body. The gradient of the total energy density ψ is computed by the chain rule, where $\frac{\partial\psi}{\partial\mathbf{x}}|_{\mathrm{expl.}}$ accounts for any explicit dependence of ψ on $\mathbf{x}$ (inhomo-

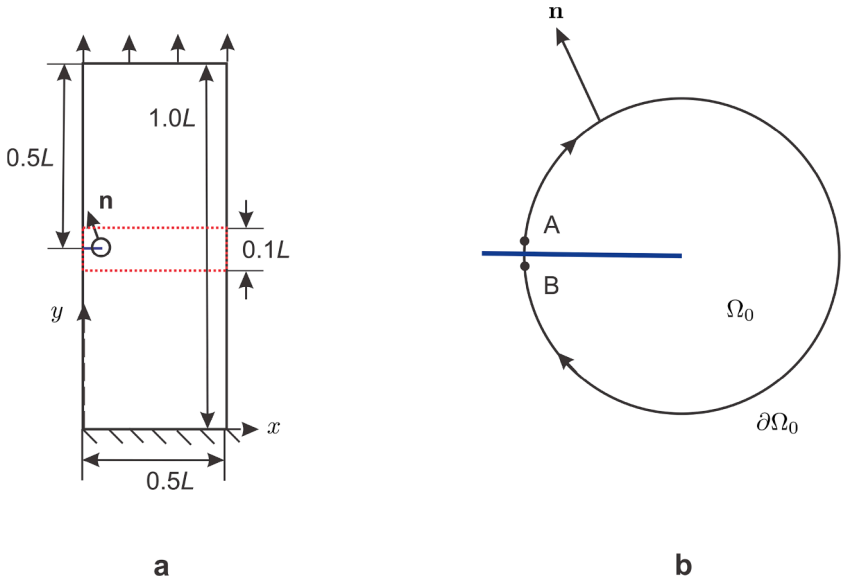

Fig. 1. **a**: the definition of the numerical example with an initial crack of length. The inhomogeneous area is marked with the red rectangle. Additionally, integrals are evaluated over a sufficiently large domain around the crack tip; **b**: control volume around the crack tip for configurational force evaluation. (For interpretation of the references to colour in this figure legend, the reader is referred to the web version of this article.)

geneous material etc.) and $\mathbf{x}^{\text{tip}}$ is the location of the crack tip[1]

$$\nabla\psi = \frac{\partial\psi}{\partial\boldsymbol{\varepsilon}} : \nabla\boldsymbol{\varepsilon} + \frac{\partial\psi}{\partial s}\nabla s + \frac{\partial\psi}{\partial\nabla s}\cdot\left(\nabla s\otimes\nabla\right) + \frac{\partial\psi}{\partial D}\nabla D + \frac{\partial\psi}{\partial\mathbf{x}}|_{\text{expl.}} + \frac{\partial\psi}{\partial\mathbf{x}^{\text{tip}}}\cdot\nabla\mathbf{x}^{\text{tip}}. \tag{12}$$

Noting the relation

$$\frac{\partial\psi}{\partial\nabla s}\cdot\left(\nabla s\otimes\nabla\right) = -\nabla\cdot\left(\frac{\partial\psi}{\partial\nabla s}\right)\nabla s + \nabla\cdot\left(\nabla s\otimes\frac{\partial\psi}{\partial\nabla s}\right) \tag{13}$$

and

$$\frac{\partial\psi}{\partial\boldsymbol{\varepsilon}} : \nabla\boldsymbol{\varepsilon} = -\nabla\mathbf{u}^T\nabla\cdot\boldsymbol{\sigma} + \nabla\cdot\left(\nabla\mathbf{u}^T\boldsymbol{\sigma}\right), \tag{14}$$

Eq. (12) is rewritten as

$$\begin{aligned}\nabla\psi \;=\; & -\nabla\mathbf{u}^T\nabla\cdot\boldsymbol{\sigma} + \nabla\cdot\left(\nabla\mathbf{u}^T\boldsymbol{\sigma}\right)\\ & + \frac{\partial\psi}{\partial s}\nabla s - \nabla\cdot\left(\frac{\partial\psi}{\partial\nabla s}\right)\nabla s + \nabla\cdot\left(\nabla s\otimes\frac{\partial\psi}{\partial\nabla s}\right)\\ & + \frac{\partial\psi}{\partial D}\nabla D + \frac{\partial\psi}{\partial\mathbf{x}}|_{\text{expl.}} + \frac{\partial\psi}{\partial\mathbf{x}^{\text{tip}}}\cdot\nabla\mathbf{x}^{\text{tip}}.\end{aligned} \tag{15}$$

$$\begin{aligned}& \nabla\cdot\underbrace{\left(\psi\mathbf{I} - \nabla\mathbf{u}^T\boldsymbol{\sigma} - \nabla s\otimes\frac{\partial\psi}{\partial\nabla s}\right)}_{\boldsymbol{\Sigma}}\\ & + \underbrace{\frac{1}{M}\frac{\mathrm{d}s}{\mathrm{d}N}\nabla s - \nabla\mathbf{u}^T\boldsymbol{f} - \frac{\partial\psi}{\partial D}\nabla D - \frac{\partial\psi}{\partial\mathbf{x}}|_{\text{expl.}} - \frac{\partial\psi}{\partial\mathbf{x}^{\text{tip}}}\cdot\nabla\mathbf{x}^{\text{tip}}}_{\mathbf{g}} = \mathbf{0}.\end{aligned} \tag{16}$$

We have thus obtained the configurational force balance

$$\nabla\cdot\boldsymbol{\Sigma} + \mathbf{g} = \operatorname{div}\boldsymbol{\Sigma} + \mathbf{g} = \mathbf{0}, \tag{17}$$

where the tensor $\boldsymbol{\Sigma}$ denotes the generalized Eshelby stress tensor and the vector $\mathbf{g}$ denotes the generalized configurational volume forces [17]. This equation gives a simple and elegant relation that defines the energetic forces driving crack growth in the phase field model: the tensor $\boldsymbol{\Sigma}$ defines a stress-like energetic driving force, while the force $\mathbf{g}$ acts as a volume force.

Noting Eq. (16), the generalized Eshelby stress tensor can be split into

$$\begin{aligned}\boldsymbol{\Sigma} \;&=\; \psi\mathbf{I} - \nabla\mathbf{u}^T\boldsymbol{\sigma} - \nabla s\otimes\frac{\partial\psi}{\partial\nabla s}\\ &=\; \underbrace{(g(s)+\eta)\psi^e\mathbf{I} - \nabla\mathbf{u}^T\boldsymbol{\sigma}}_{\boldsymbol{\Sigma}^e} + \underbrace{\psi^s\mathbf{I} - \nabla s\otimes\frac{\partial[(g(s)+\eta)\psi^e + \psi^s]}{\partial\nabla s}}_{\boldsymbol{\Sigma}^s} + \underbrace{h(s)\psi^{\text{ad}}\mathbf{I} - \nabla s\otimes\frac{\partial h(s)\psi^{\text{ad}}}{\partial\nabla s}}_{\boldsymbol{\Sigma}^{\text{ad}}},\end{aligned} \tag{18}$$

By means of the equilibrium of the stress field Eq. (10) and the evolution of the crack field Eq. (11) in cyclic domain, Eq. (15) can be further simplified to yield

where the tensor $\boldsymbol{\Sigma}^e$ denotes the elastic part, the tensor $\boldsymbol{\Sigma}^s$ denotes the surface component, and the tensor $\boldsymbol{\Sigma}^{\text{ad}}$ denotes the fatigue part. Similarly, a decomposition for the general configurational forces yields

$$\mathbf{g} = \underbrace{\frac{1}{M}\frac{\mathrm{d}s}{\mathrm{d}N}\nabla s}_{\mathbf{g}^{\text{dis}}} \underbrace{- \nabla\mathbf{u}^T\boldsymbol{f}}_{\mathbf{g}^{\text{vol}}} \underbrace{- \frac{\partial\psi}{\partial D}\nabla D}_{\mathbf{g}^D} \underbrace{- \frac{\partial\psi}{\partial\mathbf{x}}|_{\text{expl.}}}_{\mathbf{g}^{\text{inh}}} - \underbrace{\frac{\partial\psi}{\partial\mathbf{x}^{\text{tip}}}\cdot\nabla\mathbf{x}^{\text{tip}}}_{\mathbf{g}^{\text{tip}}}, \tag{19}$$

where the force $\mathbf{g}^{\text{dis}}$ denotes the dissipative part, the force $\mathbf{g}^{\text{vol}}$ denotes the volume forces part, the force $\mathbf{g}^D$ denotes the fatigue damage part, the

[1] The term $\frac{\partial\psi}{\partial\nabla s}\cdot(\nabla s\otimes\nabla)$ is computed as $\frac{\partial\psi}{\partial s_j}s_{jk}$

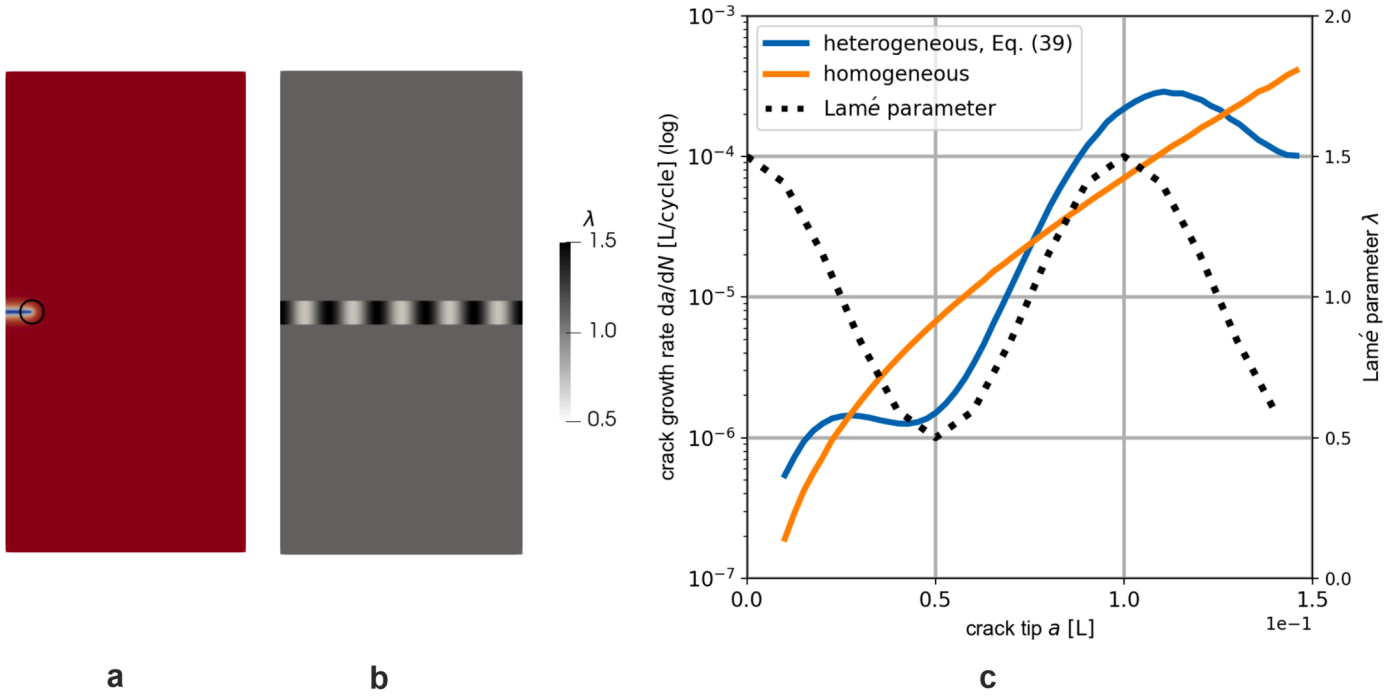

Fig. 2. **a**: in crack mode I, the crack extends in horizontal direction though the inhomogeneous area; **b**: a color-map of the Lamé parameter λ; **c**: the crack growth rate is influenced by the elastic property. The dotted line shows the profile of the Lamé parameter λ.

force $\mathbf{g}^{\text{inh}}$ denotes the inhomogeneity part, and the last term $\mathbf{g}^{\text{tip}}$ denotes the total configurational force around the crack tip. In the following section, the meaning of each component will be discussed.

4. Evaluation of the phase field model on configurational forces

In order to investigate the physical meaning of the configurational force balance and to identify the roles played by each component, a mode I loading scenario with a horizontally extending crack is evaluated (see Fig. 1**a**). A cyclic traction loading with constant amplitude $\boldsymbol{t} = 0.005\sqrt{2\mu\mathscr{G}_c/L}$ is applied to the top of the rectangular domain and its bottom is fixed. An initial crack ($s = 0$) with length of $0.01L$ in the middle of the left side of the domain is predefined. In particular, a material inhomogeneity with a width of $0.1L$ is introduced in the middle of the domain (between the dashed red lines).

Since volume forces $\boldsymbol{f}$ are neglected in the demonstrated example, the volume force contribution to the configurational force vanishes

$$\mathbf{g}^{\text{vol}} = \mathbf{0}. \tag{20}$$

The configurational force acting on the crack tip is the center point of our study because it describes the total energetic force during the evolution of the position of the crack tip in the material configuration i.e., crack growth. Thus, it is evaluated by integration around a sufficiently large domain used as a control volume (see Fig. 1**b**). The "sufficiently large" means that the evaluated domain should be large enough to cover the entire crack transition zone in order to collect all information necessary for the computation of the configurational forces. A discussion of the influence of the choice of control volume can be found in [36].

The integration on the elastic part of the generalized Eshelby stress tensor yields

$$\mathbf{G}^e = -\int_{\partial\Omega} \operatorname{div}\boldsymbol{\Sigma}^e \mathrm{d}V. \tag{21}$$

With the divergence theorem, the divergence of a vector field in the volume can be rewritten into a surface integral over the boundary of the volume

$$\mathbf{G}^e = -\int_{\Omega} \operatorname{div}\boldsymbol{\Sigma}^e \mathrm{d}V = -\int_{\partial\Omega_0} \boldsymbol{\Sigma}^e \mathbf{n}\mathrm{d}A = -\int_{\partial\Omega_{0_{A\to B}}} \boldsymbol{\Sigma}^e \mathbf{n}\mathrm{d}A - \int_{\partial\Omega_{0_{B\to A}}} \boldsymbol{\Sigma}^e \mathbf{n}\mathrm{d}A. \tag{22}$$

Recalling the meaning of the parameter ϵ, the damage-free area (from A to B in Fig. 1**b**) can be seen to be significantly larger compared to the crack surface when the parameter $\epsilon \to 0$ [19]. Thus, the configurational force $\mathbf{G}^e$ can be approximated by integration only from the path A to B with $g(s) \equiv 1$ [19]

$$\begin{aligned} \mathbf{G}^e &= -\int_{\partial\Omega_{0_{A\to B}}} \boldsymbol{\Sigma}^e \mathbf{n}\mathrm{d}A \underset{\epsilon\to 0}{=} -\int_{\partial\Omega_{0_{A\to B}}} \left[\psi^e \mathbf{I} - \nabla\mathbf{u}^{\mathrm{T}}\boldsymbol{\sigma}\right]\mathbf{n}\mathrm{d}A \\ &= -\mathscr{J}\,\mathbf{e}_x, \end{aligned} \tag{23}$$

where $\mathbf{e}_x$ denotes the unit vector in the x-direction. It is noted that the component of the configurational force due to elastic deformation is equivalent to the negative $\mathscr{J}$-integral in the sense of classic fracture mechanics. The $\mathscr{J}$-integral represents the strain energy release rate [26], capturing the intensity of the loading applied at the crack tip.

Performing the same procedure on the surface part $\mathbf{g}^s$ yields

$$\mathbf{G}^s = -\int_{\Omega} \operatorname{div}\boldsymbol{\Sigma}^s \mathrm{d}V = -\int_{\partial\Omega_0} \boldsymbol{\Sigma}^s \mathbf{n}\mathrm{d}A = -\int_{\partial\Omega_{0_{A\to B}}} \boldsymbol{\Sigma}^s \mathbf{n}\mathrm{d}A - \int_{\partial\Omega_{0_{B\to A}}} \boldsymbol{\Sigma}^s \mathbf{n}\mathrm{d}A. \tag{24}$$

It is straightforward to verify that the fracture surface part of the generalized Eshelby tensor $\boldsymbol{\Sigma}^s$ vanishes at the damage-free area (A to B) with $s \equiv 1$, and the remaining integration contour from B to A can be seen as a 1D problem in the y-direction. As shown in [17], the 1D solution of the fatigue crack field profile reads

$$s(x) = 1 - \exp\left(-\frac{|x|}{2\epsilon}\right). \tag{25}$$

Inserting Eq. (25) in Eq. (24) and considering the transition area is sufficiently small, e.g. $\epsilon \to 0$, yields [17]

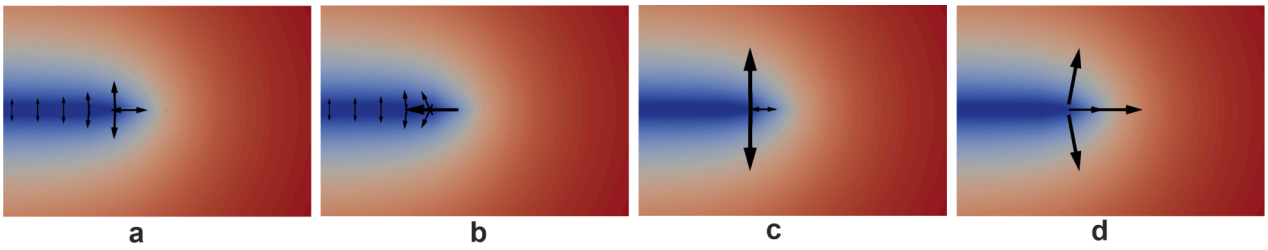

Fig. 3. The local configurational forces for every node near the crack tip. **a**: the total configuration force at the crack tip $\mathbf{g}^{\text{tip}}$; **b**: the fracture surface part $\mathbf{g}^{s}$; **c**: the fatigue part $\mathbf{g}^{\text{ad}}$; **d**: the fatigue damage part $\mathbf{g}^{D}$.

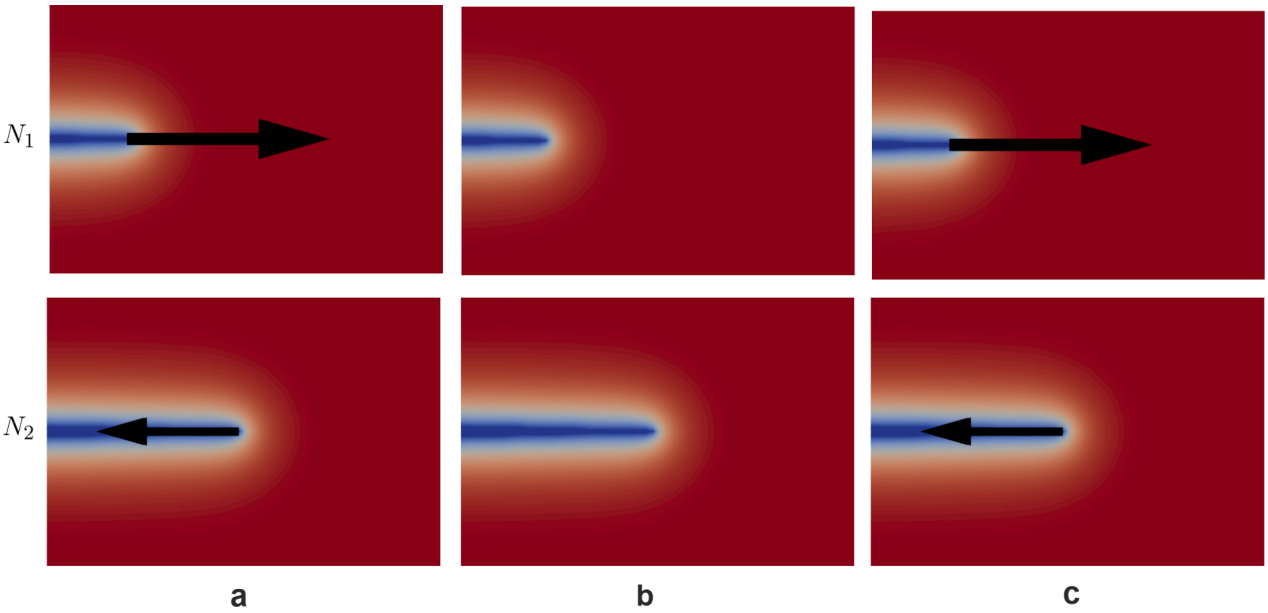

Fig. 4. The inhomogeneity parts of local configurational forces for several nodes near the crack tip. **a**: the total inhomogeneity part $\mathbf{g}^{\text{inh}}$; **b**: elastic inhomogeneity contribution $\mathbf{g}^{\text{inh},e}$; **c**: fatigue inhomogeneity contribution $\mathbf{g}^{\text{inh,ad}}$. All arrows are scaled by a factor 100 for clarity.

$$\begin{aligned}\mathbf{G}^{s} &= -\int_{\partial\Omega_{0B\to A}} \boldsymbol{\Sigma}^{s}\mathbf{n}\mathrm{d}A \\ &= -\int_{\partial\Omega_{0B\to A}} \left[\mathscr{G}_c\left(\frac{(1-s)^2}{4\epsilon}+\epsilon|\nabla s|^2\right)\mathbf{I}-2\mathscr{G}_c\nabla s\otimes\nabla s\right]\mathbf{n}\mathrm{d}A \\ &= \mathscr{G}_c\mathbf{e}_x.\end{aligned} \tag{26}$$

It is noted that the configurational force $\mathbf{G}^{s}$ corresponds to the crack resistance $\mathscr{G}_c$. Thus, this part is interpreted as a resistance of energetic forces against the crack extension.

As shown in [37], the fatigue driving force $\widehat{\sigma}$ is only pronounced within the broken area. Thus, the last term $\boldsymbol{\Sigma}^{\text{ad}}$ only needs to be integrated from the point B to A

$$\begin{aligned}\mathbf{G}^{\text{ad}} &= -\int_{\Omega_0}\mathrm{div}\boldsymbol{\Sigma}^{\text{ad}}\mathrm{d}V = -\int_{\partial\Omega_0}\boldsymbol{\Sigma}^{\text{ad}}\mathbf{n}\mathrm{d}A = -\int_{\partial\Omega_0|_{B\to A}}\boldsymbol{\Sigma}^{\text{ad}}\mathbf{n}\mathrm{d}A \\ &= -\int_{\partial\Omega_0|_{B\to A}} h(s)q<D_0+\frac{\mathrm{d}N}{n_D}\left(\frac{\widehat{\sigma}}{A_D}\right)^{k}-D_c>^{b}\mathbf{n}\mathrm{d}x.\end{aligned} \tag{27}$$

The configurational forces $\mathbf{G}^{\text{ad}}$ summarize the accumulated fatigue driving forces, and can be seen as energetic forces opposing the crack self-healing.

The dissipative part of the configurational forces at the crack tip is defined as

$$\mathbf{G}^{\text{dis}} = \int_{\Omega_0}\mathbf{g}^{\text{dis}}\mathrm{d}V = \int_{\Omega_0}\frac{1}{M}\frac{\mathrm{d}s}{\mathrm{d}N}\nabla s\mathrm{d}V. \tag{28}$$

This dissipative part is an artifact which stems from introducing the dissipative part in the phase field evolution equation (Eq. (11)), which is nonetheless required in quasi-static computation. Furthermore, this part captures the energy dissipation during the crack evolution and has a relation to the crack tip velocity [17].

The fatigue damage part is the energetic force due to the accumulated pointwise fatigue damage

$$\begin{aligned}\mathbf{G}^{D} &= \int_{\Omega_0}\mathbf{g}^{D}\mathrm{d}V = \int_{\Omega_0}-\frac{\partial\psi}{\partial D}\nabla D\mathrm{d}V = \int_{\Omega_0}-\frac{\partial\psi^{\text{ad}}}{\partial D}\nabla D\mathrm{d}V \\ &= \int_{\Omega_0}-h(s)q<D-D_c>^{b-1}\nabla D\mathrm{d}V,\end{aligned} \tag{29}$$

which accelerates the crack evolution since the fatigue damage parameter D continuously increases during the simulation. This damage part of the configurational force is the main driving force of crack growth.

The inhomogeneity part represents the influence of possible material inhomogeneity on the crack propagation

$$\begin{aligned}\mathbf{G}^{\text{inh}} &= \int_{\Omega_0}\mathbf{g}^{\text{inh}}\mathrm{d}V = \int_{\Omega_0}-\frac{\partial\psi}{\partial\mathbf{x}}|_{\text{expl.}}\mathrm{d}V \\ &= \int_{\Omega_0}\left(-g(s)\frac{\partial\psi^{e}}{\partial\mathbf{x}}|_{\text{expl.}}-\frac{\partial\psi^{s}}{\partial\mathbf{x}}|_{\text{expl.}}-h(s)\frac{\partial\psi^{\text{ad}}}{\partial\mathbf{x}}\Big|_{\text{expl.}}\right)\mathrm{d}V.\end{aligned} \tag{30}$$

In general, the inhomogeneity of the material can be caused by the inhomogeneity of the elastic material properties, e.g., the Lamé parameter λ; or it can be caused by the inhomogeneity of the material fracture

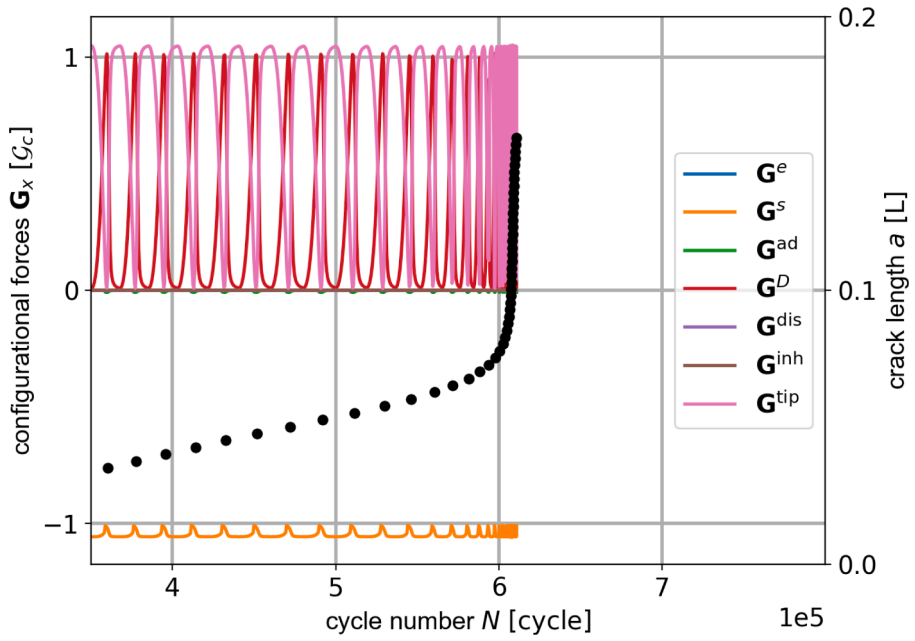

Fig. 5. The integrated configurational forces around the crack tip in relation to the cycle number together with the crack length displayed as black dots.

$$\begin{aligned}\mathbf{G}^{\mathrm{inh,ad}} &= \int_{\Omega_0}\mathbf{g}^{\mathrm{inh,ad}}\mathrm{d}V = \int_{\Omega_0} -h(s)\frac{\partial\psi^{\mathrm{ad}}}{\partial\mathbf{x}}|_{\mathrm{expl.}}\mathrm{d}V = \int_{\Omega_0} -h(s)\frac{\partial\psi^{\mathrm{ad}}}{\partial D}\frac{\partial D}{\partial\widehat{\sigma}}\frac{\partial\widehat{\sigma}}{\partial\boldsymbol{\sigma}}:\frac{\partial\boldsymbol{\sigma}}{\partial\lambda}\frac{\partial\lambda}{\partial\mathbf{x}}\mathrm{d}V \\ &= \int_{\Omega_0} -h(s)qb<D-D_c>^{b-1}k\frac{\mathrm{d}N}{n_D A_D^k}\widehat{\sigma}^{k-1}\mathrm{tr}\left(\mathbf{T}^T\begin{bmatrix}1&0&0\\0&0&0\\0&0&0\end{bmatrix}\mathbf{T}\right)\nabla\cdot\mathbf{u}\nabla\lambda\mathrm{d}V.\end{aligned} \tag{33}$$

properties, e.g., the fracture toughness $\mathcal{G}_c$.

For simplicity, it is assumed that only the Lamé parameter $\lambda(\mathbf{x})$ depends on the position vector $\mathbf{x}$. Here the term $\frac{\partial\psi^s}{\partial\mathbf{x}}|_{\mathrm{expl.}}$ is absent because the fracture surface energy density ψ^s is not related to the elastic material properties. In this case, the inhomogeneity part of the configurational force is given as

$$\mathbf{G}^{\mathrm{inh}} = \int_{\Omega_0}\Bigg(\underbrace{-g(s)\frac{\partial\psi^e}{\partial\mathbf{x}}|_{\mathrm{expl.}}}_{\mathbf{g}^{\mathrm{inh},e}}\underbrace{-h(s)\frac{\partial\psi^{\mathrm{ad}}}{\partial\mathbf{x}}|_{\mathrm{expl.}}}_{\mathbf{g}^{\mathrm{inh,ad}}}\Bigg)\mathrm{d}V. \tag{31}$$

The term $\mathbf{g}^{\mathrm{inh},e}$ denotes the pointwise inhomogeneity influences of the elastic material properties on the fatigue crack evolution, where its integration around the crack tip is given as

$$\begin{aligned}\mathbf{G}^{\mathrm{inh},e} &= \int_{\Omega_0}\mathbf{g}^{\mathrm{inh},e}\mathrm{d}V = \int_{\Omega_0} -g(s)\frac{\partial\psi^e}{\partial\mathbf{x}}|_{\mathrm{expl.}}\mathrm{d}V = \int_{\Omega_0} -g(s)\frac{\partial\psi^e}{\partial\lambda}\frac{\partial\lambda}{\partial\mathbf{x}}\mathrm{d}V \\ &= \int_{\Omega_0} -g(s)\frac{1}{2}\mathrm{tr}^2(\boldsymbol{\epsilon})\nabla\lambda\mathrm{d}V.\end{aligned} \tag{32}$$

The term $\mathbf{g}^{\mathrm{inh,ad}}$ denotes the inhomogeneity influence working on the accumulated fatigue driving forces, and integrating it around the crack tip yields[2]

The matrix $\mathbf{T}$ gives the transformation of the stress tensor $\boldsymbol{\sigma}$ to the principal reference system, in which the columns are eigenvectors of the stress tensor. Specially, when the body is under a mode I loading situation, the tensile stress in the y-direction dominates in the vicinity of the crack tip

$$\boldsymbol{\sigma}\approx\begin{bmatrix}0&0&0\\0&\sigma_1&0\\0&0&0\end{bmatrix} = \begin{bmatrix}0&0&0\\0&\widehat{\sigma}&0\\0&0&0\end{bmatrix}, \tag{34}$$

and the transformation matrix $\mathbf{T}$ degenerates to

$$\mathbf{T} = \begin{bmatrix}0&1&0\\1&0&0\\0&0&1\end{bmatrix}. \tag{35}$$

Thus, the configurational force $\mathbf{G}^{\mathrm{inh,ad}}$ in this case can be simplified to

$$\mathbf{G}^{\mathrm{inh,ad}} = \int_{\Omega_0} -h(s)qb<D-D_c>^{b-1}k\frac{\mathrm{d}N}{n_D A_D^k}\widehat{\sigma}^{k-1}\nabla\cdot\mathbf{u}\nabla\lambda\mathrm{d}V \tag{36}$$

The total inhomogeneity part of the configurational force combines those effects together according to Eq. (31)

$$\mathbf{G}^{\mathrm{inh}} = \mathbf{G}^{\mathrm{inh},e} + \mathbf{G}^{\mathrm{inh,ad}}. \tag{37}$$

Allocating all the above definitions, the total configurational force around the crack tip $\mathbf{G}^{\mathrm{tip}} = \int_\Omega \mathbf{g}^{\mathrm{tip}}\mathrm{d}V$ is given by

[2] A detailed derivation of Eq. (33) can be found in Appendix.

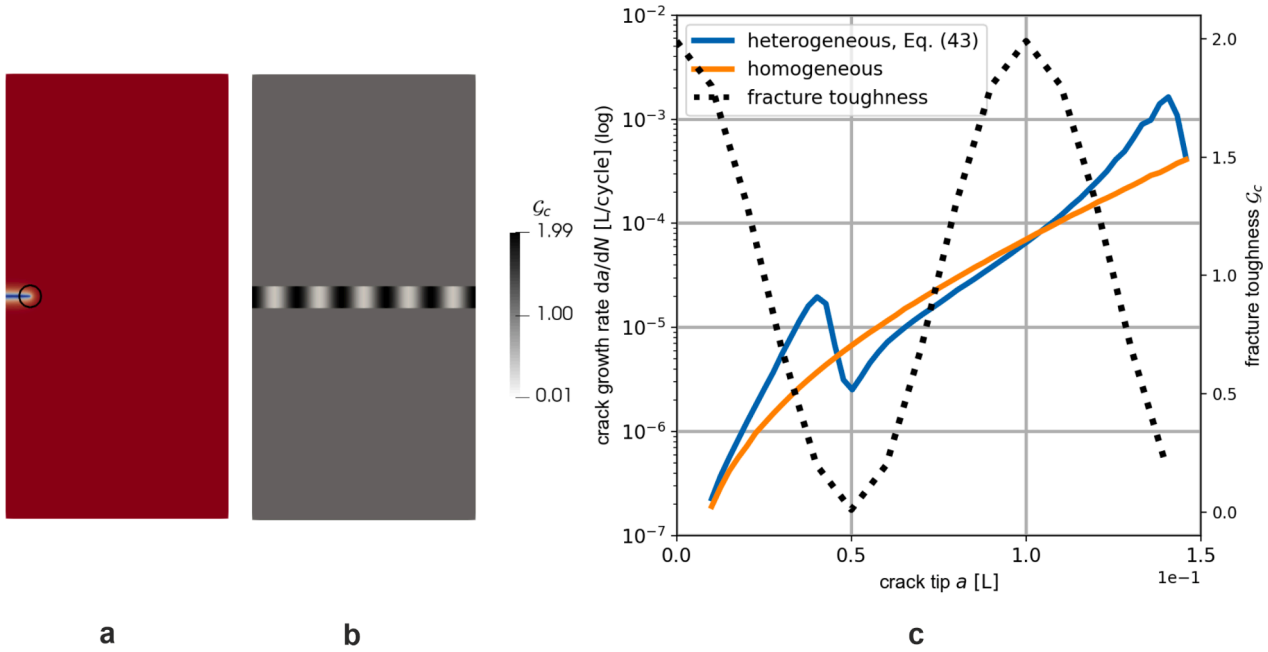

Fig. 6. **a**: in crack mode I, the crack runs through the inhomogeneous area horizontally; **b**: a color-map of the fracture toughness $\mathcal{G}_c$; **c**: the influence of an inhomogeneous fracture toughness on the crack growth rate. The dotted line shows the profile of the fracture toughness $\mathcal{G}_c$.

$$\mathbf{G}^{\text{tip}} = \mathbf{G}^{e} + \mathbf{G}^{s} + \mathbf{G}^{\text{ad}} - \mathbf{G}^{D} - \mathbf{G}^{\text{inh}} - \mathbf{G}^{\text{dis}}. \tag{38}$$

This energetic force $\mathbf{G}^{\text{tip}}$ can be interpreted as the driving force for the crack evolution with all the influences of crack extension taken into account.

Assuming that the Lamé parameter varies continuously in the marked area (see Fig. 2**b**), e.g.,

$$\lambda(\mathbf{x}) = 0.5\cos\left(\frac{20x\pi}{L}\right)\lambda_0 + \lambda_0 \quad \text{with} \quad \lambda_0 = 1,\ x \in [0, L]. \tag{39}$$

Fig. 2 reports the crack growth rate in a material with inhomogeneous elastic property compared to a domain with homogeneous material $\lambda_0 = 1$. The crack growth rate is strongly influenced by the Lamé parameter: it has a similar cosine-form as the parameter λ. A higher local value of λ results in a faster crack propagation rate. Fig. 3 reports the local configurational forces (**a**: total configuration forces at the crack tip $\mathbf{g}^{\text{tip}}$; **b**: fracture surface part $\mathbf{g}^{s}$; **c**: fatigue part $\mathbf{g}^{\text{ad}}$; **d**: damage part $\mathbf{g}^{D}$) for several nodes near the crack tip for clarity. Other configurational forces, such as elastic part $\mathbf{g}^{e}$ and dissipative part $\mathbf{g}^{\text{dis}}$, are not pronounced because they are relatively small in the fatigue scenario.

The fracture surface part $\mathbf{g}^{s}$ and fatigue part $\mathbf{g}^{\text{ad}}$ act in the opposite direction compared to the crack propagation, because they illustrate energetic forces that resist the crack growth. The fatigue damage part $\mathbf{g}^{D}$ acts also in the direction, providing the primary energetic force for the crack propagation. In addition, Fig. 4 reports the inhomogeneity part of the configurational forces (**a**: total inhomogeneity part $\mathbf{g}^{\text{inh}}$; **b**:

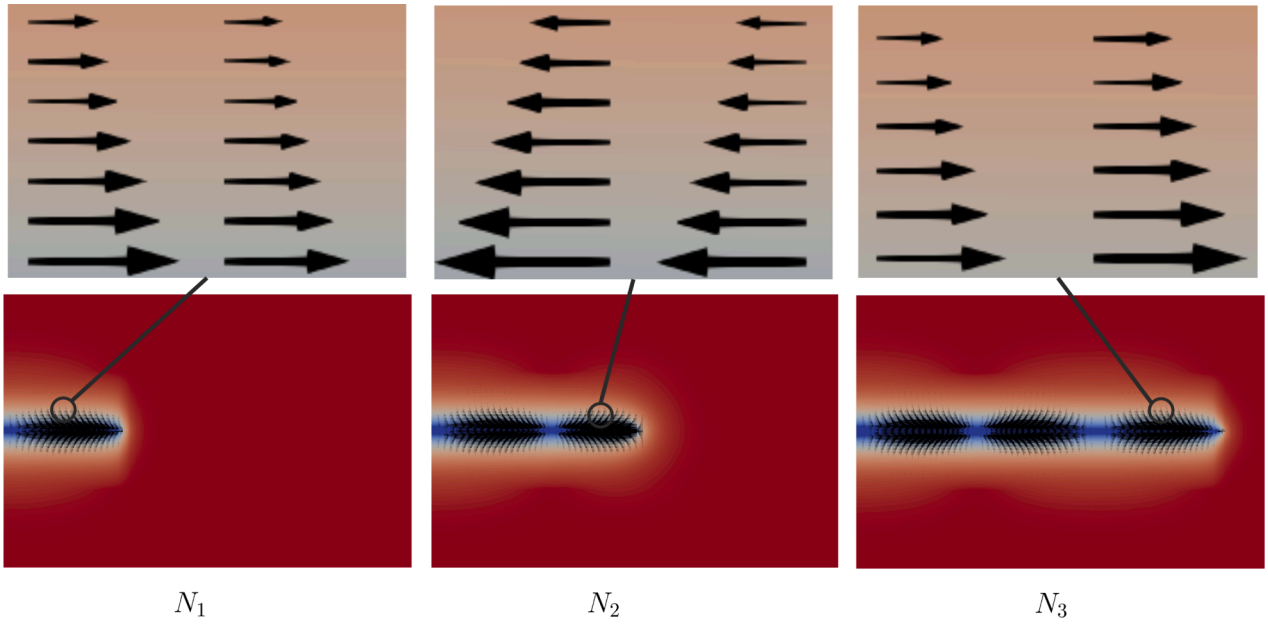

Fig. 7. The local inhomogeneity part of the configurational forces $\mathbf{g}^{\text{inh}}$ in the total cracks area at different cycles.

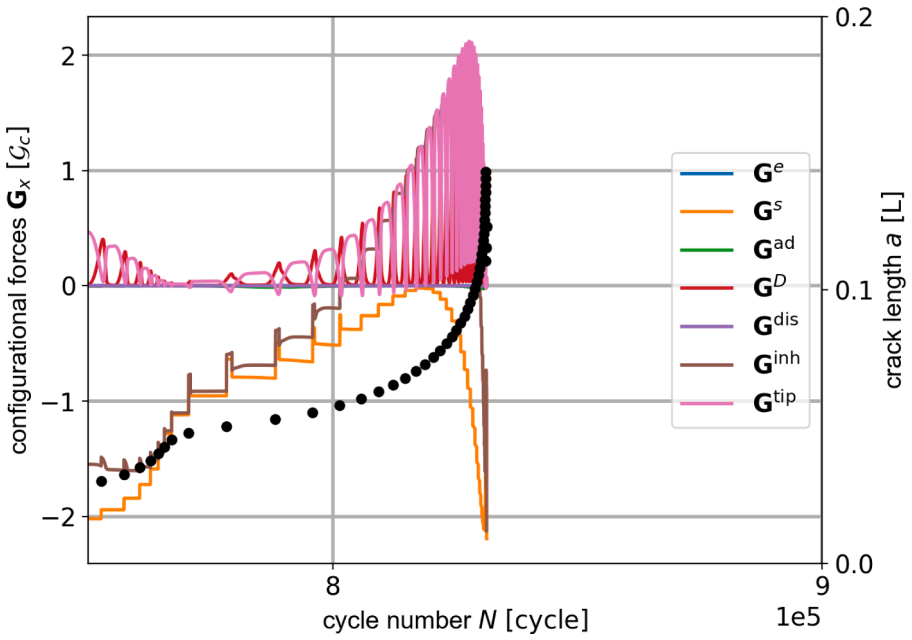

Fig. 8. The integrated configurational forces around the crack tip in relation to the cycle number together with the crack length displayed as black dots.

inhomogeneity due to elastic part $\mathbf{g}^{\text{inh},e}$; **c**: inhomogeneity due to fatigue part $\mathbf{g}^{\text{inh,ad}}$). It is important to note that these components provide an additional energetic force for crack evolution; however, they are less powerful than the force damage part $\mathbf{g}^D$ of the configurational. Furthermore, it is noticed that the total inhomogeneity part $\mathbf{g}^{\text{inh}}$ (Fig. 4**a**) is almost completely built up by its fatigue component (Fig. 4**c**) whereas the elastic contribution $\mathbf{g}^{\text{inh},e}$ (Fig. 4**b**) is significantly smaller. The inhomogeneity component $\mathbf{g}^{\text{inh}}$ propagates the crack in the same direction as the crack tip $x^{\text{tip}} \in (0, 0.05L)$. In contrast, when the crack tip is between $0.05L$ and $0.1L$, the inhomogeneity part opposes the further propagation of the crack. The different directions can be explained by the gradient term $\nabla\lambda$ in Eq. (36), which comes out as a sine function according to the definition.

In Fig. 5, different configurational force contributions are computed by integration throughout the simulation as the crack grows. We ignore the beginning of the simulation, where the integration domain cuts the boundary of the geometry. After that, the fracture surface part $\mathbf{G}^s$ remains close to the value of $\mathcal{G}_c$ which was shown mathematically earlier. The damaged contribution $\mathbf{G}^D$ oscillates along with the crack propagate; especially, the onset of cracking happens when the total configurational force on the crack tip vanish ($\mathbf{G}^{\text{tip}} = 0$), where the damage part $\mathbf{G}^D$ and fracture surface part $\mathbf{G}^s$ cancel. The fatigue crack can be seen to propagate faster at the later stage of the simulation, as the total configurational force $\mathbf{G}^{\text{tip}}$ declines more often to zero.

In an additional scenario, we consider an inhomogeneous fracture toughness in the area (see Fig. 6**b**). In this case, the inhomogeneity part is only related to the fracture surface energy density

$$\mathbf{G}^{\text{inh}} = \int_{\Omega_0} \underbrace{-\frac{\partial \psi^s}{\partial \mathbf{x}}|_{\text{expl.}}}_{\mathbf{g}^{\text{inh},s}} \mathrm{d}V. \tag{40}$$

Proceeding to define

$$\mathbf{G}^{\text{inh},s} = \int_{\Omega_0} \mathbf{g}^{\text{inh},s} \mathrm{d}V = \int_{\Omega_0} \frac{\partial \psi^s}{\partial \mathcal{G}_c} \frac{\partial \mathcal{G}_c}{\partial \mathbf{x}} \mathrm{d}V = \int_{\Omega_0} \left(\frac{(1-s)^2}{4\epsilon} + \epsilon |\nabla s|^2 \right) \nabla \mathcal{G}_c \mathrm{d}V, \tag{41}$$

the energetic force $\mathbf{G}^{\text{inh},s}$ gives the inhomogeneity influence due to a change of the fracture toughness and contributes to the crack evolution

$$\mathbf{G}^{\text{inh}} = \mathbf{G}^{\text{inh},s}. \tag{42}$$

The fracture toughness $\mathcal{G}_c$ is assumed to have the following form

$$\mathcal{G}_c(\mathbf{x}) = 0.99 \cos\left(\frac{20x\pi}{L}\right) \mathcal{G}_{c0} + \mathcal{G}_{c0} \quad \text{with} \quad \mathcal{G}_{c0} = 1,\ x \in [0, L]. \tag{43}$$

Generally speaking, the crack growth rate in relation to the crack tip correlates to a sine function as shown in Fig 6**c**, which agrees with the gradient of the fracture toughness $\nabla\mathcal{G}_c$ in Eq. (41). This finding can be explained by Fig. 7, which depicts the local inhomogeneity part of the configurational forces $\mathbf{g}^{\text{inh}}$ at different cycles. Different from the previous discussion of configurational forces $\mathbf{g}^{\text{inh,ad}}$, the configurational force $\mathbf{g}^{\text{inh},s}$ does not vanish as cracks extend, because the fracture surface energy ψ^s is not associated with a degradation function. As shown in Fig. 7, a positive configurational force contributes to the crack propagation and a negative configurational force prevents the crack extension, whose directions are determined by the gradient of the fracture toughness $\nabla\mathcal{G}_c$.

In order to analyze the total configurational force at the crack tip, Fig. 8 reports the individual, integrated contributions to the total configurational force. After the integration domain moves out of the left boundary of the domain, the magnitudes of each of the configurational forces vary depending on the position of the crack tip. The fracture surface part $\mathbf{G}^s$ is strongly relevant to the fracture toughness $\mathcal{G}_c$, and the magnitude of the inhomogeneity part $\mathbf{G}^{\text{inh}}$ varies in the same way as the fracture toughness gradient $\nabla\mathcal{G}_c$. The same observation can be noticed that the crack propagates further when the total configurational force acting on the crack direction decrease to zero.

In the second scenario, we consider a rectangular specimen with shear loading on its top and a pre-defined crack $a_0 = 0.1L$ in the middle of the left side. In the marked area (red dotted square), the geometry is under different material inhomogeneities by varied Lamé parameter λ or fracture toughness $\mathcal{G}_c$ along the y-axis (see Fig. 9), given as

$$\lambda(\mathbf{x}) = 0.5 \cos\left(\frac{20y\pi}{L}\right) \lambda_0 + \lambda_0 \quad \text{with} \quad \lambda_0 = 1,\ y \in [0.4L, 0.6L] \tag{44}$$

or

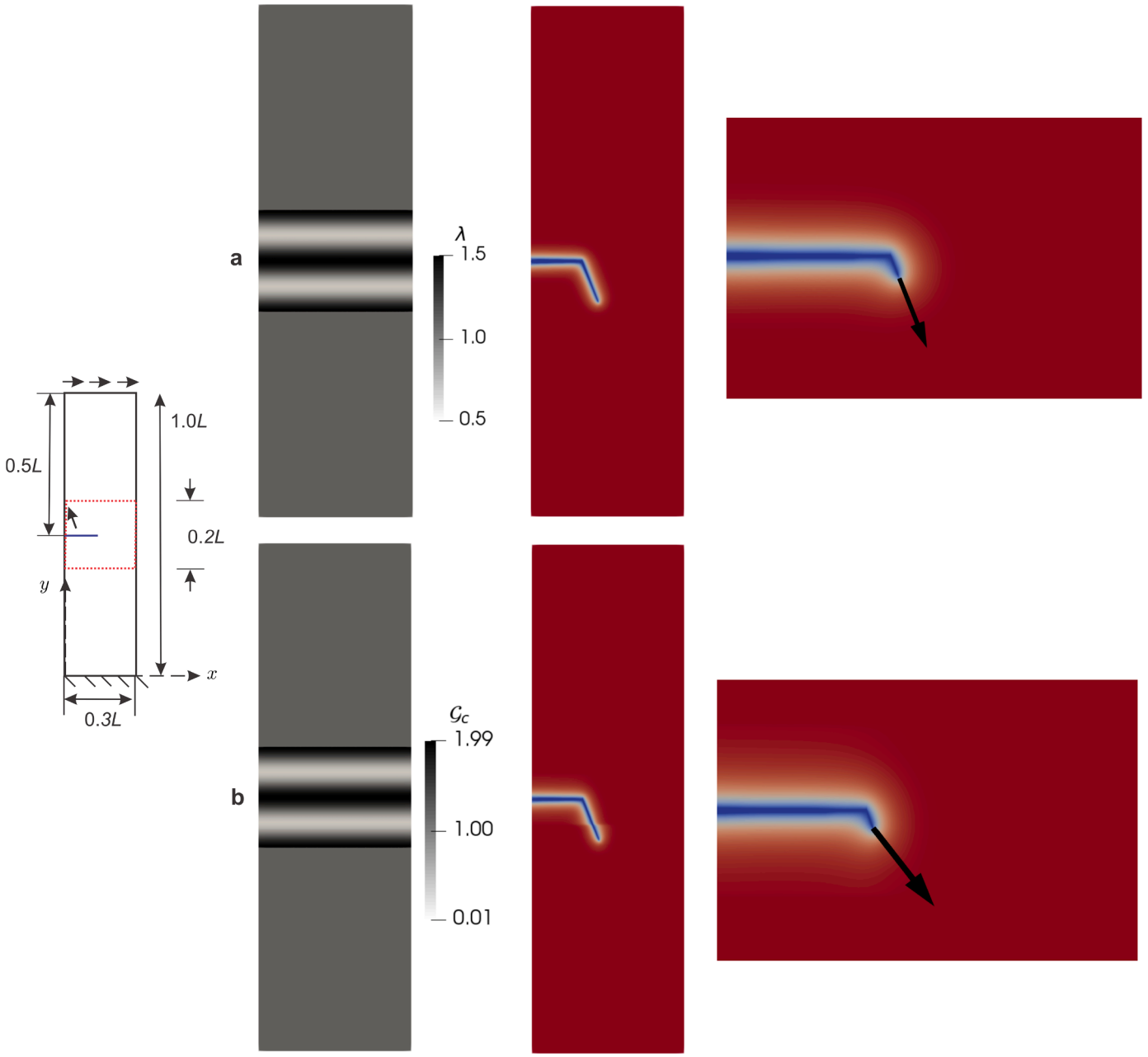

Fig. 9. A rectangular specimen under shear loading with varied elastic or fracture parameter in the marked area on the y-direction (**a**: Lamé parameter; **b**: fracture toughness). The crack follows a kink from the edges of a pre-existing crack, where the integrated total configurational force (black arrow) represents the energetic forces for the crack extension.

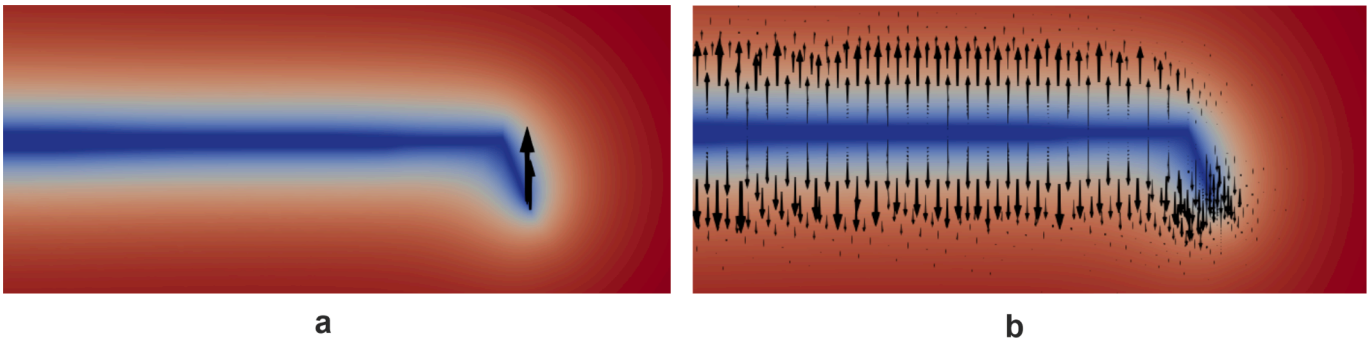

Fig. 10. The local inhomogeneity part of the configurational forces $\mathbf{g}^{\text{inh}}$ act both in the y-direction for this case **a**: the inhomogeneity part of the configurational forces from elastic parameter (scaled by factor 1000); **b**: the inhomogeneity part of the configurational forces from fracture parameter.

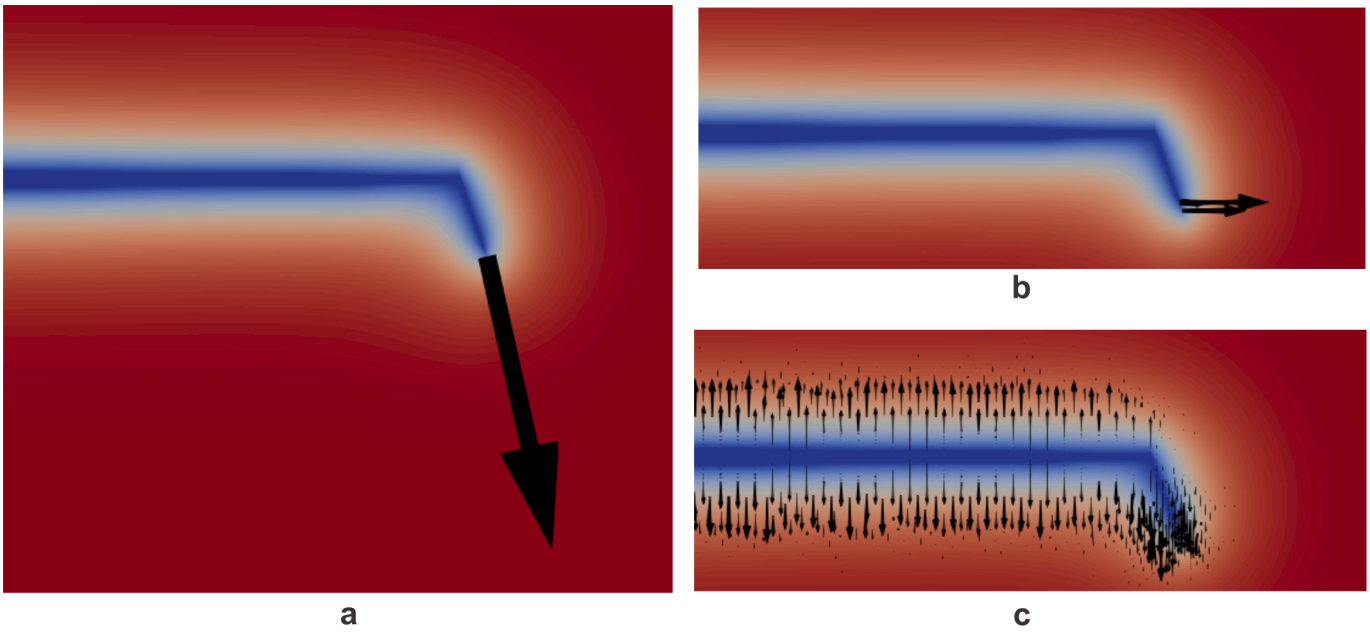

Fig. 11. Configurational forces for the specimen with a heterogeneity profile varying along both x- and y-direction: **a**: the integrated total configurational force around the crack tip; **b**: the local inhomogeneity part of the configurational forces from elastic parameter (scaled by factor 1000); **c**: the local inhomogeneity part of the configurational forces from fracture parameter).

$$\mathscr{G}_c(\mathbf{x}) = 0.99\cos\left(\frac{20y\pi}{L}\right)\mathscr{G}_{c0} + \mathscr{G}_{c0} \quad \text{with} \quad \mathscr{G}_{c0} = 1,\ y \in [0.4L, 0.6L]. \tag{45}$$

Different from the mode I loading, the crack develops a kink from the edges of a pre-existing crack under shear loading as shown in Fig. 9. Nevertheless, the same observations regarding the configurational forces can be noticed. It is noted that the integrated total configurational force around the crack tip (black arrow) is once again the energetic force responsible for the crack extension. However, the inhomogeneity parts of the configurational forces perform differently in this case as shown in Fig. 10. They both point in the y-direction, which can be explained by the gradient term from their definitions as we detailed discussed in the first example for the pure tension loading.

In the next example, we take the previously proposed rectangular specimen in Fig. 9 under shear loading, especially, a heterogeneity profile varying along both x- and y-direction is imposed in this case. The Lamé parameter λ varies on x-direction, given as in Eq. (39); and fracture toughness $\mathscr{G}_c$ varies on y-direction, given as in Eq. (45). The result in Fig. 11 confirms again our finding, that the integrated total configurational force represents the driving force for the crack propagation. Especially, the inhomogeneity parts of the configurational forces work independently for the crack extension as their directions are determined of the gradient term ($\nabla\lambda$ or $\nabla\mathscr{G}_c$).

5. Conclusion

Despite the well-established phase field model for fracture mechanics, it is difficult to understand the energetic driving forces causing the crack evolution behavior from the phase field equations in an intuitive manner. We propose a link between generalized configurational forces and crack propagation in a phase field fatigue model. In general, the total generalized configurational force represents the total energetic forces responsible for the crack extension. The onset of crack propagation can be observed when the total generalized configurational force in the crack propagation direction vanish, and crack growth only occurs if a Griffith-type energy principle is fulfilled. Unlike previous studies, our work considers various types of material inhomogeneity for fatigue fracture simulation: A higher Lamé parameter λ or lower fracture toughness $\mathscr{G}_c$ can increase the crack propagation rate. It is demonstrated that configurational forces associated with material inhomogeneity provide an additional contribution to the rate of crack growth. When the configurational forces show the same direction as the crack propagation, it accelerates the crack extension; otherwise it acts against further crack growth. Our results show that the concepts of configurational forces can be used to illustrate how the different energy components of the phase field fatigue model influence crack the evolution.

Declaration of Competing Interest

The authors declare that they have no known competing financial interests or personal relationships that could have appeared to influence the work reported in this paper.

Data availability

Data will be made available on request.

Acknowledgment

Funded by the Deutsche Forschungsgemeinschaft (DFG, German Research Foundation) - 252408385 - IRTG 2057

Appendix A

We use index-notation to derivate the part of the inhomogeneity influence working on the accumulated fatigue driving forces.

$$g_i^{\mathrm{inh,ad}} = -h\frac{\psi^{\mathrm{ad}}}{x_i}. \tag{A.1}$$

Applying the chain rule on $\frac{\psi^{\mathrm{ad}}}{x_i}$ yields

$$\frac{\psi^{\mathrm{ad}}}{x_i} = \frac{\partial\psi^{\mathrm{ad}}}{\partial D}\frac{\partial D}{\partial\widehat{\sigma}}\frac{\partial\widehat{\sigma}}{\partial\sigma_{\alpha\beta}}\frac{\partial\sigma_{\alpha\beta}}{\partial\lambda}\frac{\partial\lambda}{\partial x_i}. \tag{A.2}$$

Recalling the definition of the additional energy density ψ^{ad} and the damage parameter D, the first- and second term in Eq. (A.12) read

$$\frac{\partial\psi^{\mathrm{ad}}}{\partial D} = qb < D - D_c >^{b-1} \tag{A.3}$$

and

$$\frac{\partial D}{\partial\widehat{\sigma}} = \frac{\partial \mathrm{d}D}{\partial\widehat{\sigma}} = k\frac{\mathrm{d}N}{n_D A_D^k}\widehat{\sigma}^{k-1}. \tag{A.4}$$

Applying the chain rule again on the term $\frac{\partial\widehat{\sigma}}{\partial\sigma_{\alpha\beta}}$ yields

$$\frac{\partial\widehat{\sigma}}{\partial\sigma_{\alpha\beta}} = \frac{\partial\widehat{\sigma}}{\partial\sigma_{\xi\zeta}}\frac{\partial\sigma_{\xi\zeta}}{\partial\sigma_{\alpha\beta}} \tag{A.5}$$

with

$$\sigma_{\xi\zeta} = T_{\xi\alpha}\sigma_{\alpha\beta}T_{\beta\zeta} \tag{A.6}$$

as the transformation from an arbitrary stress tensor $\sigma_{\alpha\beta}$ to the stress tensor in the principal planes $\sigma_{\xi\zeta}$. The transformation tensor is given as

$$T_{\xi\alpha} = e_\xi e_\alpha \quad \text{and} \quad T_{\beta\zeta} = e_\beta e_\zeta, \tag{A.7}$$

where the vectors e_α, e_β, e_ξ, and e_ζ are the unit vectors in both coordinate systems. In the phase field model, the driving force is taken as the first principal stress $\widehat{\sigma} = \sigma_1$, it yields

$$\frac{\partial\widehat{\sigma}}{\partial\sigma_{\xi\zeta}} = \frac{\partial\sigma_1}{\partial\sigma_{\xi\zeta}} = \delta_{1\xi}\delta_{\xi\zeta} = \delta_{1\zeta} \tag{A.8}$$

with Kronecker Delta δ. The latter term in Eq. (A.5) is computed as

$$\frac{\partial\sigma_{\xi\zeta}}{\partial\sigma_{\alpha\beta}} = T_{\xi\alpha}T_{\beta\zeta}. \tag{A.9}$$

Noting the constitution law, the stress tensor has the relation with the Lamé parameters

$$\sigma_{\alpha\beta} = \lambda\frac{\partial u_j}{\partial x_j}\delta_{\alpha\beta} + \mu\left(\frac{\partial u_\alpha}{\partial x_\beta} + \frac{\partial u_\beta}{\partial x_\alpha}\right), \tag{A.10}$$

it leads to

$$\frac{\partial\sigma_{\alpha\beta}}{\partial\lambda} = \frac{\partial u_j}{\partial x_j}\delta_{\alpha\beta}. \tag{A.11}$$

Allocating all above equations yields

$$
\begin{aligned}
g_i^{\text{inh,ad}} &= -h\frac{\psi^{\text{ad}}}{x_i} = -h\frac{\partial\psi^{\text{ad}}}{\partial D}\frac{\partial D}{\partial\widehat{\sigma}}\frac{\partial\widehat{\sigma}}{\partial\sigma_{\alpha\beta}}\frac{\partial\sigma_{\alpha\beta}}{\partial\lambda}\frac{\partial\lambda}{\partial x_i}. \\
&= -hqb < D - D_c >^{b-1} k\frac{\mathrm{d}N}{n_D A_D^k}\widehat{\sigma}^{k-1}\delta_{1\zeta}T_{\xi\alpha}T_{\beta\zeta}\frac{\partial u_j}{\partial x_j}\delta_{\alpha\beta}\frac{\partial\lambda}{\partial x_i} \\
&= -hqb < D - D_c >^{b-1} k\frac{\mathrm{d}N}{n_D A_D^k}\widehat{\sigma}^{k-1}T_{\xi\alpha}\left(\delta_{1\zeta}\delta_{\alpha\beta}\right)T_{\beta\zeta}\frac{\partial u_j}{\partial x_j}\delta_{\alpha\beta}\frac{\partial\lambda}{\partial x_i} \\
&= -hqb < D - D_c >^{b-1} k\frac{\mathrm{d}N}{n_D A_D^k}\widehat{\sigma}^{k-1}T_{\xi\alpha}\delta_{1\beta}T_{\beta\zeta}\frac{\partial u_j}{\partial x_j}\delta_{\alpha\beta}\frac{\partial\lambda}{\partial x_i} \\
\Rightarrow \mathbf{g}^{\text{inh,ad}} &= -hqb < D - D_c >^{b-1} k\frac{\mathrm{d}N}{n_D A_D^k}\widehat{\sigma}^{k-1}\mathrm{tr}\left(\mathbf{T}^T\begin{bmatrix}1&0&0\\0&0&0\\0&0&0\end{bmatrix}\mathbf{T}\right)\nabla\cdot\mathbf{u}\nabla\lambda
\end{aligned}
\tag{A.12}
$$

References

[1] R. Alessi, S. Vidoli, L. De Lorenzis, A phenomenological approach to fatigue with a variational phase-field model: the one-dimensional case, Eng. Fract. Mech. 190 (2018) 53–73.

[2] H. Amor, J.-J. Marigo, C. Maurini, Regularized formulation of the variational brittle fracture with unilateral contact: numerical experiments, J. Mech. Phys. Solids 57 (8) (2009) 1209–1229.

[3] M.J. Borden, T.J. Hughes, C.M. Landis, C.V. Verhoosel, A higher-order phase-field model for brittle fracture: formulation and analysis within the isogeometric analysis framework, Comput. Methods Appl. Mech. Eng. 273 (2014) 100–118.

[4] M.J. Borden, C.V. Verhoosel, M.A. Scott, T.J. Hughes, C.M. Landis, A phase-field description of dynamic brittle fracture, Comput. Methods Appl. Mech. Eng. 217 (2012) 77–95.

[5] B. Bourdin, G.A. Francfort, J.-J. Marigo, Numerical experiments in revisited brittle fracture, J. Mech. Phys. Solids 48 (4) (2000) 797–826.

[6] B. Bourdin, G.A. Francfort, J.-J. Marigo, The variational approach to fracture, J. Elast. 91 (1–3) (2008) 5–148.

[7] B. Bourdin, C.J. Larsen, C.L. Richardson, A time-discrete model for dynamic fracture based on crack regularization, Int. J. Fract. 168 (2) (2011) 133–143.

[8] M. Braun, Configurational forces induced by finite-element discretization, Proc. Estonian Acad. Sci. Phys. Math. 46 (1/2) (1997) 24–31.

[9] P. Carrara, M. Ambati, R. Alessi, L. De Lorenzis, A framework to model the fatigue behavior of brittle materials based on a variational phase-field approach, Comput. Methods Appl. Mech. Eng. 361 (2020) 112731.

[10] J. Chaboche, P. Lesne, A non-linear continuous fatigue damage model, Fatigue Fract. Eng. Mater. Struct. 11 (1) (1988) 1–17.

[11] J.D. Eshelby, Energy relations and the energy-momentum tensor in continuum mechanics. Fundamental Contributions to the Continuum Theory of Evolving Phase Interfaces in Solids, Springer, 1999, pp. 82–119.

[12] G.A. Francfort, J.-J. Marigo, Revisiting brittle fracture as an energy minimization problem, J. Mech. Phys. Solids 46 (8) (1998) 1319–1342.

[13] A.A. Griffith, VI. The phenomena of rupture and flow in solids, Philos. Trans. R. Soc. London Ser. A 221 (582–593) (1921) 163–198.

[14] M.E. Gurtin, Generalized Ginzburg-Landau and Cahn-Hilliard equations based on a microforce balance, Physica D 92 (3–4) (1996) 178–192.

[15] M.E. Gurtin, Configurational Forces as Basic Concepts of Continuum Physics vol. 137, Springer Science & Business Media, 1999.

[16] M.M. Hasan, T. Baxevanis, A phase-field model for low-cycle fatigue of brittle materials, Int. J. Fatigue 150 (2021) 106297.

[17] C. Kuhn. Numerical and analytical investigation of a phase field model for fracture, Technische Universität Kaiserslautern, 2013 doctoralthesis.http://nbn-resolving.de/urn:nbn:de:hbz:386-kluedo-35257

[18] C. Kuhn, R. Müller, Configurational forces in a phase field model for fracture. 18th European Conference on Fracture. DVM, 2010.

[19] C. Kuhn, R. Müller, A continuum phase field model for fracture, Eng. Fract. Mech. 77 (18) (2010) 3625–3634.

[20] C. Kuhn, R. Müller, A discussion of fracture mechanisms in heterogeneous materials by means of configurational forces in a phase field fracture model, Comput. Methods Appl. Mech. Eng. 312 (2016) 95–116.

[21] G.A. Maugin, Material Inhomogeneities in Elasticity, CRC Press, 2020.

[22] C. Miehe, F. Welschinger, M. Hofacker, Thermodynamically consistent phase-field models of fracture: variational principles and multi-field fe implementations, Int. J. Numer. Methods Eng. 83 (10) (2010) 1273–1311.

[23] M.A. Miner, Cumulative damage in fatigue, J. Appl. Mech. (1945).

[24] R. Mueller, G. Maugin, On material forces and finite element discretizations, Comput. Mech. 29 (2002) 52–60.

[25] K. Pham, J.-J. Marigo, From the onset of damage to rupture: construction of responses with damage localization for a general class of gradient damage models, Continuum Mech. Thermodyn. 25 (2013) 147–171.

[26] J.R. Rice, A path independent integral and the approximate analysis of strain concentration by notches and cracks, 1968.

[27] A. Schlüter, C. Kuhn, R. Müller, Configurational forces in a phase field model for dynamic brittle fracture. Advances in Mechanics of Materials and Structural Analysis: In Honor of Reinhold Kienzler, 2018, pp. 343–364.

[28] C. Schreiber, Phase Field Modeling of Fracture: Fatigue and Anisotropic Fracture Resistance, Technische Universität Kaiserslautern, 2021.

[29] C. Schreiber, C. Kuhn, R. Müller, T. Zohdi, A phase field modeling approach of cyclic fatigue crack growth, Int. J. Fract. 225 (1) (2020) 89–100.

[30] C. Schreiber, R. Müller, C. Kuhn, Phase field simulation of fatigue crack propagation under complex load situations, Arch. Appl. Mech. (2020) 1–15.

[31] M. Seiler, T. Linse, P. Hantschke, M. Kästner, An efficient phase-field model for fatigue fracture in ductile materials, Eng. Fract. Mech. 224 (2020) 106807.

[32] K. Seleš, F. Aldakheel, Z. Tonković, J. Sorić, P. Wriggers, A general phase-field model for fatigue failure in brittle and ductile solids, Comput. Mech. 67 (5) (2021) 1431–1452.

[33] C. Steinke, K. Özenç, G. Chinaryan, M. Kaliske, A comparative study of the r-adaptive material force approach and the phase-field method in dynamic fracture, Int. J. Fract. 201 (2016) 97–118.

[34] F. Vicentini, P. Carrara, L. De Lorenzis, Phase-field modeling of brittle fracture in heterogeneous bars, Eur. J. Mech.-A/Solids 97 (2023) 104826.

[35] S. Yan, R. Müller, An efficient phase field model for fatigue fracture. WCCM-APCOM 2022 Volume 100 Fracture, Damage and Failure Mechanics, 2022.

[36] S. Yan, A. Schlüter, R. Müller, Configurational forces in a phase field model for fatigue, PAMM 22 (1) (2023) e202200034.

[37] S. Yan, C. Schreiber, R. Müller, An efficient implementation of a phase field model for fatigue crack growth, Int. J. Fract. (2022) 1–14.

3. Summary, discussion, and outlook

As phase field fracture models boomed at the beginning of the twentieth century, different phase field methods for fatigue fracture have also been proposed. Phase field computer simulation demonstrates significant economic advantages compared to traditional fatigue experiments.; at the same time, the huge time cost of experiments can be skipped by using the computational method. One of the successful phase field fatigue models was introduced by Schreiber et al. [91, 92], in which a fatigue damage parameter was taken from Wöhler curve. As the damage parameter grows during the simulation, it will contribute additional energy to the total energy formulation through a newly introduced fatigue energy density. Although it was demonstrated that this model can reproduce the most essential fatigue features, there is still a gap in applying the phase field fatigue model to predict the lifetime of the structure and simulate crack behavior in practice. In this spirit, this thesis tries to fill the gap and demonstrate the usability of the model in a real manufacturing scenario.

The first problem that occurs in the phase field fatigue simulation for complex problems is its huge demand for computing resources. Speaking of high cycle fatigue of material, the number of cycles to failure is usually around tens of thousands or even more, which makes the phase field simulation computationally expensive if the classical fatigue simulation scheme is still employed. The first step of an efficient integration concept is proposed by Chaboche [27] with a non-linear cumulative damage model, where cycles with similar loading are bundled into blocks. Following this idea, [35][91] utilized a cycle-resolved simulation scheme to transfer “cycles” to “time”. It is noticed that the choice of the cycle increment plays an important role in phase field fatigue simulation, since it has a high impact on both crack pattern and simulation time. Classically, the cycle increment in phase-field fatigue simulations is treated as a constant, without accounting for the natural fatigue properties in different phases of crack evolution. For this reason, the computing time for an entire fatigue simulation can take weeks, which is inefficient for complex problems. Thanks to the introduction of the damage parameter in the phase field model, an adaptive cycle number adjustment algorithm (*ACNAA*) proposed by us in this work enables the phase field fatigue simulation under a moderate computing time without losing accuracy. The essential idea of *ACNAA* is to try to control the cycle increment by controlling of the damage increment; especially, the entire simulation is segregated into

different stages, and different damage increment controlling methods are applied for each different stage. Results show that by using *ACNAA* in phase field simulations, computing time can be reduced to nearly 3% compared to a constant cycle number increment (e.g. five cycles).

After introducing the adaptive cycle number adjustment algorithm and improving the efficiency of the phase field fatigue model, the next problem we faced is how to extend the existing phase field model to various applications and scenarios. In the second attribution, we show that by using the different fatigue parameters (k, N_D, A_D), the phase field fatigue model can capture arbitrary crack growth rates and SN curves under complex loading situations, including different temperatures and frequencies of loading. In addition to fatigue resulting from cyclic mechanical loading, fatigue failure can also be caused by fluctuating cyclic thermal loading, known as thermal fatigue. There have been very few studies on thermomechanical fatigue using phase field modeling in the literature. The other key feature of this work is that we propose a phase field model to simulate thermomechanical fatigue. The idea of this formulation is to introduce a second fatigue driving force from thermal stress, which brings an additional contribution to the crack evolution. Results show that this extended phase field model can simulate thermomechanical fatigue problems, where the thermal stress has a strong influence on the fatigue crack nucleation.

As we show in Chapter II and Chapter III, the phase field fatigue model is able to capture the most important fatigue properties under complex circumstances and reproduce the crack evolution path in an efficient fashion; however, it is still hard to understand how the phase field model works on the fatigue fracture. The reason for this difficulty is that the phase field model is based on an energetic formulation – the total energy of the body, and it is derived solely from a variational principle. It is desirable to understand the phase field model in a straightforward way. In this spirit, we borrow the concept of configurational forces and examine the energetic driving forces of the phase field model in this work. The beauty of the configurational force framework is that it is based on the material manifold itself, but not the traditional spatial coordinates. It is shown that the phase field model contains different types of energetic forces, which contribute to crack propagation in an individual manner. In general, when the configurational forces point in the same direction as the crack progresses, it accelerates the crack propagation; otherwise, it hinders further crack extension. Lastly, we show that the proposed tool of configurational forces complies with the Griffith energy criterion, where the onset of a crack happens when the total configurational force on the crack tip vanishes.

Given the complex nature of phase field models and fatigue fracture, further investigation on this topic remains necessary. Although a "cycle"-"time" transformation for the phase field model has been proposed in the literature, it is largely based on an intuitive

relationship without any physical input. One possibility is to explore the “cycle”-"time" transform and try to establish a quantitative description for this relation. At the same time, the determination of the damage increment size could also be studied for the adaptive cycle scheme, which is currently selected only based on experience. Although it has been shown that the proposed phase field fatigue model can be easily extended for simple 3D simulations [107], it still fails when applied to more complex 3D problems with arbitrary geometries and complicated boundary conditions. The reason for this shortcoming is that the phase field model requires a fine mesh to accurately describe and capture the narrow transition zone, which can lead to excessive computing time. Thus, it could also be beneficial to exploit the advantages of the *ACNAA* acceleration scheme and extend the phase field model to address 3D complex problems. Another important missing point of the phase field model for thermal fatigue is the heat transfer effect. Since the heat transfer effect is ignored in the current work, the evolution of the temperature field is absent, which could potentially influence crack evolution behavior during both nucleation and propagation. The heat transfer equation could probably be included in the phase field model in order to yield more precise results. It is expected that the increased temperature resulting from the evolution of the temperature field will be coupled into crack evolution, which could accelerate crack propagation. Furthermore, it is worth studying how to extend the presented phase field fatigue model into the low-cycle fatigue regime, where material plasticity can be strongly coupled. As the presented phase field fatigue model is more suitable for brittle materials and high-cycle fatigue, the plastic deformation and the plastic energy of the material is not explicitly modeled. Thus, it is worth trying to include the plastic energy density into the total energy formulation for low-cycle fatigue problems. At the same time, the plastic stress could provide an additional contribution to the fatigue driving force. It is also worthwhile to continue studying how to use the phase field method to model contact fatigue. In such applications, it may be more suitable to use von Mises stress instead of principal stress as the fatigue driving force. It is anticipated that cracks will nucleate below the contact surface due to the shear stress effect in these scenarios. The presented phase field fatigue model could be applied to more engineering applications, such as studying the influence of surface roughness on fatigue life. For these research studies, it would be advantageous if more experimental data could be provided for validation.

Bibliography

[1] R. Ahluwalia and W. Cao. Effect of surface induced nucleation of ferroelastic domains on polarization switching in constrained ferroelectrics. *Journal of applied physics*, 93(1):537–544, 2003.

[2] F. Aldakheel, C. Schreiber, R. Müller, and P. Wriggers. Phase-field modeling of fatigue crack propagation in brittle materials. In *Current Trends and Open Problems in Computational Mechanics*, pages 15–22. Springer, 2022.

[3] R. Alessi, J.-J. Marigo, C. Maurini, and S. Vidoli. Coupling damage and plasticity for a phase-field regularisation of brittle, cohesive and ductile fracture: one-dimensional examples. *International Journal of Mechanical Sciences*, 149:559–576, 2018.

[4] R. Alessi and J. Ulloa. Endowing griffith's fracture theory with the ability to describe fatigue cracks. *Engineering Fracture Mechanics*, page 109048, 2023.

[5] R. Alessi, S. Vidoli, and L. De Lorenzis. A phenomenological approach to fatigue with a variational phase-field model: The one-dimensional case. *Engineering fracture mechanics*, 190:53–73, 2018.

[6] M. Ambati and L. De Lorenzis. Phase-field modeling of brittle and ductile fracture in shells with isogeometric nurbs-based solid-shell elements. *Computer Methods in Applied Mechanics and Engineering*, 312:351–373, 2016.

[7] M. Ambati, T. Gerasimov, and L. De Lorenzis. A review on phase-field models of brittle fracture and a new fast hybrid formulation. *Computational Mechanics*, 55:383–405, 2015.

[8] L. Ambrosio and V. M. Tortorelli. Approximation of functional depending on jumps by elliptic functional via t-convergence. *Communications on Pure and Applied Mathematics*, 43(8):999–1036, 1990.

[9] G. Amendola, M. Fabrizio, and J. M. Golden. Thermomechanics of damage and fatigue by a phase field model. *Journal of Thermal Stresses*, 39(5):487–499, 2016.

[10] H. Amor, J.-J. Marigo, and C. Maurini. Regularized formulation of the variational brittle fracture with unilateral contact: Numerical experiments. *Journal of the Mechanics and Physics of Solids*, 57(8):1209–1229, 2009.

[11] T. L. Anderson. *Fracture mechanics: fundamentals and applications*. CRC press, 2017.

[12] I. Aranson, V. Kalatsky, and V. Vinokur. Continuum field description of crack propagation. *Physical review letters*, 85(1):118, 2000.

[13] ASTM. ASTM E606, Standard test method for strain-controlled fatigue testing. Technical report, 2021. `http://www.astm.org`.

[14] S. Banerjee and A. Roy. *Linear algebra and matrix analysis for statistics*. Crc Press, 2014.

[15] C. Bathias. There is no infinite fatigue life in metallic materials. *Fatigue & fracture of engineering materials & structures (Print)*, 22(7):559–565, 1999.

[16] W. Becker and D. Gross. *Mechanik elastischer Körper und Strukturen*. Springer-Verlag, 2013.

[17] M. Benedetti, A. Du Plessis, R. O. Ritchie, M. Dallago, N. Razavi, and F. Berto. Architected cellular materials: A review on their mechanical properties towards fatigue-tolerant design and fabrication. *Materials Science and Engineering: R: Reports*, 144:100606, 2021.

[18] M. J. Borden, T. J. Hughes, C. M. Landis, A. Anvari, and I. J. Lee. A phase-field formulation for fracture in ductile materials: Finite deformation balance law derivation, plastic degradation, and stress triaxiality effects. *Computer Methods in Applied Mechanics and Engineering*, 312:130–166, 2016.

[19] M. J. Borden, T. J. Hughes, C. M. Landis, and C. V. Verhoosel. A higher-order phase-field model for brittle fracture: Formulation and analysis within the isogeometric analysis framework. *Computer Methods in Applied Mechanics and Engineering*, 273:100–118, 2014.

[20] M. J. Borden, C. V. Verhoosel, M. A. Scott, T. J. Hughes, and C. M. Landis. A phase-field description of dynamic brittle fracture. *Computer Methods in Applied Mechanics and Engineering*, 217:77–95, 2012.

[21] B. Bourdin. Numerical implementation of the variational formulation for quasi-static brittle fracture. *Interfaces and free boundaries*, 9(3):411–430, 2007.

[22] B. Bourdin, G. A. Francfort, and J.-J. Marigo. Numerical experiments in revisited brittle fracture. *Journal of the Mechanics and Physics of Solids*, 48(4):797–826, 2000.

[23] B. Bourdin, C. J. Larsen, and C. L. Richardson. A time-discrete model for dynamic fracture based on crack regularization. *International journal of fracture*, 168(2):133–143, 2011.

[24] E. C. Bryant and W. Sun. A mixed-mode phase field fracture model in anisotropic rocks with consistent kinematics. *Computer Methods in Applied Mechanics and Engineering*, 342:561–584, 2018.

[25] M. Caputo and M. Fabrizio. Damage and fatigue described by a fractional derivative model. *Journal of Computational Physics*, 293:400–408, 2015.

[26] P. Carrara, M. Ambati, R. Alessi, and L. De Lorenzis. A framework to model the fatigue behavior of brittle materials based on a variational phase-field approach. *Computer Methods in Applied Mechanics and Engineering*, 361:112731, 2020.

[27] J. L. Chaboche and P. M. Lesne. A non-linear continuous fatigue damage model. *Fatigue & fracture of engineering materials & structures*, 11(1):1–17, 1988.

[28] M. Ciavarella, P. D'antuono, and A. Papangelo. On the connection between palmgren-miner rule and crack propagation laws. *Fatigue & Fracture of Engineering Materials & Structures*, 41(7):1469–1475, 2018.

[29] L. F. Coffin. Concept of frequency separation in life prediction for time-dependent fatigue. Technical report, General Electric Co., Schenectady, NY (USA), 1976.

[30] M. Dittmann, F. Aldakheel, J. Schulte, P. Wriggers, and C. Hesch. Variational phase-field formulation of non-linear ductile fracture. *Computer Methods in Applied Mechanics and Engineering*, 342:71–94, 2018.

[31] W. Dornisch, D. Schrade, B.-X. Xu, M.-A. Keip, and R. Müller. Coupled phase field simulations of ferroelectric and ferromagnetic layers in multiferroic heterostructures. *Archive of Applied Mechanics*, 89:1031–1056, 2019.

[32] N. Dowling, C. Calhoun, and A. Arcari. Mean stress effects in stress-life fatigue and the walker equation. *Fatigue & Fracture of Engineering Materials & Structures*, 32(3):163–179, 2009.

[33] F. Erdogan and G. Sih. On the crack extension in plates under plane loading and transverse shear. *Journal of Basic Engineering*, 85:519–525, 1963.

[34] J. A. Ewing and J. C. W. Humfrey. The fracture of metals under repeated alternations of stress. *Proceedings of the Royal Society of London Series I*, 71:79, 1902.

[35] J. Fish and Q. Yu. Computational mechanics of fatigue and life predictions for composite materials and structures. *Computer methods in applied mechanics and engineering*, 191(43):4827–4849, 2002.

[36] G. A. Francfort and J.-J. Marigo. Revisiting brittle fracture as an energy minimization problem. *Journal of the Mechanics and Physics of Solids*, 46(8):1319–1342, 1998.

[37] G. A. Francfort and J.-J. Marigo. Griffith theory of brittle fracture revisited: merits and drawbacks. *Latin American Journal of Solids and Structures*, 2(1):57–64, 2005.

[38] V. L. Ginzburg. On the theory of superconductivity. *Il Nuovo Cimento (1955-1965)*, 2:1234–1250, 1955.

[39] R. V. Gol'dstein and R. L. Salganik. Brittle fracture of solids with arbitrary cracks. *International journal of Fracture*, 10:507–523, 1974.

[40] J. Goodman. *Mechanics applied to engineering*. Longmans, Green, 1919.

[41] A. A. Griffith. Vi. the phenomena of rupture and flow in solids. *Philosophical transactions of the royal society of london. Series A, containing papers of a mathematical or physical character*, 221(582-593):163–198, 1921.

[42] D. Gross and T. Seelig. *Fracture mechanics: with an introduction to micromechanics*. Springer, 2017.

[43] B. E. Grossman-Ponemon, A. Mesgarnejad, and A. Karma. Phase-field modeling of continuous fatigue via toughness degradation. *Engineering Fracture Mechanics*, 264:108255, 2022.

[44] M. E. Gurtin. *An introduction to continuum mechanics*. Academic press, 1982.

[45] M. E. Gurtin. Generalized ginzburg-landau and cahn-hilliard equations based on a microforce balance. *Physica D: Nonlinear Phenomena*, 92(3-4):178–192, 1996.

[46] M. M. Hasan and T. Baxevanis. A phase-field model for low-cycle fatigue of brittle materials. *International Journal of Fatigue*, 150:106297, 2021.

[47] G. A. Haveroth, M. G. Vale, M. L. Bittencourt, and J. L. Boldrini. A non-isothermal thermodynamically consistent phase field model for damage, fracture and fatigue evolutions in elasto-plastic materials. *Computer Methods in Applied Mechanics and Engineering*, 364:112962, 2020.

[48] H. Henry and H. Levine. Dynamic instabilities of fracture under biaxial strain using a phase field model. *Physical review letters*, 93(10):105504, 2004.

[49] M. Hofacker and C. Miehe. Continuum phase field modeling of dynamic fracture: variational principles and staggered fe implementation. *International journal of fracture*, 178(1):113–129, 2012.

[50] M. Hofacker and C. Miehe. A phase field model of dynamic fracture: Robust field updates for the analysis of complex crack patterns. *International Journal for Numerical Methods in Engineering*, 93(3):276–301, 2013.

[51] C. E. Inglis. Stresses in a plate due to the presence of cracks and sharp corners. *Trans Inst Naval Archit*, 55:219–241, 1913.

[52] G. R. Irwin. Analysis of stresses and strains near the end of a crack traversing a plate. *Journal of Applied Mechanics*, 24(3):361–364, 1957.

[53] M. Kalina, T. Schneider, J. Brummund, and M. Kästner. Overview of phase-field models for fatigue fracture in a unified framework. *Engineering Fracture Mechanics*, 288:109318, 2023.

[54] K. Kanazawa and S. Nishijima. Fatigue fracture of low alloy steel at ultra-high-cycle region under elevated temperature condition. *Journal of the Society of Materials Science, Japan*, 46, 1997.

[55] A. Karma, D. A. Kessler, and H. Levine. Phase-field model of mode iii dynamic fracture. *Physical Review Letters*, 87(4):045501, 2001.

[56] M. Kikuchi, H. Ueda, and T. Naito. Fatigue behavior of carburized steel with internal oxides near the surface. *Metallurgical Transactions A*, 18(1):156–158, 1987.

[57] S. K. Koh and R. I. Stephens. Mean stress effects on low cycle fatigue for a high strength steel. *Fatigue & Fracture of Engineering Materials & Structures*, 14(4):413–428, 1991.

[58] C. Kuhn and R. Müller. A continuum phase field model for fracture. *Engineering Fracture Mechanics*, 77(18):3625–3634, 2010.

[59] C. Kuhn, T. Noll, and R. Müller. On phase field modeling of ductile fracture. *GAMM-Mitteilungen*, 39(1):35–54, 2016.

[60] W. M. Lai, D. Rubin, and E. Krempl. *Introduction to continuum mechanics*. Butterworth-Heinemann, 2009.

[61] C. J. Larsen, C. Ortner, and E. Süli. Existence of solutions to a regularized model of dynamic fracture. *Mathematical Models and Methods in Applied Sciences*, 20(07):1021–1048, 2010.

[62] S. Lee, B. Min, and M. F. Wheeler. Correction to: Optimal design of hydraulic fracturing in porous media using the phase field fracture model coupled with genetic algorithm. *Computational Geosciences*, 22(6):1583–1583, 2018.

[63] B. Li, C. Peco, D. Millán, I. Arias, and M. Arroyo. Phase-field modeling and simulation of fracture in brittle materials with strongly anisotropic surface energy. *International Journal for Numerical Methods in Engineering*, 102(3-4):711–727, 2015.

[64] Y.-S. Lo, M. J. Borden, K. Ravi-Chandar, and C. M. Landis. A phase-field model for fatigue crack growth. *Journal of the Mechanics and Physics of Solids*, 132:103684, 2019.

[65] P. J. Loew, B. Peters, and L. A. Beex. Fatigue phase-field damage modeling of rubber using viscous dissipation: Crack nucleation and propagation. *Mechanics of Materials*, 142:103282, 2020.

[66] S. S. Manson, G. R. Halford, and M. H. Hirschberg. Creep-fatigue analysis by strain-range partitioning. In *ASME symposium for design for elevated temperature environment, San Francisco, USA*, 1971.

[67] G. B. McFadden. Phase-field models of solidification. *Contemporary Mathematics*, 306:107–146, 2002.

[68] A. Mesgarnejad, A. Imanian, and A. Karma. Phase-field models for fatigue crack growth. *Theoretical and Applied Fracture Mechanics*, 103:102282, 2019.

[69] C. Miehe, F. Aldakheel, and A. Raina. Phase field modeling of ductile fracture at finite strains: A variational gradient-extended plasticity-damage theory. *International Journal of Plasticity*, 84:1–32, 2016.

[70] C. Miehe, M. Hofacker, and F. Welschinger. A phase field model for rate-independent crack propagation: Robust algorithmic implementation based on operator splits. *Computer Methods in Applied Mechanics and Engineering*, 199(45-48):2765–2778, 2010.

[71] C. Miehe, F. Welschinger, and F. Aldakheel. Variational gradient plasticity at finite strains. part ii: Local–global updates and mixed finite elements for additive plasticity in the logarithmic strain space. *Computer Methods in Applied Mechanics and Engineering*, 268:704–734, 2014.

[72] C. Miehe, F. Welschinger, and M. Hofacker. Thermodynamically consistent phase-field models of fracture: Variational principles and multi-field fe implementations. *International journal for numerical methods in engineering*, 83(10):1273–1311, 2010.

[73] M. A. Miner. Cumulative damage in fatigue. *Journal of Applied Mechanics*, 1945.

[74] H. Mughrabi. Microstructural mechanisms of cyclic deformation, fatigue crack initiation and early crack growth. *Philosophical Transactions of the Royal Society A: Mathematical, Physical and Engineering Sciences*, 373(2038):20140132, 2015.

[75] D. Mumford and J. Shah. Boundary detection by minimizing functionals. In *IEEE Conference on Computer Vision and Pattern Recognition*, volume 17, pages 137–154. San Francisco, 1985.

[76] S. Nambu and D. A. Sagala. Domain formation and elastic long-range interaction in ferroelectric perovskites. *Physical Review B*, 50(9):5838, 1994.

[77] R. Neu and H. Sehitoglu. Thermomechanical fatigue, oxidation, and creep: Part i. damage mechanisms. *Metallurgical transactions A*, 20:1755–1767, 1989.

[78] T. T. Nguyen, J. Réthoré, and M.-C. Baietto. Phase field modelling of anisotropic crack propagation. *European Journal of Mechanics-A/Solids*, 65:279–288, 2017.

[79] R. Nuismer. An energy release rate criterion for mixed mode fracture. *International journal of fracture*, 11:245–250, 1975.

[80] P. Paris and F. Erdogan. A critical analysis of crack propagation laws. *Journal of Basic Engineering*, 85(4):528–533, 1963.

[81] O. Penrose and P. C. Fife. Thermodynamically consistent models of phase-field type for the kinetic of phase transitions. *Physica D: Nonlinear Phenomena*, 43(1):44–62, 1990.

[82] J. Polák. The effect of intermediate annealing on the electrical resistivity and shear stress of fatigued copper. *Scripta Metallurgica*, 4(10):761–764, 1970.

[83] J. R. Rice. A path independent integral and the approximate analysis of strain concentration by notches and cracks. *Journal of Applied Mechanics*, 35(2):379–386, 1968.

[84] R. O. Ritchie. Mechanisms of fatigue-crack propagation in ductile and brittle solids. *International journal of Fracture*, 100(1):55–83, 1999.

[85] M. D. Sangid. The physics of fatigue crack initiation. *International journal of fatigue*, 57:58–72, 2013.

[86] J. Schijve. Significance of fatigue cracks in micro-range and macro-range. In *Fatigue crack propagation*. ASTM International, 1967.

[87] J. Schijve. *Fatigue of structures and materials*. Springer, 2009.

[88] A. Schlüter, A. Willenbücher, C. Kuhn, and R. Müller. Phase field approximation of dynamic brittle fracture. *Computational Mechanics*, 54(5):1141–1161, 2014.

[89] D. Schrade, R. Müller, D. Gross, M.-A. Keip, H. Thai, and J. Schröder. An invariant formulation for phase field models in ferroelectrics. *International Journal of Solids and Structures*, 51(11-12):2144–2156, 2014.

[90] C. Schreiber. *Phase Field Modeling of Fracture: Fatigue and Anisotropic Fracture Resistance*. Technische Universität Kaiserslautern, 2021.

[91] C. Schreiber, C. Kuhn, R. Müller, and T. Zohdi. A phase field modeling approach of cyclic fatigue crack growth. *International Journal of Fracture*, 225(1):89–100, 2020.

[92] C. Schreiber, R. Müller, and C. Kuhn. Phase field simulation of fatigue crack propagation under complex load situations. *Archive of Applied Mechanics*, pages 1–15, 2020.

[93] W. Schütz. A history of fatigue. *Engineering fracture mechanics*, 54(2):263–300, 1996.

[94] M. Seiler, T. Linse, P. Hantschke, and M. Kästner. An efficient phase-field model for fatigue fracture in ductile materials. *Engineering Fracture Mechanics*, 224:106807, 2020.

[95] K. Seleš, F. Aldakheel, Z. Tonković, J. Sorić, and P. Wriggers. A general phase-field model for fatigue failure in brittle and ductile solids. *Computational Mechanics*, 67(5):1431–1452, 2021.

[96] K. Seleš, Z. Tomić, and Z. Tonković. Microcrack propagation under monotonic and cyclic loading conditions using generalised phase-field formulation. *Engineering Fracture Mechanics*, 255:107973, 2021.

[97] P. Shanthraj, L. Sharma, B. Svendsen, F. Roters, and D. Raabe. A phase field model for damage in elasto-viscoplastic materials. *Computer Methods in Applied Mechanics and Engineering*, 312:167–185, 2016.

[98] S. Taira. Lifetime of structures subjected to varying load and temperature. In *Creep in Structures: Colloquium Held at Stanford University, California July 11–15, 1960*, pages 96–124. Springer, 1962.

[99] A. Tsakmakis and M. Vormwald. Phase field modelling of ductile fracture in the frameworks of non-conventional thermodynamics and continuum damage mechanics. *International Journal of Solids and Structures*, 262:112049, 2023.

[100] J. Ulloa, J. Wambacq, R. Alessi, G. Degrande, and S. François. Phase-field modeling of fatigue coupled to cyclic plasticity in an energetic formulation. *Computer Methods in Applied Mechanics and Engineering*, 373:113473, 2021.

[101] K. Walker. The effect of stress ratio during crack propagation and fatigue for 2024-t3 and 7075-t6 aluminum. *ASTM Special Technical Publication (American Society for Testing and Materials)*, 462:1–14, 1970.

[102] J. Wang and J. Zhang. A real-space phase field model for the domain evolution of ferromagnetic materials. *International Journal of Solids and Structures*, 50(22-23):3597–3609, 2013.

[103] J. A. Warren, R. Kobayashi, A. E. Lobkovsky, and W. C. Carter. Extending phase field models of solidification to polycrystalline materials. *Acta materialia*, 51(20):6035–6058, 2003.

[104] A. A. Wheeler, W. J. Boettinger, and G. B. McFadden. Phase-field model for isothermal phase transitions in binary alloys. *Physical Review A*, 45(10):7424, 1992.

[105] Q. Xin. *Diesel engine system design*. Elsevier, 2011.

[106] Q. Xin. Durability and reliability in diesel engine system design. *Diesel Engine System Design*, pages 113–202, 2013.

[107] S. Yan and R. Müller. An efficient phase field model for fatigue fracture. *WCCM-APCOM 2022*, Volume 100 Fracture, Damage and Failure Mechanics, 2022.

[108] S. Yan, C. Schreiber, and R. Müller. An efficient implementation of a phase field model for fatigue crack growth. *International Journal of Fracture*, pages 1–14, 2022.

[109] M. Yi and B.-X. Xu. A constraint-free phase field model for ferromagnetic domain evolution. *Proceedings of the Royal Society A: Mathematical, Physical and Engineering Sciences*, 470(2171):20140517, 2014.

[110] P. Yin, W. Zhang, Y. Zhang, Q. Yang, F. Liang, L. Chang, and C. Zhou. Cyclic deformation mechanism and fracture behaviour of 316l stainless steel under thermomechanical fatigue loading. *Journal of Materials Research and Technology*, 24:4484–4499, 2023.

[111] S. Zhou, X. Zhuang, and T. Rabczuk. A phase-field modeling approach of fracture propagation in poroelastic media. *Engineering Geology*, 240:189–203, 2018.

A. Additional paper

Published in:
Proceedings of the 3rd Conference on Physical Modeling for Virtual Manufacturing Systems and Processes, pp 16–31 (2023)
DOI: https://doi.org/10.1007/978-3-031-35779-4_2

A.1. Objectives of the additional paper

During the decades, the phase field fatigue has been well-established for various loading situations within an advanced computing strategy [91] [92] [108]. The next frontier before us is how to use the phase field fatigue model to solve manufacturing problems. In manufacturing and engineering processes, fatigue failure is one of the most critical and dangerous issues since it is hard to detect and prevent. Thus, it is desired to simulate the fatigue process in advance, proactively avoiding such failures.

In this paper, the phase field fatigue model is used to simulate the fatigue process of the cold forging process. First, we give a comprehensive review of the key contributions of the presented phase field fatigue model. For efficient computing, the existing phase field model needs to extend into a cylindrical coordinate system in this work. Next, the cold forge die is simulated with the proposed phase field model. The results demonstrate that the phase field model can reliably predict the fatigue life and crack propagation of the die geometry in advance within different case studies.

Phase Field Simulations for Fatigue Failure Prediction in Manufacturing Processes

S. Yan[1( )], R. Müller[2], and B. Ravani[3]

[1] Institute of Applied Mechanics, University of Kaiserslautern-Landau, Kaiserslautern, Germany
sikang.yan@rptu.de
[2] Institute for Mechanics, Technical University of Darmstadt, Darmstadt, Germany
[3] Department of Mechanical and Aerospace Engineering, University of California Davis, Davis, USA

Abstract. Fatigue failure is one of the most crucial issues in manufacturing and engineering processes. Stress cycles can cause cracks to form and grow over time, eventually leading to structural failure. To avoid these failures, it is important to predict fatigue crack evolution behavior in advance. In the past decade, the phase field method for crack evoluation analysis has drawn a lot of attention for its application in fracture mechanics. The biggest advantage of the phase field model is its uniform description of all crack evolution behaviors by one evolution equation. The phase field method simultaneously models crack nucleation and crack propagation which will be particularly useful manufacturing problems. In this work, we show that the phase field method is capable to reproduce the most important fatigue features, e.g., Paris' law, mean stress effect, and load sequence effects. For efficient computing, a "cycle"- "time" transformation is introduced to convert individual cycle numbers into a continuous time domain. In order to exploit the symmetry property of the demonstrated examples, a phase field model in cylindrical coordinates is presented. Finally, the fatigue modeling approach presented is applied to study a cold forging process in manufacturing.

1 Introduction

The phase field model was initially used to solve the interfacial problem, like ferromagnetism, ferroelectrics, and solidification dynamics [1]. Moreover, the phase field model can also be applied in fracture mechanics [2–6]. The method has the advantage that it takes a monolithic approach to simulate crack initiation, branching, bifurcation, and unification. It also overcomes stress singularity, displacement jumps, or interface tracking during the fracture simulation. Differing from other methods, neither remeshing nor finite elements with special shape functions are needed in the phase field model; the simulation is performed on a fixed mesh. The core idea of a phase field fracture model is to introduce an additional field variable to represent cracks. This scalar field variable interpolates smoothly between the values of 0 and 1, representing cracked and undamaged material, respectively. The relevant equations are derived from the total energy of

J. C. Aurich et al. (Eds.): IRTG 2023, *Proceedings of the 3rd Conference on Physical Modeling for Virtual Manufacturing Systems and Processes*, pp. 16–31, 2023.
https://doi.org/10.1007/978-3-031-35779-4_2

the system by a variational principle (one equation models the equilibrium of the stress field, and a second models the evolution of the crack field). Consequently, contour plots of a scalar field variable used allow for the visualization of the progression of fracture and reproduce the crack situation. A phase field model has been successfully applied for quasi-static [7–9] and dynamic cases [6, 10–14]. Further recent model extensions also allow the consideration of ductile fracture [15–18], anisotropic fracture properties [19–21], and the evolution of fracture in various multi-physics scenarios [22–25].

In manufacturing processes like cutting, the dynamic loads typically do not cause an immediate failure of a tool; instead, tool failure can occur due to fatigue fracture development over numerous loading cycles. Thus, a phase field model which can handle the fatigue scenarios is required. In this paper the application of the model presented is focused on the fatigue failure of manufacturing tools. Since the driving mechanisms of fatigue failure significantly differ from those of classical linear elastic fracture mechanics, it was necessary to make appropriate adjustments to the evolution equation of the fracture field to model fatigue crack growth in manufacturing. Time-resolved simulations are impractical since fatigue failure only happens after a significant number of cycles; hence the evolution equation must be written in the context of cycles. The numerical implementation must be able to consolidate multiple cycles into a pseudo time to achieve the efficiency needed for the use of the model in actual production processes. In this work, we present a phase field model for cyclic fatigue. Since fatigue cracks won't appear until several loading cycles have been completed, fatigue simulations generally consume high computing time. We introduce an adaptive cycle increment algorithm, which provides a moderate computing time without losing accuracy compared to the classical computing strategies.

This paper proceeds as follows: in Sect. 2, a phase field model for cyclic fatigue is presented. In addition, a "cycle"- "time" transfer is proposed to bundle several cycles to a pseudo time domain for efficient computing. An adaptive cycle increment algorithm is then developed to reduce the computational cost without losing accuracy. In Sect. 3, an example of a manufacturing problem is modeled by the phase field fatigue model. In Sect. 4, the conclusions are stated.

2 A Phase Field Model for Cyclic Fatigue

The phase field fracture model introduces an additional field variable to represent cracks [7, 26]. The crack field s is 1 if the material is undamaged and if it is 0 where cracks occur. Furthermore, it is postulated that the displacement field $\mathbf{u}$ and crack field s locally minimize the total energy of a loaded body Ω. This yields the equilibrium of the stress field and the evolution of the crack field for fatigue fracturing. The extended total energy $\mathcal{E}$ with $\boldsymbol{t}$ as the external traction and $\boldsymbol{f}$ as the volume forces on the body is given by

$$\mathcal{E} = \int_{\Omega} \psi \mathrm{d}V - \int_{\partial\Omega} \boldsymbol{t} \mathrm{d}A - \int_{\Omega} \boldsymbol{f} \mathrm{d}V \tag{1}$$

where ψ denotes the total energy density of the body

$$\psi = (g(s) + \eta)\psi^{e}(\boldsymbol{\varepsilon}) + \psi^{s}(s, \nabla s) + h(s)\psi^{\mathrm{ad}}(D), \tag{2}$$

which consists of three parts: elastic part, fracture surface part and additional fatigue part.

The strain energy density

$$\psi^e(\boldsymbol{\varepsilon}) = \frac{1}{2}\boldsymbol{\varepsilon} : \mathbb{C}(\boldsymbol{\varepsilon}) \tag{3}$$

is the elastic energy stored inside of a body with $g(s)$ as a degradation function, which models the loss of stiffness of the broken material. The tensor $\boldsymbol{\varepsilon}$ is the infinitesimal strain, defined by

$$\boldsymbol{\varepsilon} = \begin{bmatrix} \varepsilon_{xx} & \varepsilon_{xy} & \varepsilon_{xz} \\ \varepsilon_{yx} & \varepsilon_{yy} & \varepsilon_{yz} \\ \varepsilon_{zx} & \varepsilon_{zy} & \varepsilon_{zz} \end{bmatrix} = \begin{bmatrix} \frac{\partial u_x}{\partial x} & \frac{1}{2}\left(\frac{\partial u_y}{\partial x} + \frac{\partial u_x}{\partial y}\right) & \frac{1}{2}\left(\frac{\partial u_x}{\partial x} + \frac{\partial u_z}{\partial z}\right) \\ \frac{1}{2}\left(\frac{\partial u_y}{\partial x} + \frac{\partial u_x}{\partial y}\right) & \frac{\partial u_y}{\partial y} & \frac{1}{2}\left(\frac{\partial u_y}{\partial z} + \frac{\partial u_z}{\partial y}\right) \\ \frac{1}{2}\left(\frac{\partial u_z}{\partial x} + \frac{\partial u_x}{\partial z}\right) & \frac{1}{2}\left(\frac{\partial u_z}{\partial y} + \frac{\partial u_y}{\partial z}\right) & \frac{\partial u_z}{\partial z} \end{bmatrix} \tag{4}$$

The crack surface density

$$\psi^s(s, \nabla s) = \mathcal{G}_c\left(\frac{(1-s)^2}{4\epsilon} + \epsilon|\nabla s|^2\right) \tag{5}$$

is the energy required to separate the material to generate a crack, which is assumed to be proportional to the crack surface. The parameter $\mathcal{G}_c$ denotes fracture resistance and can be related to fracture toughness. The numerical parameter ϵ – not to be confused with strain tensor - models the width of the smooth transition zone between the broken and unbroken material.

The fatigue energy density

$$\psi^{\mathrm{ad}}(D) = q < D - D_c >^b \quad \text{with} \quad D = D_0 + \mathrm{d}D \tag{6}$$

is introduced to account for the accumulated fatigue driving forces, which is associated with a fatigue damage parameter D. This parameter D models the damage related to fatigue, inspired by Miner rule [28], which is accumulated during the simulation. The parameter D_0 is the previous damage and

$$\mathrm{d}D = \frac{\mathrm{d}N}{n_D}\left(\frac{\widehat{\sigma}}{A_D}\right)^k \tag{7}$$

is the damage increment, which is associated with the cycle increment $\mathrm{d}N$, where the parameters n_D, A_D and k are extracted from the Wöhler curve of experiments [29]. This formulation allows the phase field fatigue model to incorporate all the influences from the environment into the fatigue propagation behavior [30]. In the phase field model, the first principal stress $\widehat{\sigma}_1$ from the undegraded stress field

$$\widehat{\sigma}_1 = [\mathbb{C}\boldsymbol{\varepsilon}]_1 \tag{8}$$

is used as the fatigue driving force for high cycle fatigue. It is noted that it is not claimed that this choice of the driving force is suitable for all materials. Other effective stress

quantities, e.g. the von-Mises stress, might be more suitable for ductile material and low cycle fatigue [31, 32]. Moreover, a mean stress corrector can be applied to include the mean stress effect on the fatigue crack propagation [27, 33]. The parameter D_c is a damage threshold, which models the crack nucleation process. With the Macauley brackets ($< \bullet >$), the additional fatigue energy ψ^{ad} will not contribute when the damage D is below this threshold. After the crack nucleation stage, the parameters q and b are parameters controlling how intense the additional fatigue energy drives the crack. A discussion of different choices of the parameters q and b can be found in [34]. The degradation function $h(s)$ - similarly as $g(s)$ - models the loss of the stiffness of broken material due to cyclic fatigue. A discussion of different choices of the degradation functions can be found in [34, 36].

With the variational principle of Eq. (1), four coupled equations are derived

$$\text{div}\frac{\partial \psi}{\partial \nabla \mathbf{u}} + \boldsymbol{f} = 0 \tag{9}$$

$$\frac{\partial \psi}{\partial s} - \text{div}\frac{\partial \psi}{\partial \nabla s} = 0 \tag{10}$$

$$\frac{\partial \psi}{\partial \nabla s} \cdot \mathbf{n} = 0 \quad \text{on} \quad \partial\Omega_{\nabla s} \tag{11}$$

$$\left(\frac{\partial \psi}{\partial \nabla \boldsymbol{u}}\right)\mathbf{n} = \boldsymbol{t} \quad \text{on} \quad \partial\Omega_t \tag{12}$$

Equation (9) describes the equilibrium condition of the stress field; Eq. (10) described the evolution behavior of the crack field; Eq. (11) and Eq. (12) are the Neumann boundary conditions for the crack field and displacement field. Those equations define the fatigue fracture problem.

The phase field fatigue model can reproduce the most important fatigue properties. In the following evaluation, the material parameters are taken from [26] with a CT specimen [37] as a numerical example. The crack growth rate is depicted in Fig. 1 for various maximum stress amplitude values. It is to observe that even though different stress amplitudes for the simulation are applied, the rate of crack growth can be described with the same Paris' law. The result matches Paris' law with $m = 5.54$ very well. Radhakrishnan [38] shows that in some materials the constant C and the slope m depend on the stress ratio R. The stress ratio R is defined as the ratio between the minimum stress and the maximum stress. At high positive mean stress, a decrease in fatigue life is associated with multiple crack initiation sites at the specimen surface. Fatigue limit is highly affected by the tensile mean stress and stress ratio since the maximum stress approaches near yield stress and it causes cyclic ratcheting [39]. Figure 2 displays the effect of mean stress on the crack growth rate, which reflects the fact that higher mean stress increases the rate of crack growth [40]. Figure 3 reports the effect of the loading sequence on the crack growth rate. Results show that a high-low loading sequence results in short fatigue life. This phenomenon is called the loading sequence effect [41, 42]. It has been shown that the material with a low-high load sequxsence results in a longer fatigue life because the low load level is mostly involved in the crack nucleation and the high load level is contributed to the crack propagation [43]. This effect can be explained

by the residual stresses and crack closure near the crack tip [44]. Although Miner's rule does not include the loading sequence effect, the damage quantity D with a low load level increases slowly, such that it reaches the critical damage state D_c later than a high load level.

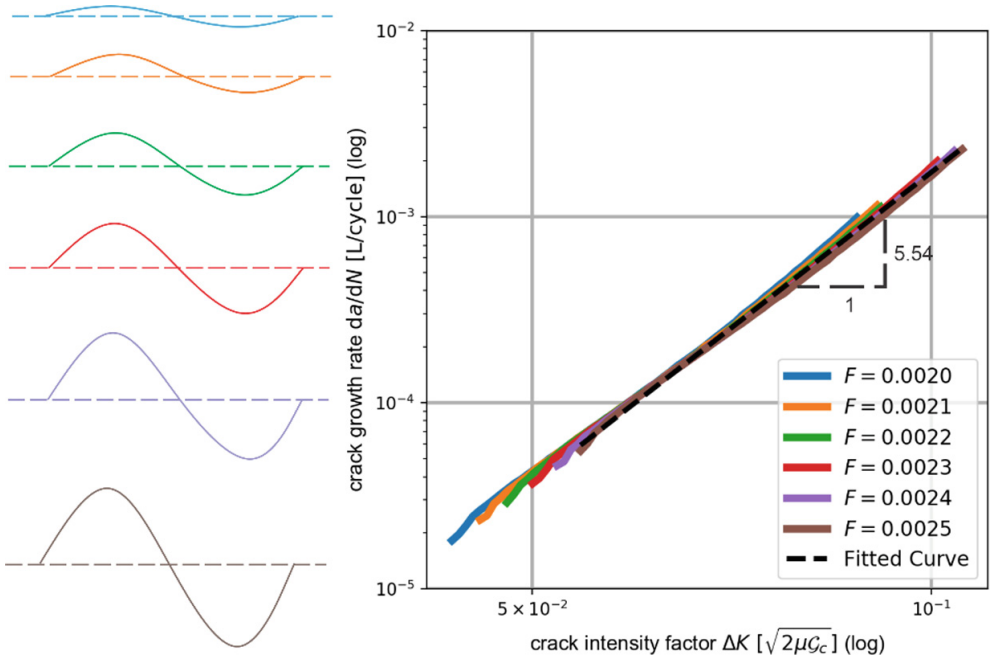

Fig. 1. Different maximum load amplitude [35].

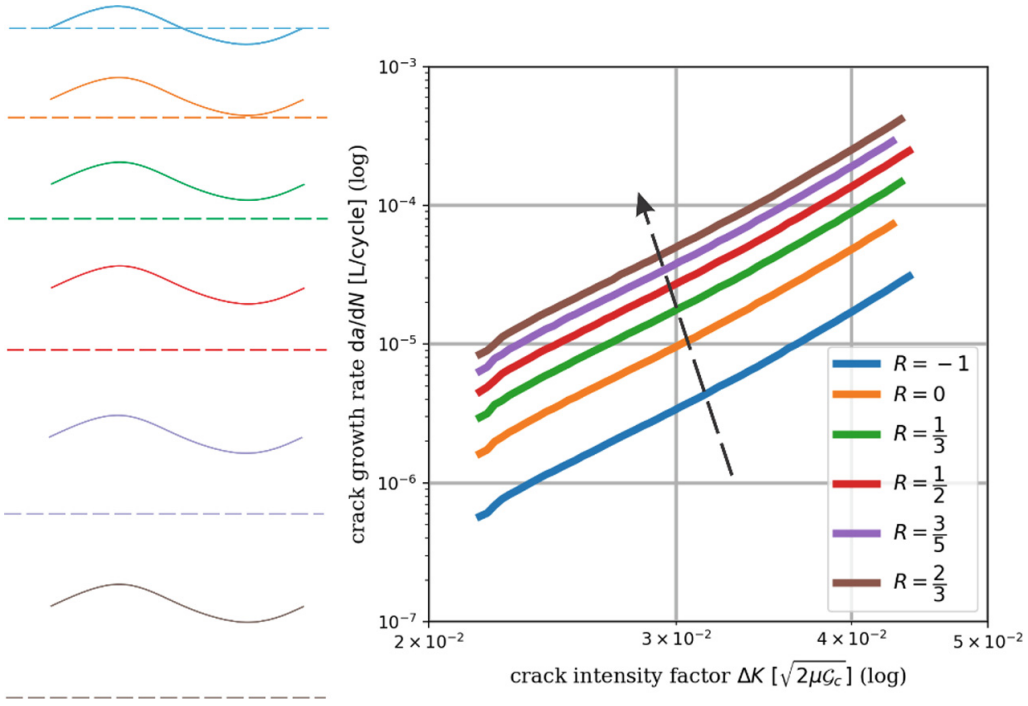

Fig. 2. Different mean stress [35].

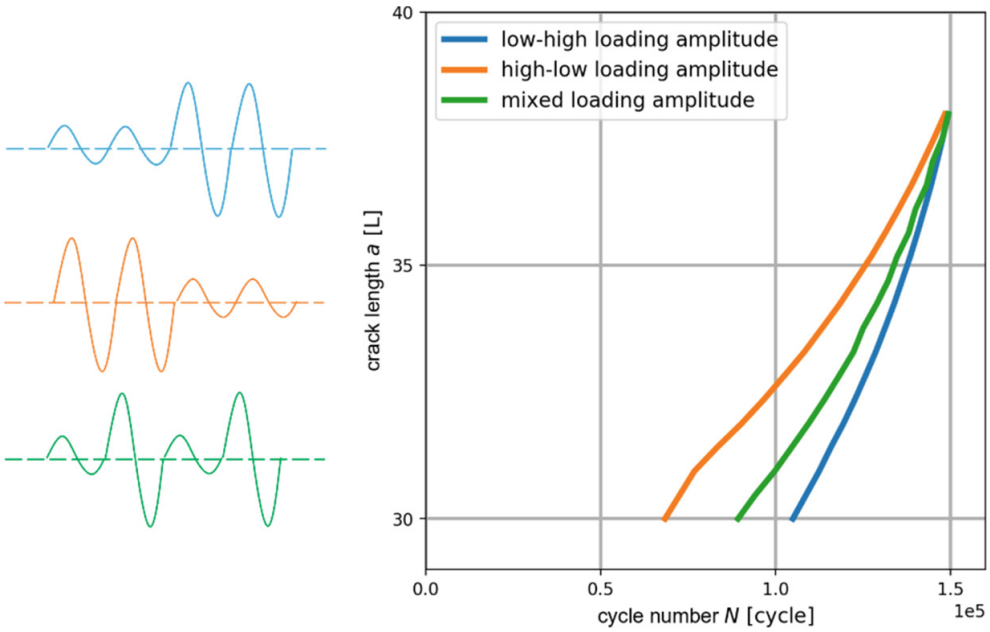

Fig. 3. Different loading sequences.

2.1 A Time-Cycle Transformation in the Phase Field Fatigue Model

As the discussion in the previous section, the phase field fatigue model is more suitable for high cycle fatigue. Speaking of high cycle fatigue, the number of cycles to failure is usually around tens of millions or even more. Thus, it is not feasible to simulate the accumulated cycles one after another.

The first step of an efficient integration concept is proposed by Chaboche [45] with a non-linear cumulative damage model, where cycles with similar loading are bundled into blocks. The "time"- "cycle" transfer of the phase field model is similar to this idea. It is to assume a constant block size of cycle number per time $\frac{\mathrm{d}N}{\mathrm{d}t}$ representing a certain evolution of fatigue damage [26]. Thus, the individual single loading cycle is not used in the proposed phase field fatigue model; rather, the cycle is converted into continuous pseudo "time" as illustrated in Fig. 4. The red line in Fig. 4 represents the envelope loading, which approximates the actual discrete cyclic loading. In addition, several load cycles are combined into one block in order to reduce the overall number of load cycles: in one simulation step, the incremental change in pseudo "time" is connected to a specific number of load cycles.

In addition, for irregular loading sequences, the rain flow algorithm is used to convert a loading sequence of varying stress into an equivalent set of constant amplitude stress [19, 46].

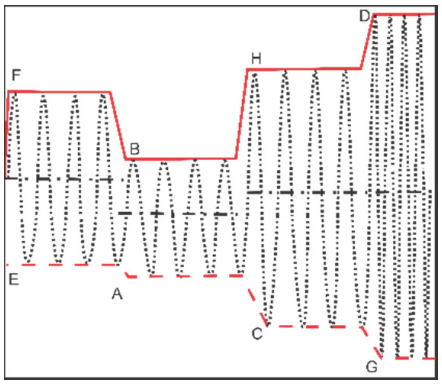

Fig. 4. A "cycle" - "time" transformation

However, the cycle number increment is usually determined by a trade-off between the computing time of simulation and the accuracy of the result. The choice of the number of the cycle increment is critical in the phase field fatigue model, not only because it determines the simulation time, but also because it has a strong influence on the crack topology [34].

The damage parameter D is introduced in the phase field model to model material damage caused by fatigue. Additionally, the "cycle"- "time" transform captures the loading with similar fatigue damage influence together. To reduce the computational effect, the adaptive cycle number adjustment algorithm (*ACNAA*) works by associating the cycle number increment with the damage increment. The simulation of fatigue fracture is divided into three stages based on the damage state (see Fig. 5):

1. $D < D_c$: The fatigue energy term disappears at this point, so it can be viewed as a pure static mechanical state. The cycle increment should be as large as possible in order to reach the critical fatigue state as quickly as possible.
2. $D \approx D_c$: The material is about to break at this point, and the cycle number increment $\mathrm{d}N$ should be chosen so that the damage increment $\mathrm{d}D$ is small enough to simulate the transient process.
3. $D > D_c$: The fatigue crack begins to propagate. The damage increment $\mathrm{d}D$ is regulated at this stage to achieve a moderate growth rate of the fatigue energy.

Our method has been shown to reduce computing time to nearly 3% when compared to constant cycle number increments with $\mathrm{d}N = 5$ [34]. The reason is that the huge computing time involved in the crack nucleation is dramatically reduced. Additionally, the adaptive cycle number adjustment method is also suitable for parallel computing [35]. With parallel computing (e.g. MPI), an additional significant decrease in computing time can be obtained, which keeps a 3D simulation within a reasonable time limit [35].

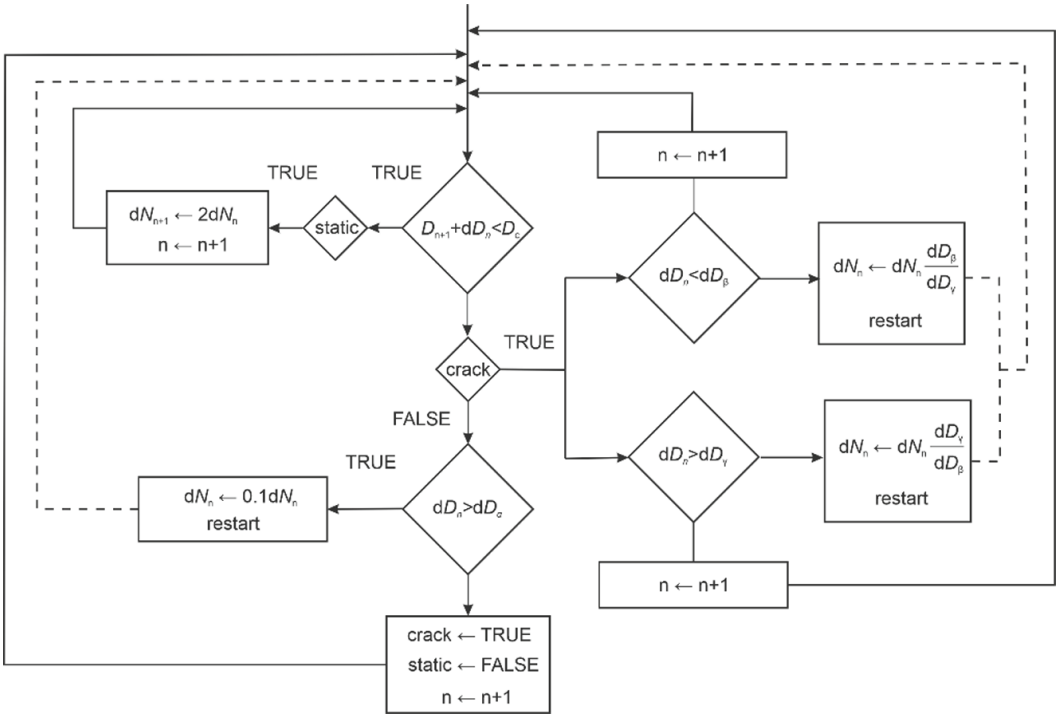

Fig. 5. A flowchart illustrates the idea of ACNAA [35]. dD_α, dD_β, dD_γ are suitable numerical parameters.

3 Phase Field Model in the Context of Manufacturing Process

3.1 Application in the Cold Forging Process

In the past decades, cold forging has gained a lot of attention and has become a economic production method for complex geometries with net-shaped or near-net-shaped surfaces. The cold forge is characterized by the circumstance that the forming of the workpiece begins at room temperature and without external heating. The major advantages of cold forging are close dimensional tolerances, good surface finish quality, and interchangeability as well as reproducibility due to its simple process [47, 48]. During the cold forging process, the material of a metal billet is put into a container (called a die). The material, compressed by a ram, flows through the container and is formed into the desired shape. In general, the cold forging process involves 5 steps (see Fig. 6):

a. lubrication: the workpiece is lubricated to avoid sticking to the die and to maintain a low temperature.
b. insertion: the workpiece is inserted onto a die with the shape of the final part.
c. stroke: a great force is stroked onto the workpiece to create the desired form.
d. flash: the excess metal around the dice is trimmed.
e. removing: the workpiece is removed from the die.

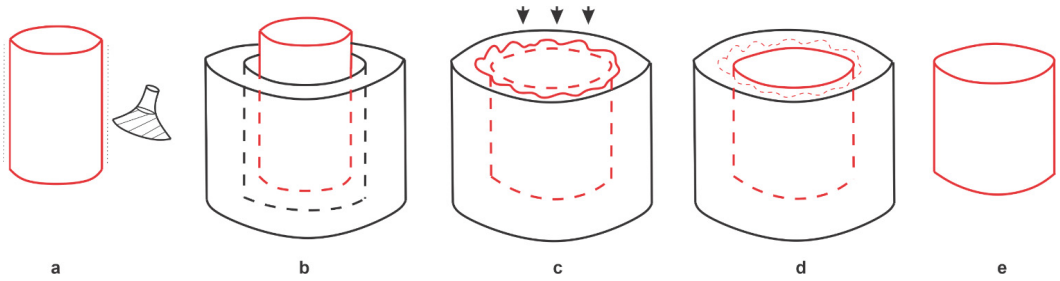

Fig. 6. Cold forging process: (a: lubrication; b: insertion; c: stroke; d: flash; e: removing).

3.2 Modeling Cold Forging Process Using Phase Field Method

In this paper, the cold forging process is modeled by the phase field method, and the fatigue life, where the crack propagation behavior are the main focus. The die geometry is adopted from Lang et al. [49] shown in Fig. 7. To reduce the computational cost, a 2D slice from the die cross-section is extracted for the finite element simulation. The opening angle α and the die length L can be seen as design parameters of the die. In this paper, we evaluate two different die geometries, which are listed in Table 1.

Table 1. Die geometry

α	L
45°	23 mm
60°	25 mm

This design of the die enables high stresses at the fillet radius to generate the fatigue crack initiation and crack growth after a short number of production cycles [49]. The material of the die is AISI 2D [50, 51]. The simulation loading settings are motivated by the experiments of Dalbosco et al. [52]. One contribution of his work for this application is the different assumptions regarding the interference between the workpiece and the die.

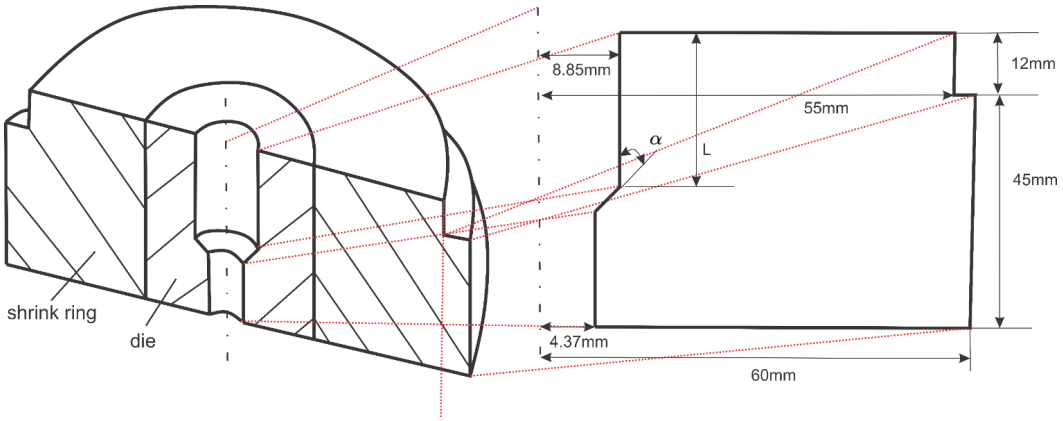

Fig. 7. The cold forging tool geometry presented in [49] and a 2D slice for finite element simulation.

In our first simulation setting (see Fig. 8a) the entire inner face of the die is assumed compressed with a constant distributed load, and the bottom of the cold forging tool is fixed by Dirichlet boundary conditions. In a different design of the die (see Fig. 8b), there is no interference from the point of transition radius until the bottom of the die in the second example. This is caused by a lack of material apposition, resulting in stress vacancy along this area of the die. For the sake of simplicity, we assume a constant load only applying it to the inner face of the die. Moreover, as an alternative design, it is also considered that the inner wall can shrunk less due to the lower shrink-fit of the die material on this part as shown in Fig. 8c. As shown in this last Figure, only the fillet of the die is under the tension loading.

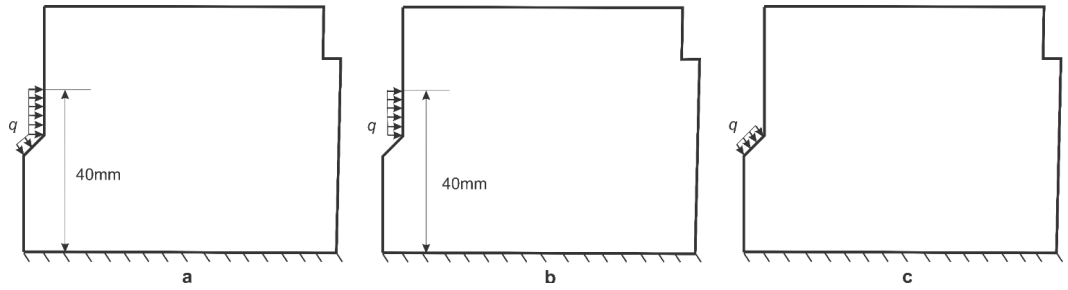

Fig. 8. **a**: both fillet and inner wall are loaded; **b**: only inner wall is loaded; **c**: only fillet is loaded.

3.3 Phase Field Fatigue Model in Cylindrical Coordinate System

In the *cartesian* coordinate system, the positions of points are determined with respect to three mutually perpendicular planes, giving the length-, width- and height coordinates. For a suitable computational cost, a 2D slice from the cross-section of the die is chosen for the finite element calculation Fig. 9a. This simplification in a sense of a cartesian coordinate system is to assume that the width of the body is infinite and all the derivatives regarding z-direction are zero. However, the cold forging die does not have an endless width, rather say, it is symmetric around its axis. Thus, a proper way to simulate the cold forging process with less computational resources is to bring this 2D slice cross-section of the die into a cylindrical coordinate system to exploit its rotational symmetry. A cylindrical coordinate system is specified by a radial position, an angular position, and a height position as shown in Fig. 9b.

The total energy of the body reads

$$\mathcal{E} = \int \Big[(g(s) + \eta)\psi^e\Big(\boldsymbol{\varepsilon}^{\mathrm{cyl}}\Big) + \psi^s\Big(s, \nabla^{\mathrm{cyl}} s\Big) + h\Big(s, \nabla^{\mathrm{cyl}} s\Big)\psi^{\mathrm{ad}}(\mathrm{D})\Big] \mathrm{d}\, V^{\mathrm{cyl}}, \tag{13}$$

where $\boldsymbol{\varepsilon}^{\mathrm{cyl}}$ is the strain tensor in the cylindrical coordinates and $\mathrm{d}V^{\mathrm{cyl}}$ is the infinite cylinder volume element.

Let r be the radius, θ be the circumferential angle and z be the height, the transformation between the cartesian coordinates (x, y, z) and cylindrical coordinates (r, θ, z) can be given as

$$x = r\cos\theta \quad y = r\sin\theta \quad z = z, \tag{14}$$

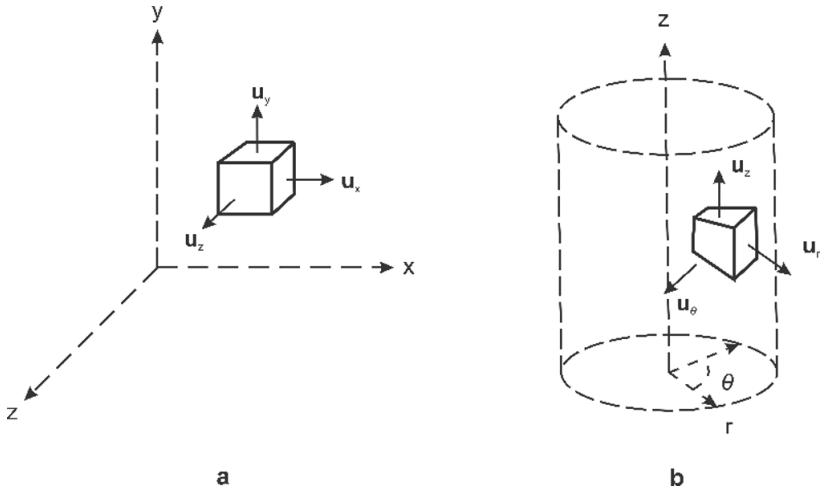

Fig. 9. **a**: cartesian coordinate system; **b**: cylindrical coordinate system.

and the *Jacobian* matrix transforming the infinitesimal vectors from cartesian coordinates to cylindrical coordinates is given as

$$J = \begin{bmatrix} \frac{\partial x}{\partial r} & \frac{\partial y}{\partial r} & \frac{\partial z}{\partial r} \\ \frac{\partial x}{\partial \theta} & \frac{\partial y}{\partial \theta} & \frac{\partial z}{\partial \theta} \\ \frac{\partial x}{\partial z} & \frac{\partial y}{\partial z} & \frac{\partial z}{\partial z} \end{bmatrix} = \begin{bmatrix} \cos\theta & \sin\theta & 0 \\ -r\sin\theta & r\cos\theta & 0 \\ 0 & 0 & 1 \end{bmatrix}. \tag{15}$$

The displacement vector in the cylindrical coordinate system with rotational symmetry properties is given as

$$\mathbf{u}^{\text{cyl}} = [u_r, u_\theta, u_z]^T \underset{rot.\ sym.}{\Longrightarrow} [u_r, 0, u_z]^T, \tag{16}$$

where u_r and u_z are the width and height components of the displacement vector.

For rotational sysmmetry, the derivative in angular direction vanishes, thus, the strain tensor is given by.

$$\boldsymbol{\varepsilon}^{\text{cyl}} = \begin{bmatrix} \frac{\partial u_r}{\partial r} & 0 & \frac{1}{2}\left(\frac{\partial u_r}{\partial z} + \frac{\partial u_z}{\partial r}\right) \\ 0 & \frac{u_r}{r} & 0 \\ \frac{1}{2}\left(\frac{\partial u_z}{\partial r} + \frac{\partial u_r}{\partial z}\right) & 0 & \frac{\partial u_z}{\partial z} \end{bmatrix}. \tag{17}$$

It is noted that the entry in the middle $\frac{u_r}{r}$ provides an additional contribution into the energy density, which is omitted in the cartesian coordinates system for 2D. The fatigue driving force $\widehat{\sigma}^{\text{cyl}}$ can be given with the constitutive law and taking as the first principal stress

$$\widehat{\sigma}^{\text{cyl}} = \left[\mathbb{C}\boldsymbol{\varepsilon}^{\text{cyl}}\right]_1 \tag{18}$$

where the stiffness tensor $\mathbb{C}$ remains the same as it is in the cartesian coordinate system because of its isotropic character. The crack field s itself does not need to be modified into a cylindrical coordinate system since it is a scalar variable to indicate the broken

state of the material. The gradient of the crack field $\nabla^{\text{cyl}} s$ in the cylindrical coordinate system is given as

$$\nabla^{\text{cyl}} s = [\frac{\partial s}{\partial r} 0 \frac{\partial s}{\partial z}]^T .$$

3.4 Phase Field Simulation of Cold Forging Process

In the our first analysis, it is assumed that the fillet and the inner wall of the die are completely loaded, two different geometries of the die are investigated. The angle of crack propagation is nearly 30° in Fig. 10a and nearly 40° in Fig. 10b. Those angles of the crack propagation directions can be explained by the mixed energy fracture criterion [53], since the tools are under a mixed mode I/II load situation. The bigger angle of fracture initiation in Fig. 10b can be explained by the dominant influence of shear stress from mode II in comparison to the tension stress from mode I. Furthermore, the first initialized crack can be found after around 3,000 production cycles at the forging tool with an opening angle of 45° and the fatigue life of the second tool ($\alpha = 60°$) is only around 500 cycles of production. This analysis reveals the fact that the dominated shear stress on the inner wall of the die shortens the fatigue life of the tool.

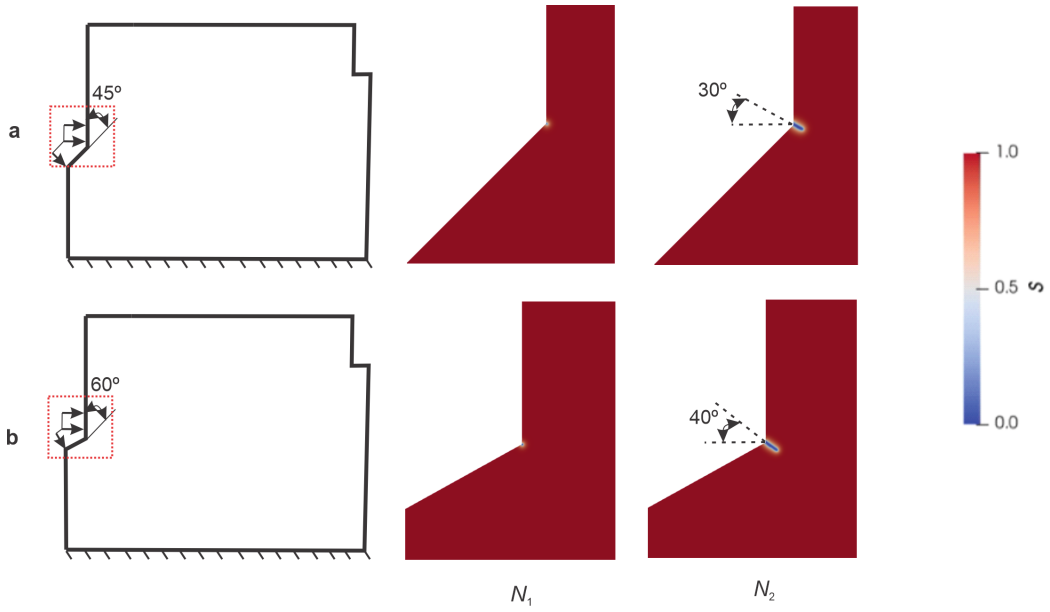

Fig. 10. The simulation of the cold forging process at first crack N_1 and final stage N_2 (**a**: opening angle $\alpha = 45°$; **b**: opening angle $\alpha = 60°$).

For further investigations, the cold forging tools are simulated with different loading assumptions (Fig. 8) as shown in Fig. 11. Results show that loading acts merely on the inner wall of the die and can dramatically increase the fatigue life of the die. In the analysis that was performed itt yielded the highest fatigue life at around 55,000 production cycles for the opening angle of 45° (Fig. 11b). Different loading assumptions lead to different patterns of crack propagation. In Fig. 11a and Fig. 11b, the crack propagates first sloping

downward, which is influenced by a mixed mode loading situation. After these stages, the crack curves moves in a nearly horizontal direction because of the mainly vertical tensile stress. In contrast, loads acting only on the inner wall yield almost the same crack propagation patterns, where the angle of crack propagation is around 70°. This can be explained by a pure shear mode II loading situation. These crack propagation behaviors from the phase field simulations have been found similarly in reported experiments [52].

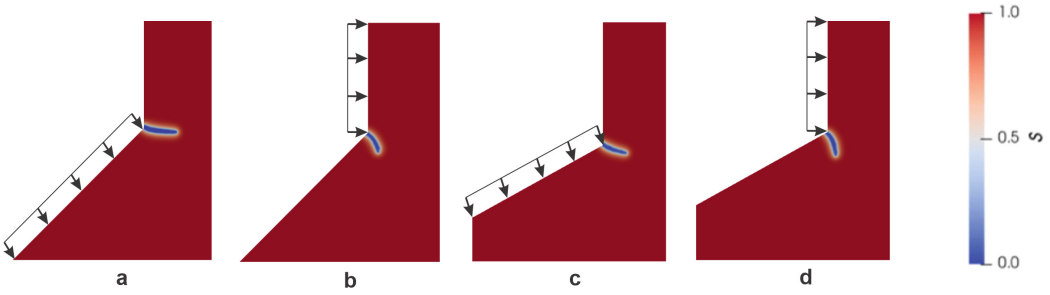

Fig. 11. The simulation of the cold forging process by different loading conditions.

4 Conclusion

In this paper, we presented a phase field model for cyclic fatigue, which is used to analyze manufacturing process namely the cold forging process. The phase field model introduces an additional phase field variable to model the broken material. The entire crack evolution behavior can be derived by considering the total energy of the body. The total energy consists of three parts: an elastic energy part, which represents the energy stored inside of the body; a fracture surface energy part, which represents the energy to generate cracks; and an additional fatigue energy part, which represents the additional driving forces associated with fatigue evolution. Inspired by Miner rule, a damage parameter is introduced to model the accumulative fatigue damage. The phase field fatigue model can reproduce the most important fatigue properties, e.g., the Paris' law, the mean stress effect, and the loading sequence effect. Moreover, a "cycle"- "time" transfer is presented which would transform the cycle domain into the pseudo time domain for an efficient fatigue simulation. For irregular loading sequences, the rain flow counting algorithm is used to convert the load cycles into several blocks of regular uniform loading. The existing fatigue simulation methods usually suffers from its huge computational demand. In order to further reduce the computational time without losing accuracy, different numerical strategies are proposed. The core idea of the *ACNAA* is to associate the damage increment with the cycle increment. Additional computing time reduction can be obtained by applying parallel computing.

The main contribution of this work is that we apply the phase field model to the manufacturing problem to predict fatigue life and crack patterns. We used the cold forging process as the demonstrated example since it is an important manufacturing methods for producing parts with complex geometries. To exploit the rotational symmetry property of the problem, a phase field fatigue model for cylindrical coordinates is introduced. Different cold forging die geometries and load conditions in the processing are presented

to analyze the fatigue life and crack patterns. Results show that the phase field model can be effectively applied to cold forging process. This enables a physics-based prediction of the lifetime of manufacturing tools and the identification of process parameters relevant to detect the onset of damage.

Acknowledgment. Funded by the Deutsche Forschungsgemeinschaft (DFG, German Research Foundation) – 252408385 – IRTG 2057.

References

1. Steinbach, I.: Phase-field models in materials science. Modell. Simul. Mater. Sci. Eng. **17**(7), 073001 (2009)
2. Griffith, A.A.: VI. The phenomena of rupture and flow in solids. Philosophical Transactions of the Royal Society of London. Series A, Containing Papers of a Mathematical or Physical Character **221**(582–593), 163–198 (1921)
3. Francfort, G.A., Marigo, J.J.: Revisiting brittle fracture as an energy minimization problem. J. Mech. Phys. Solids **46**(8), 1319–1342 (1998)
4. Bourdin, B., Francfort, G.A., Marigo, J.J.: Numerical experiments in revisited brittle fracture. J. Mech. Phys. Solids **48**(4), 797–826 (2000)
5. Bourdin, B.: Numerical implementation of the variational formulation for quasi-static brittle fracture. Interfaces and Free Boundaries **9**(3), 411–430 (2007)
6. Bourdin, B., Larsen, C.J., Richardson, C.L.: A time-discrete model for dynamic fracture based on crack regularization. Int. J. Fract. **168**(2), 133–143 (2011)
7. Kuhn, C., Müller, R.: A continuum phase field model for fracture. Eng. Fract. Mech. **77**(18), 3625–3634 (2010)
8. Amor, H., Marigo, J.J., Maurini, C.: Regularized formulation of the variational brittle fracture with unilateral contact: numerical experiments. J. Mech. Phys. Solids **57**(8), 1209–1229 (2009)
9. Miehe, C., Welschinger, F., Hofacker, M.: Thermodynamically consistent phase-field models of fracture: variational principles and multi-field FE implementations. Int. J. Numer. Meth. Eng. **83**(10), 1273–1311 (2010)
10. Larsen, C.J., Ortner, C., Süli, E.: Existence of solutions to a regularized model of dynamic fracture. Math. Models Methods Appl. Sci. **20**(07), 1021–1048 (2010)
11. Borden, M.J., Verhoosel, C.V., Scott, M.A., Hughes, T.J., Landis, C.M.: A phase-field description of dynamic brittle fracture. Comput. Methods Appl. Mech. Eng. **217**, 77–95 (2012)
12. Hofacker, M., Miehe, C.: Continuum phase field modeling of dynamic fracture: variational principles and staggered FE implementation. Int. J. Fract. **178**(1), 113–129 (2012)
13. Hofacker, M., Miehe, C.: A phase field model of dynamic fracture: robust field updates for the analysis of complex crack patterns. Int. J. Numer. Meth. Eng. **93**(3), 276–301 (2013)
14. Schlüter, A., Willenbücher, A., Kuhn, C., Müller, R.: Phase field approximation of dynamic brittle fracture. Comput. Mech. **54**(5), 1141–1161 (2014). https://doi.org/10.1007/s00466-014-1045-x
15. Miehe, C., Aldakheel, F., Raina, A.: Phase field modeling of ductile fracture at finite strains: a variational gradient-extended plasticity-damage theory. Int. J. Plast **84**, 1–32 (2016)

16. Ambati, M., De Lorenzis, L.: Phase-field modeling of brittle and ductile fracture in shells with isogeometric NURBS-based solid-shell elements. Comput. Methods Appl. Mech. Eng. **312**, 351–373 (2016)
17. Borden, M.J., Hughes, T.J., Landis, C.M., Anvari, A., Lee, I.J.: A phase-field formulation for fracture in ductile materials: finite deformation balance law derivation, plastic degradation, and stress triaxiality effects. Comput. Methods Appl. Mech. Eng. **312**, 130–166 (2016)
18. Kuhn, C., Noll, T., Müller, R.: On phase field modeling of ductile fracture. GAMM-Mitteilungen **39**(1), 35–54 (2016)
19. Li, B., Peco, C., Millán, D., Arias, I., Arroyo, M.: Phase-field modeling and simulation of fracture in brittle materials with strongly anisotropic surface energy. Int. J. Numer. Meth. Eng. **102**(3–4), 711–727 (2015)
20. Nguyen, T.T., Réthoré, J., Baietto, M.C.: Phase field modelling of anisotropic crack propagation. Eur. J. Mech.-A/Solids **65**, 279–288 (2017)
21. Schreiber, C., Ettrich, T., Kuhn, C., Müller, R.: A phase field modeling approach of crack growth in materials with anisotropic fracture toughness. In: 2nd International Conference of the DFG International Research Training Group 2057–Physical Modeling for Virtual Manufacturing (iPMVM 2020). Schloss Dagstuhl-Leibniz-Zentrum für Informatik (2021)
22. Xu, B.X., Schrade, D., Gross, D., Mueller, R.: Phase field simulation of domain structures in cracked ferroelectrics. Int. J. Fract. **165**(2), 163–173 (2010)
23. Miehe, C., Schaenzel, L.M., Ulmer, H.: Phase field modeling of fracture in multi-physics problems. Part I. Balance of crack surface and failure criteria for brittle crack propagation in thermo-elastic solids. Comput. Methods Appl. Mech. Eng. **294**, 449–485 (2015)
24. Miehe, C., Hofacker, M., Schänzel, L.M., Aldakheel, F.: Phase field modeling of fracture in multi-physics problems. Part II. Coupled brittle-to-ductile failure criteria and crack propagation in thermo-elastic–plastic solids. Comput. Methods Appl. Mech. Eng. **294**, 486–522 (2015)
25. Miehe, C., Mauthe, S.: Phase field modeling of fracture in multi-physics problems. Part III. Crack driving forces in hydro-poro-elasticity and hydraulic fracturing of fluid-saturated porous media. Comput. Methods Appl. Mech. Eng. **304**, 619–655 (2016)
26. Schreiber, C., Kuhn, C., Müller, R., Zohdi, T.: A phase field modeling approach of cyclic fatigue crack growth. Int. J. Fract. **225**(1), 89–100 (2020). https://doi.org/10.1007/s10704-020-00468-w
27. Schreiber, C., Müller, R., Kuhn, C.: Phase field simulation of fatigue crack propagation under complex load situations. Arch. Appl. Mech. **91**(2), 563–577 (2020). https://doi.org/10.1007/s00419-020-01821-0
28. Miner, M.A.: Cumulative damage in fatigue (1945)
29. ASTM E739 10 - Standard Practice for Statistical Analysis of Linear or Linearized Stress-Life (S-N) and Strain-Life (ε-N) Fatigue Data
30. Yan, S., Müller, R., Ravani, B.: Simulating Fatigue Crack Growth including Thermal Effects Using the Phase Field Method (2022)
31. Mises, R.V.: Mechanik der festen Körper im plastisch-deformablen Zustand. Nachrichten von der Gesellschaft der Wissenschaften zu Göttingen, Mathematisch-Physikalische Klasse **1913**, 582–592 (1913)
32. Bathias, C., Pineau, A.: Fatigue of Materials and Structures: Fundamentals. Hoboken, (2010)
33. Walker, K.: The effect of stress ratio during crack propagation and fatigue for 2024-T3 and 7075-T6 aluminum (1970)
34. Yan, S., Schreiber, C., Müller, R.: An efficient implementation of a phase field model for fatigue crack growth. Int. J. Fract., 1–14 (2022). https://doi.org/10.1007/s10704-022-00628-0
35. Yan, S., Müller, R.: An efficient phase field model for fatigue fracture. In: 15th World Congress on Computational Mechanics (WCCM-XV) and 8th Asian Pacific Congress on Computational Mechanics (APCOM-VIII) (2022)

36. Kuhn, C.: Numerical and analytical investigation of a phase field model for fracture. Technische Universität Kaiserslautern (2013)
37. ASTM: ASTM E399-09, Standard test method for linear-elastic plane-strain fracture toughness k ic of metallic materials. http://www.astm.org (2009)
38. Radhakrishnan, V.M.: Parameter representation of fatigue crack growth. Eng. Fract. Mech. **11**(2), 359–372 (1979)
39. Pradhan, D., et al.: Effect of stress ratio and mean stress on high cycle fatigue behavior of the superalloy IN718 at elevated temperatures. Mater Res Express **6**(9), 0965a6 (2019)
40. Kamaya, M., Kawakubo, M.: Mean stress effect on fatigue strength of stainless steel. Int. J. Fatigue **74**, 20–29 (2015)
41. Paepegem, W.V., Degrieck, J.: Effects of load sequence and block loading on the fatigue response of fiber-reinforced composites. Mech. Adv. Mater. Struct. **9**(1), 19–35 (2002)
42. Kamaya, M., Kawakubo, M.: Loading sequence effect on fatigue life of type 316 stainless steel. Int. J. Fatigue **81**, 10–20 (2015)
43. Stephens, R.I., Fatemi, A., Stephens, R.R., Fuchs, H.O.: Metal Fatigue in Engineering. John Wiley & Sons (2000)
44. Stephens, R.I.: Fatigue crack growth under spectrum loads. ASTM International (2011)
45. Chaboche, J.L., Lesne, P.M.: A non-linear continuous fatigue damage model. Fatigue Fract. Eng. Mater. Struct. **11**(1), 1–17 (1988)
46. Yan, S., Müller, R., Ravani, B.: A phase field fatigue model for complex loading situations. In: 15th International Conference on Fracture (2023)
47. Fritz, A.H., Schulze, G. (eds.): Fertigungstechnik. Springer Berlin Heidelberg, Berlin, Heidelberg (2004)
48. Fritz, A.H.: Umformen. In: Fritz, A.H. (ed.) Fertigungstechnik. S, pp. 133–223. Springer, Heidelberg (2018). https://doi.org/10.1007/978-3-662-56535-3_3
49. Lange, K., Hettig, A., Knoerr, M.: Increasing tool life in cold forging through advanced design and tool manufacturing techniques. J. Mater. Process. Technol. **35**(3–4), 495–513 (1992)
50. Bringas, J.E.: Handbooks of comparative world steel standards (2004)
51. Pyun, Y.S., et al.: Development of D2 tool Steel trimming knives with nanoscale microstructure. In: AISTECH-Conference Proceedings, vol. 2, p. 465. Association for Iron Steel Technology
52. Dalbosco, M., da Silva Lopes, G., Schmitt, P.D., Pinotti, L., Boing, D.: Improving fatigue life of cold forging dies by finite element analysis: a case study. J. Manuf. Process. **64**, 349–355 (2021)
53. Kfouri, A.P., Brown, M.W.: A fracture criterion for cracks under mixed-mode loading. Fatigue Fract. Eng. Mater. Struct. **18**(9), 959–969 (1995)